OCS Study
BOEM 2021-008

Tracking Movements of Migratory Shorebirds in the U.S. Atlantic Outer Continental Shelf Region

US Department of the Interior
Bureau of Ocean Energy Management
Office of Renewable Energy Programs

BOEM
Bureau of Ocean Energy Management

OCS Study
BOEM 2021-008

Tracking Movements of Migratory Shorebirds in the US Atlantic Outer Continental Shelf Region

January 2021

Authors:

Pamela H. Loring, US Fish and Wildlife Service (USFWS), Division of Migratory Birds, Hadley, MA
Ariel K. Lenske, Environment and Climate Change Canada, Science & Technology Branch, Ontario, CA
James D. McLaren, Inst. Chemistry & Biology of Marine Environments, Univ. of Oldenburg, Germany
Marley Aikens, Trent University, Peterborough, ON, Canada
Alexandra M. Anderson, Trent University, Peterborough, ON, Canada
Yves Aubry, Canadian Wildlife Service, Québec, QC, Canada
Evan Dalton, Manomet Inc., Manomet, MA, USA
Amanda Dey, New Jersey Division of Fish and Wildlife, Trenton, NJ, USA
Christian Friis, Canadian Wildlife Service, Toronto, ON, Canada
Diana Hamilton, Mount Allison University, Sackville, NB, Canada
Rebecca Holberton, University of Maine, Orono, ME, USA
Debra Kriensky, New York City Audubon, New York, NY, USA
David Mizrahi, New Jersey Audubon, Cape May Court House, NJ, USA
Lawrence Niles, Wildlife Restoration Partnerships LLC, Greenwich, NJ, USA
Kaitlyn L. Parkins, New York City Audubon, New York, NY, USA
Julie Paquet, Canadian Wildlife Service, Sackville, NB, Canada
Felicia Sanders, South Carolina Department of Natural Resources, McClellanville, SC, USA
Adam Smith, USFWS, National Wildlife Refuge System, Athens, GA, USA
Yves Turcotte, Collège de La Pocatière, La Pocatière, QC, Canada
Andrew Vitz, Massachusetts Division of Fisheries & Wildlife, Westborough, MA, USA
Paul A. Smith, Environment and Climate Change Canada, Science & Technology Branch, ON, Canada

Prepared under BOEM Intra-Agency Agreement No. M18PG00021

By
US Department of Interior
US Fish and Wildlife Service
Division of Migratory Birds
300 Westgate Center Dr.
Hadley, MA 01035

US Department of the Interior
Bureau of Ocean Energy Management
Office of Renewable Energy Programs

BOEM
Bureau of Ocean Energy Management

DISCLAIMER

This study was funded, in part, by the U.S. Department of the Interior, Bureau of Ocean Energy Management, Office of Renewable Energy Programs, Washington, DC, through Inter-Agency Agreement Number M18PG00021 with the US Department of Interior, US Fish and Wildlife Service, Division of Migratory Birds, Hadley, MA. This report has been technically reviewed by BOEM, and it has been approved for publication. The views and conclusions contained in this document are those of the authors and should not be interpreted as representing the opinions or policies of the US Government, nor does mention of trade names or commercial products constitute endorsement or recommendation for use.

REPORT AVAILABILITY

To download a PDF file of this report, go to the US Department of the Interior, Bureau of Ocean Energy Management Data and Information Systems webpage (http://www.boem.gov/Environmental-Studies-EnvData/), click on the link for the Environmental Studies Program Information System (ESPIS), and search on 20xx-xxx. The report is also available at the National Technical Reports Library at https://ntrl.ntis.gov/NTRL/.

CITATION

Loring PH, Lenske AK, McLaren JD, Aikens M, Anderson AM, Aubrey Y, Dalton E, Dey A, Friis C, Hamilton D, Holberton B, Kriensky D, Mizrahi D, Niles L, Parkins K.L. Paquet J, Sanders F, Smith A, Turcotte Y, Vitz A, Smith PA. 2020. Tracking Movements of Migratory Shorebirds in the US Atlantic Outer Continental Shelf Region. Sterling (VA): US Department of the Interior, Bureau of Ocean Energy Management. OCS Study BOEM 2021-008. 104 p.

ABOUT THE COVER

Shorebirds in James Bay, Ontario, Canada. Photo by Amie MacDonald, Trent University.

ACKNOWLEDGMENTS

For study administration, guidance, and oversight, we thank David Bigger, Mary Boatman, and Tim White from the Bureau of Ocean Energy Management (BOEM); Dominique Bruce-Morton from the Bureau of Safety and Environmental Enforcement, as well as Scott Johnston, Caleb Spiegel, and Pamela Toschik from the US Fish and Wildlife Service (USFWS). We thank Annelee Motta and Laurie Racine from the USFWS administrative support.

The data analyzed in this report are the product of immense efforts in the field, spread across 21 sites. Innumerable people contributed to these field studies, and we thank them all for their contributions. Key individuals are listed by site below.

At Bathurst Island, Nunavut, Canada: Paul Woodard, Beth Macdonald, Fletcher Smith, Julie Belliveau, Mark Dodds, Keara Nelson, and Kiersten Shulhan. Many thanks also to the pilots of Kenn Borek Air Ltd. for safely delivering us to the field site, and staff of the Polar Continental Shelf Program in Resolute Bay for providing logistical support.

At Southampton and Coats Islands, Nunavut, Canada: Lisa Kennedy, Scott Flemming, Willow English, the many dedicated field staff, and the community of Coral Harbour for their ongoing support.

At Churchill, Manitoba, Canada: Christophe Buidin, Florence Masson, Kenneth Mills, Erica Nol, Yann Rochepault. Additional thanks to the dedicated staff at Churchill Northern Studies Centre and Parks Canada for logistical support.

Polar Bear Provincial Park (Burnt Point), Ontario, Canada: Hannah MacKellar, Lisa Pollock, Glen Brown, Kim Bennett, Rod Brook.

At James Bay, Ontario, Canada: Ross Wood, Amie MacDonald, Rod Brook, Kim Bennet, Sarah Hagey, Bernie McLeod, field staff, and the numerous volunteers that make the project a success. A special thank you to the Gagnon family, the Wesley family, the Cheechoo family, and Rickard family for field site accommodations.

At the Mingan Islands, Quebec, Canada: Yann Rochepault, Christophe Buidin, and the volunteers and staff of Parks Canada and the Mingan Islands National Park Reserve. At the Saint Lawrence River, Quebec, Canada: Christine Pomerleau

At Lameque and Miscou Islands, New Brunswick, Canada: For field work and research, Mount Allison University students Avery Nagy-MacArthur, Hannah MacKellar, Jessie MacIntyre and Erica Geldart. Also, Fletcher Smith, Bryan Watts and Barry Truitt at the Center for Conservation Biology, Lewnanny Richardson at Nature New Brunswick, and the many summer staff that contributed to this project. Landowners who hosted Motus stations on their property include the Nature Conservancy of Canada, Complexe des Deux Rivieres, Denise Maillet, Kouchibouguac National Park, Prince Edward Island National Park and Cape Jourimain National Wildlife Area (NWA).

At the Bay of Fundy, New Brunswick and Nova Scotia, Canada: For field work and research, Mount Allison University students Abby White, Sarah Neima, Hilary Mann, Sydney Bliss, numerous support staff and Nature Conservancy of Canada Johnson's Mills Shorebird Interpretation Center staff. Land owners who hosted Motus stations on their property include the Nature Conservancy of Canada, the Cape Enrage Interpretive Centre, Shepody NWA, The Hopewell Rocks, Beaubassin Research Station, Joggins Fossil Institute, Fundy Ocean Research Center for Energy, Burntcoat Head Park, Elmsdale Landscaping, Shirley and Merv Ferguson, Peggy and Blair Hamilton, Roy Bishop, Chester and Donna Sharp, Ginny Lee, Mary Majka and David Christie.

At the Gulf of Maine, Maine, USA: Lindsay Tudor (Maine Department of Inland Fisheries & Wildlife; MDIFW), Kate O'Brien (USFWS-Rachel Carson NWR) were major collaborators on all aspects of the field work done in Maine. USFWS-Maine Coastal Islands NWR provided additional funding and logistic support. Capture and tagging efforts were done primarily by Glenn Mittelhauser (Maine Natural History Observatory) and staff at Biodiversity Research Institute, and assisted by additional staff at MDIFW. Wes Wright and Sean Rune helped set up equipment and capture birds. The Mudge and Marshall families allowed towers to be set up on private land in Downeast Maine. Funding for work in Maine came from the Maine Outdoor Heritage Fund, USFWS, and the University of Maine Agricultural and Forestry Experimental Station.

At Plymouth Bay and Cape Cod, Massachusetts, USA: Monomoy National Wildlife Refuge staff for equipment and logistical support, and especially Stephanie Koch and Kate Iaquinto for helping to lead the field effort. We also thank our many cooperators who provided landowner permission and field support, including: Towns of Chatham, Orleans, and Eastham; National Park Service; Massachusetts Audubon

Society; Goldenrod Foundation; Biodiversity Works; and New England Wildlife Center. We also thank the numerous other USFWS staff and volunteers who assisted with field work and made the capture and tagging efforts a success.

At Jamaica Bay, New York, USA: National Park Service/Gateway National Recreation Area natural resources staff for logistical support. New York City Audubon field assistants Emilio Tobón, José Ramirez-Garofalo, Molly Adams, and Andrew Baksh. Nellie Tsipoura for her guidance in planning and help in the field.

At Delaware Bay, New Jersey, USA: New Jersey Division of Fish and Wildlife, Stephanie Feigin of Conserve Wildlife Foundation, Humphrey Sitters of International Wader Study and Joe Smith. For spring capture and tagging we also thank New Jersey Division of Fish and Wildlife, New Jersey Natural Land Trust, Conserve Wildlife Foundation of New Jersey and the entire Delaware Bay Shorebird Project and the volunteers and groups supporting the project, chief among them Citizens United to Protect the Maurice River. We thank Michelle Poulopaulos and Joe Atzert for keeping track of the birds and towers.

At South Carolina, USA: South Carolina Department of Natural Resources, particularly Janet Thibault. We thank State Wildlife Grants and USFWS for funding and numerous volunteers, especially those at Seabrook Island. Thanks to Ellen Jamieson (Trent University) for technical support.

For field and logistical support with automated radio telemetry towers along the US Atlantic Coast, we thank our many cooperators from following entities: UMass Amherst-USGS Cooperative Fish and Wildlife Unit, USFWS Southern New England-New York Bight Coastal Program, USFWS Division of Migratory Birds, University of Rhode Island, Cape Cod National Seashore, Eastern Massachusetts National Wildlife Refuge Complex, Waquoit Bay National Estuarine Research Reserve, US Army Corps of Engineers/Cape Cod Canal Field Office, Rhode Island NWR Complex, Shearwater Excursions, Nantucket Islands Land Bank, Nantucket Conservation Foundation, Napatree Point Conservation Area, Connecticut Department of Energy & Environmental Protection, American Museum of Natural History/Great Gull Island Project, Plum Island Animal Disease Center, Block Island Southeast Lighthouse Foundation, Camp Hero State Park, Fire Island National Seashore, Gateway National Recreation Area, Wildlife Conservation Society/New York Aquarium, Rutgers University Marine Field Station, Conserve Wildlife Foundation of New Jersey, New Jersey Division of Fish and Wildlife, Avalon Fishing Club, Delaware Department of Natural Resources/Cape Henlopen State Park, The Nature Conservancy Virginia Coast Reserve, Chincoteague NWR, Eastern Shore of Virginia NWR, Back Bay NWR, Mackay Island NWR, Pea Island NWR, Cedar Island NWR, Cape Romain NWR, Harris Neck NWR, Blackbeard Island NWR, and Georgia Department of Natural Resources. We also thank the many partners operating automated radio telemetry stations throughout the Western Hemisphere as part of the Motus Wildlife Tracking System.

For technical support and assistance with data management and analysis, we thank Stu Mackenzie and Lucas Berrigan (Motus Wildlife Tracking System, Bird Studies Canada); Phil Taylor and John Brzustowski (Acadia University); Mike Vandentillart (Lotek Wireless); Hua Bai and Ramakrishna Janaswamy (University of Massachusetts Amherst).

This study was funded in part by the US Department of the Interior, Bureau of Ocean Energy Management, Environmental Studies Program, Washington DC, through Intra-Agency Agreement Number M18PG00021 with the Department of Interior, Fish and Wildlife Service. This study was also supported by grants from Environment and Climate Change Canada, the Polar Continental Shelf Program, and the Natural Sciences and Engineering Research Council.

Summary

The Bureau of Ocean Energy Management (BOEM) is responsible for managing renewable energy development on the Outer Continental Shelf (OCS) of the United States. The OCS extends from the boundary of each state's jurisdictional waters (generally 3 nautical miles offshore) to the outer boundary of the US Exclusive Economic Zone (approximately 200 nautical miles offshore). In the Atlantic OCS, 7,073 km² is presently under lease agreement for development of commercial-scale offshore wind energy facilities and an additional 11,235 km² is in the planning stages for potential lease (BOEM 2019). Development in the United States to date (December 2019) is limited to a 30-MW, five turbine demonstration-scale facility in state waters off the coast of Block Island, RI and a 12-MW, two turbine pilot project under construction in Federal waters off the coast of Virginia. Herein, BOEM Lease Areas and BOEM Planning Areas are collectively referred to as Wind Energy Areas (WEAs).

With large areas of the Atlantic OCS under consideration for development of offshore wind energy facilities, information on offshore movements and flight altitudes of high-priority bird species is needed for estimating exposure of birds to collision risks in WEAs and for developing strategies to manage adverse effects (BOEM 2017). The potential effects of offshore wind turbines on avian populations vary by species and include direct mortality from collisions with infrastructure and indirect effects of disturbance and habitat loss (Fox et al. 2006, Fox and Petersen 2019). Understanding these species-specific effects, including cumulative impacts from exposure to multiple commercial-scale wind energy facilities throughout their migratory ranges, will be increasingly important as offshore wind energy development advances in US waters (Goodale and Milman 2016).

This study provides new information on the movements and flight altitudes of 12 species of shorebirds: Black-bellied Plover (*Pluvialis squatarola*); Dunlin (*Calidris alpina*); Least Sandpiper (*Calidris minutilla*); Lesser Yellowlegs (*Tringa flavipes*); Pectoral Sandpiper (*Calidris melanotos*); Red Knot (*Calidris canutus*); Ruddy Turnstone (*Arenaria interpres*); Sanderling (*Calidris alba*); Semipalmated Plover (*Charadrius semipalmatus*); Semipalmated Sandpiper (*Calidris pusilla*); Whimbrel (*Numenius phaeopus*); and White-rumped Sandpiper (*Calidris fuscicollis*). These species are long-distance migratory shorebirds that breed in Subarctic and Arctic regions of North America and winter along the coast of the southern United States to southernmost South America. These species migrate over the Atlantic OCS and land to rest and refuel at a network of stopover sites along the US Atlantic coast (O'Connell et al. 2011). While broad patterns in shorebirds' migration routes and behavior have been documented by tracking and banding studies, we still lack fine-scale information on the routes, altitudes, timing, and environmental conditions associated with flights of migratory shorebirds over the Atlantic OCS. Such fine-scale information is needed to refine assessments of exposure to offshore WEAs and to improve estimates of collision risk with offshore wind turbines (O'Connell et al. 2011).

In this study, we compiled movement data from 3,955 individuals of 17 shorebird species that were tagged with digital VHF (Very High Frequency) transmitters from 2014 to 2017 at 21 sites widely dispersed across North and South America. The movements of tagged shorebirds were tracked using a collaborative radio telemetry network, the Motus Wildlife Tracking System, which has extensive coverage from automated radio telemetry stations distributed across Eastern North America and additional coverage at key shorebird sites from Arctic Canada to South America. Our Study Area encompassed a region of the US Atlantic coast extending from Cape Cod, Massachusetts to Back Bay, Virginia, where a network of BOEM-funded automated radio telemetry stations was established for monitoring avian movements throughout adjacent waters of the Atlantic OCS (Loring et al 2018, Loring et al. 2019). These coastal stations had an effective detection radius of about 20 km, therefore the bounds of our Study Area ranged from 20 km inland to 20 km offshore. To estimate broad-scale use of our Study

Area by shorebirds, while accounting for transmitter loss, we examined the migratory tracks of all shorebirds detected by automated radio telemetry stations at least 50 km from their original tagging site and within 30 km of the Atlantic coast from Mingan QC, Canada, in the north to the Texas-Mexico border in the south. Of these individuals that retained their transmitters and were detected somewhere along the Atlantic Coast of North America (n = 1,363), 65% were detected within the Study Area.

We then analyzed movements and flight altitudes of 594 individuals of 12 shorebird species with sufficient detection data by automated radio telemetry stations within our Study Area. We implemented novel movement modeling techniques to assess the frequency and extent of offshore movements over Federal waters within the Study Area, which extended approximately 20 km offshore (corresponding to effective range of automated radio telemetry stations). Our objectives were to: 1) develop spatially-explicit, 3-dimensional models of shorebird movements in the Atlantic OCS region; 2) estimate the presence of shorebirds over Federal waters of the Atlantic OCS region during migration; 3) assess the probability of movements into Federal waters in relation to meteorological conditions (wind speed, wind direction, barometric pressure, temperature, visibility, precipitation), temporal variation (time of day, day of year, migratory season), and sex and age class (where known).

We tracked shorebirds in Federal waters of the Atlantic OCS during both fall and spring migration. In spring, the highest probability of presence in the Atlantic OCS occurred from mid-May to early June, when winds were moderate (~10 m/s) and blowing to the north-northeast. In the fall, the probability of presence in the Atlantic OCS was highest at the beginning of July, decreased through October, and increased slightly in November. Higher probability of presence in the Atlantic OCS during fall was associated with winds blowing to the south-southeast and high atmospheric pressure. During both spring and fall, precipitation during flights in the Atlantic OCS was generally low (< 3 kg/m^2).

During non-stop flights over Federal waters, model-estimated flight altitudes varied greatly (28-2,940 m) and mostly were estimated to occur above the Rotor Swept Zone (RSZ) of offshore wind turbines (25-250 m), with overall mean flight altitudes of 914 m during spring and 545 m during fall. Exposure to the RSZ was higher during fall (approximately 36% of offshore flights in RSZ), relative to spring (approximately 24% of offshore flights in RSZ).

Our array of land-based automated radio telemetry stations was effective for assessing the flight paths and behavior of shorebirds departing from the US Atlantic coast over Federal waters of the Atlantic OCS. However, using digital VHF transmitters to track movements >20 km offshore typically exceeds the limits of the technology's current capabilities. In the future, estimates of shorebird passage rates through specific lease areas located >20 km offshore could be accomplished by placing tracking stations directly within the lease areas on offshore infrastructure such as buoys or wind turbines. The digital VHF technology used in this study has the added benefit of seamless integration with the rest of the rapidly expanding Motus Wildlife Tracking System, which uses a collaborative approach to extend the scope of tracking across the Western Hemisphere. Future studies of collision risk could benefit from the application of other forms of developing technology, especially radar and satellite transmitters, which could be used in conjunction with digital VHF telemetry to collect additional location and flight altitude data at complimentary spatial and temporal scales.

Contents

List of Figures

List of Tables

List of Abbreviations and Acronyms

AHY	After Hatch Year
AMGP	American Golden-Plover
asl	above sea level
BBPL	Black-bellied Plover
BGAM	Boosted Generalized Additive Model
BOEM	Bureau of Ocean Energy Management
COP	Construction and Operations Plan
dBm	decibel-milliwatts
DOI	Department of the Interior
DUNL	Dunlin
ESA	Endangered Species Act
ESP	Environmental Studies Program
ESPIS	Environmental Studies Program Information System
EST	Eastern Standard Time
ft	foot/feet
GAM	Generalized Additive Model
GMT	Greenwich Mean Time
GOMSWG	Gulf of Maine Seabird Working Group
GW	Gigawatts
HY	Hatch Year
K	Kelvin
kg	kilogram
km	kilometer
LESA	Least Sandpiper
LEYE	Lesser Yellowlegs
m	meter
MBTA	Migratory Bird Treaty Act
MDIFW	Maine Department of Inland Fisheries and Wildlife
min	minute(s)
Motus	Motus Wildlife Tracking System
MW	Megawatts
NARR	North American Regional Reanalysis
NEPA	National Environmental Policy Act
NWA	National Wildlife Area
NWR	National Wildlife Refuge
OCS	Outer Continental Shelf
Pa	Pascal
PESA	Pectoral Sandpiper
PFR	Plastic Field Readable
PI	Principal Investigator
PO	Project Officer
PUSA	Purple Sandpiper

REKN	Red Knot
REPH	Red Phalarope
RNPH	Red-necked Phalarope
RSZ	Rotor Swept Zone
RUTU	Ruddy Turnstone
SAND	Sanderling
SBDO	Short-billed Dowitcher
SD	Standard Deviation
SEPL	Semipalmated Plover
SESA	Semipalmated Sandpiper
US	United States
USFWS	US Fish and Wildlife Service
USGS	US Geological Survey
UTM	Universal Transverse Mercator
VHF	Very High Frequency
WEA	Wind Energy Area
WHIM	Whimbrel
WHSRN	Western Hemisphere Shorebird Reserve Network
WRSA	White-rumped Sandpiper

1 Introduction

The Bureau of Ocean Energy Management (BOEM) is responsible for managing energy and mineral resources on the Outer Continental Shelf (OCS) of the United States. The OCS extends from the outer limit of each state's jurisdictional waters (approximately 3 nautical miles or 5.6 km offshore) to the outer limit of the US Exclusive Economic Zone (approximately 200 nautical miles or 370 km offshore). In the Atlantic OCS, 7,073 km² is presently under lease agreement for development of commercial-scale offshore wind energy facilities and an additional 11,235 km² is in the planning stages for potential lease (BOEM 2019). Development in the United States to date (December 2019) is limited to a 30-MW, five turbine demonstration-scale facility in state waters off the coast of Block Island, RI and a 12-MW, two turbine pilot project under construction in Federal waters off the coast of Virginia. Herein, BOEM Lease Areas and BOEM Planning Areas are broadly referred to as Wind Energy Areas (WEAs).

With large nearshore and offshore areas of the US Atlantic OCS under consideration for development, both site specific and regional-scale studies are critical for understanding potential exposure of migratory birds to WEAs (BOEM 2017). Current understanding of the effects of offshore wind turbines on birds comes primarily from studies in western Europe, where large-scale offshore wind energy facilities have been in operation since the 1990s (Langston 2013). These studies have broadly categorized adverse effects to birds from offshore wind turbines as: 1) acting as barriers to movement (e.g. between foraging and roosting sites or along migration routes); 2) destruction, modification, or displacement of habitat; and 3) direct mortality from collisions with infrastructure or pressure vortices (Exo et al. 2003; Drewitt and Langston 2006; Fox et al. 2006). However, the magnitude of these effects are species and site-specific, which highlights the importance of conducting fine-scale movement studies on priority species in areas with potential for development of offshore wind energy facilities (Furness et al. 2013).

In the Federal waters of the US, evaluations of the potential effects of development on migratory birds and their habitats are conducted in accordance with the National Environmental Policy Act (NEPA) and the Migratory Bird Treaty Act (MBTA). In addition, information regarding potential adverse effects to species listed as “Threatened” or “Endangered” under the US Endangered Species Act (ESA) is needed for risk assessments and ESA Section 7 consultations between BOEM and the USFWS.

Arctic breeding shorebirds are declining worldwide, including a large majority of North American populations (71% of species with known trends; Smith et al. *accepted*). The drivers of declines may be acting on a combination of factors on the breeding grounds, nonbreeding grounds, and during migration (Morrison et al. 2001, Zockler et al. 2003, Hope et al. 2019). Shorebirds that are long-distance migrants, including most populations that breed in the Arctic, are declining faster than those that migrate short-distances (Hope et al. 2019, NABCI Canada 2019). Declines appear to be greatest for the easternmost populations of species, such as the *rufa* subspecies of Red Knot, or the more easterly breeding populations of Semipalmated Sandpiper (Smith et al. 2012). With their globe-spanning migrations, shorebirds also are predicted to be atypically vulnerable to global anthropogenic climate change (Galbraith et al. 2014). The rapid, ongoing declines of many shorebird populations are an issue of global conservation concern. The large declines observed in North America already have led to the listing of the

rufa Red Knot in Canada and the United States, the recent listing of Hudsonian Godwit and Red-necked Phalarope as Special Concern in Canada (Rosenberg et al. 2014, Hope et al. 2019), and the identification of several additional species as high priority candidates for status review and potential listing in Canada (COSEWIC 2019).

Some species of shorebirds, including such as Red Knots, Whimbrel, Semipalmated Sandpipers, are known to make transoceanic flights (Hicklin and Gratto-Trevor 2010, Baker et al. 2013, Johnson et al. 2016). However, the risk of exposure to offshore wind energy areas in the Atlantic OCS is unknown for almost all shorebird species (O'Connell et al. 2011, but see Loring et al 2018, 2019). To improve risk assessments, more information is needed to document the timing, frequency, and altitudes of shorebird flights over the OCS during migration in the US Atlantic region. Information about meteorological conditions associated with offshore flights is also important for assessments because birds may be at higher risk of collision with offshore wind turbines during inclement weather (e.g. high winds, precipitation, low visibility) due to impaired visibility and avoidance response (Exo et al. 2003).

Information on avian movements can be obtained through individual-based tracking studies, but current tracking technologies are limited for small-bodied species (Barron et al. 2010, Green et al. 2019). Recent advances in coordinated digital-VHF telemetry provide new opportunities to investigate migratory behavior and routes of small-bodied (<100 g) birds across broad geographic scales (Taylor et al. 2017). Lightweight digital-VHF transmitters that emit uniquely identifiable signals on a shared frequency have been integrated with a coordinated network of automated telemetry receivers: the Motus Wildlife Tracking System (www.motus.org). This system comprises an intercommunicating network of tagging projects and automated radio telemetry stations, with project-specific regional arrays distributed across the Western Hemisphere (Taylor et al. 2017). With strategic deployment, automated radio telemetry stations can be used to determine the timing of avian movements within and among sites of interest, enabling researchers to assess environmental and demographic variation in movement patterns (e.g. Dossman et al. 2016, Duijns et al. 2017, Mann et al. 2017, Smetzer et al. 2017, Müller et al. 2018, Anderson et al. 2019). The integrated nature of the network of telemetry stations allows researchers to track movements of tagged animals beyond their own research sites, at regional to continental scales (Duijns et al. 2017, Gómez et al. 2017, Loring et al. 2017, Wright et al. 2018). The widespread, collaborative use of this technology has compelled the development of new analytic techniques to model flight trajectories, flight altitudes, and behavior (Taylor et al. 2017, Janaswamy et al. 2018).

In this study, we collaborated with researchers from the Motus network who collectively tagged 3,955 shorebirds representing 17 different species between 2014 to 2017. To help address information needs for assessments of offshore WEAs in the Atlantic OCS, we analyzed movement data of shorebirds detected by automated radio telemetry stations along the US Atlantic coast. Our specific objectives were to: 1) develop spatially-explicit, 3-dimensional models of shorebird movements in the Atlantic OCS; 2) estimate the exposure of shorebirds to Federal waters of the Atlantic OCS during migration; and 3) assess movements of shorebirds into Federal waters relative to meteorological conditions (wind speed, wind direction, barometric pressure, temperature, visibility, precipitation), temporal variation (time of day, day of year, migratory season) and demographic variation (age, sex).

2 Methods

2.1 Study Area

2.1.1 Atlantic OCS and Wind Energy Areas

Our Study Area extends along the US Atlantic coast and adjacent OCS waters, extending approximately 20 km inland to 20 km offshore of the coastline to encompass the effective range of automated radio telemetry stations (Fig. 1). The Study Area bounded by Cape Cod, MA to the north and Back Bay, VA to the south. To date (December 2019), there are 11 BOEM Commercial Renewable Energy Lease Areas offshore of the Study Area, as well as one Research Renewable Energy Lease Area in Virginia where two 6-MW turbines are currently under construction (Fig. 1; BOEM 2019). These BOEM Renewable Energy Lease Areas are located in Rhode Island Sound and adjacent offshore waters of Massachusetts (3,685 km²), New York Bight (321 km²), and adjacent waters offshore of New Jersey (1,391 km²), Delaware (390 km²), Maryland (323 km²), Virginia (467 km²), and North Carolina (495 km²). In total, their combined area covers 7,072 km² of the Atlantic OCS. Additional BOEM Planning Areas (under consideration for designation as lease areas) are located offshore of the Study Area in Federal waters off the coast of New York (7,022 km²).

2.1.2 Tagging Sites

This study includes data from 2014 to 2017 that were collected by project partners who tagged shorebirds at stopover, breeding and wintering sites along the Atlantic flyway as part of ongoing studies on shorebird movement and migration. Tagging sites were distributed across North America and along the coast of South America, ranging from breeding areas in Bathurst Island, Nunavut (NU), Canada in the north to wintering areas in Brazil and Suriname to the south (Fig. 2). The majority of tagging sites were located at migratory stopover sites along the Atlantic coast. In addition, the study included data from shorebirds tagged at a spring stopover location in Chaplin, Saskatchewan (SK), Canada and a fall stopover location in James Bay, Ontario (ON), Canada. Tagging sites at breeding areas were primarily distributed in the Hudson Bay region.

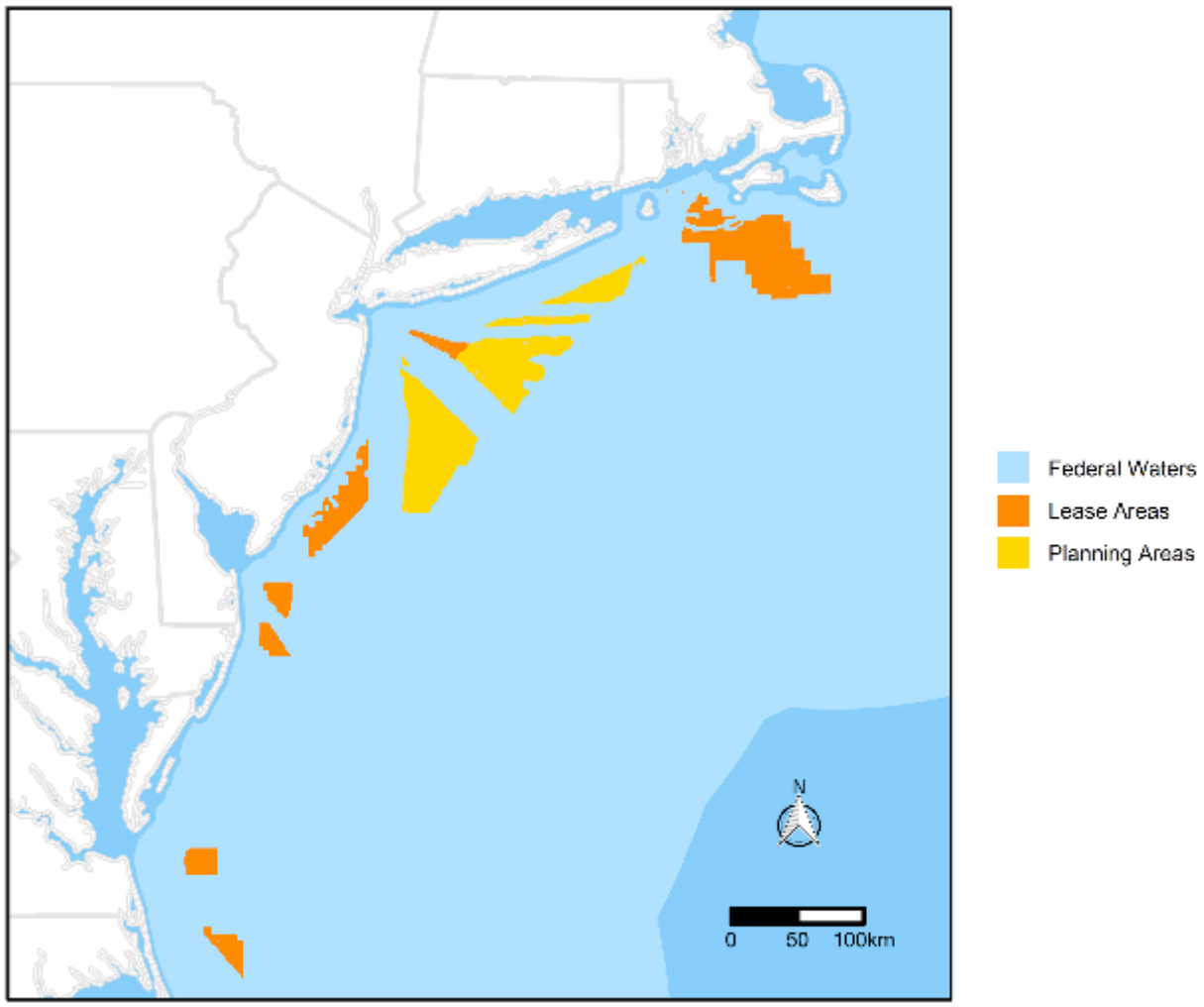

Figure 1. Map of Study Area
Federal Waters of the U.S Atlantic are shown in light blue (3 to 200 nautical miles). Within this boundary, all current (February 2019) BOEM Wind Energy Areas and Planning Areas are shown as orange and yellow polygons, respectively.

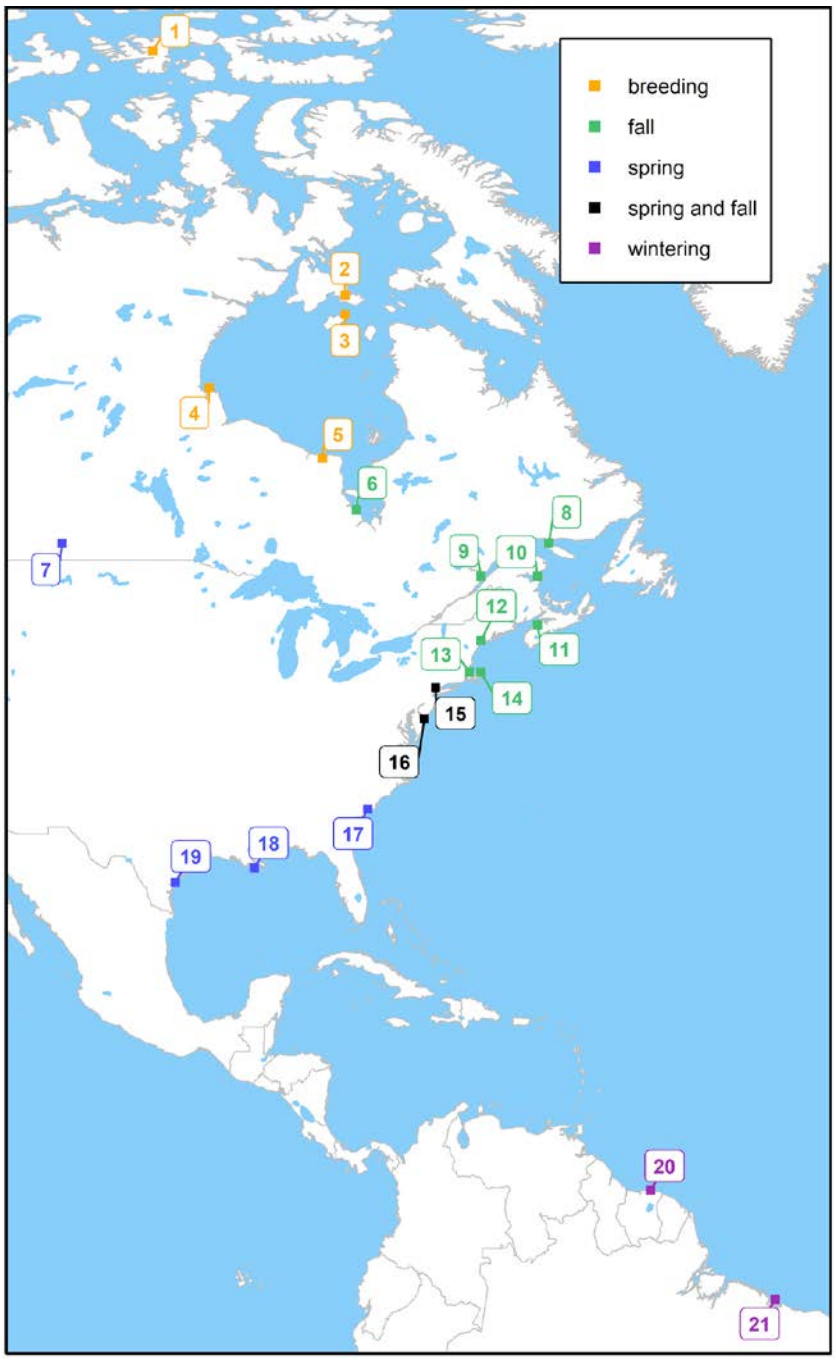

Figure 2. Locations of shorebird tagging sites, 2014-2017.
Numbers and colors indicate the tagging site and season during the annual cycle. 1 - Bathurst Island, NU, Canada; 2 - Southampton Island, NU, Canada; 3 - Coats Island, NU, Canada; 4 - Churchill, MB, Canada; 5 - Polar Bear Provincial Park, ON, Canada; 6 - James Bay, ON, Canada; 7 - Chaplin, SK, Canada; 8 - Mingan Archipelago, QC,

Canada; 9 - Saint Lawrence River, QC, Canada; 10 - Miscou Island, NB, Canada; 11 - Bay of Fundy, NB/NS, Canada; 12 - Gulf of Maine, ME, USA; 13 - Plymouth Bay, MA, USA; 14 - Cape Cod, MA, USA; 15 - Jamaica Bay, NY, USA; 16 - Delaware Bay, NJ, USA; 17 - Charleston, SC, USA; 18 - Gulf of Mexico, LA, USA; 19 - Gulf of Mexico, TX, USA; 20 - Suriname; 21 - Brazil.

2.2 Study Species

This study focuses on 12 species of shorebirds (Black-bellied Plover, Dunlin, Least Sandpiper, Lesser Yellowlegs, Pectoral Sandpiper, Red Knot, Ruddy Turnstone, Sanderling, Semipalmated Plover, Semipalmated Sandpiper, Whimbrel, White-rumped Sandpiper) that were tagged by project partners between 2014 and 2017. An additional five species were tagged by project participants but with small sample sizes or too few detections within our Study Area along the US Atlantic coast to be included as focal species. Focal species include both long- and short-distance migrants that breed in the North American Subarctic and Arctic and occur regularly on the US Atlantic coast and OCS during migration in spring, fall, or both seasons.

2.2.1 Breeding

Lesser Yellowlegs breed primarily in the Subarctic while Red Knots, Black-bellied Plovers, Sanderling, Pectoral Sandpipers, Ruddy Turnstones and White-rumped Sandpipers breed in the Arctic. The remaining focal species have breeding ranges that span both the Arctic and Subarctic (ECCC 2019). Within these broad breeding ranges, several species have recognized subspecies or morphometric variation suggestive of population structure. Importantly, for some species, declines appear to be greatest for the easternmost populations, such as the *rufa* subspecies of Red Knot (Hope et al. 2019), or the more easterly breeding populations of Semipalmated Sandpiper (Andres et al. 2012, Gratto-Trevor et al. 2012a,b, Smith et al. 2012, Brown et al. 2017). However, for most species, there is a lack of information on migratory connectivity between portions of the breeding range and the non-breeding range. Where such connectivity exists and is supported by evolutionary and/or ecological distinctiveness, the population segments can be recognized as distinct under endangered species legislation. This population structure can greatly alter the interpretation of the relative risk faced by a subspecies/population, versus the population as a whole. For many species of shorebirds, disjunct breeding ranges and widely dispersed non-breeding ranges are suggestive of population structure. However, for most species, we lack the necessary evidence to define these population segments with certainty.

2.2.2 Non-breeding

Most of the focal species in our study are long-distance migrants, wintering mainly in the southern hemisphere (ECCC 2019). Although their occurrence on the US Atlantic coast and OCS is most likely to occur during migration, several focal species have non-breeding ranges that extend along the US Atlantic coast (ECCC 2019), so exposure to WEAs could occur both during migration and throughout the non-breeding period. For example, Dunlin spend the non-breeding season primarily in the northern hemisphere (within temperate regions of southern North America and northern Mexico) and are common along the US Atlantic coast from southern New Jersey to southern Florida during winter (Warnock and Gill 1996). Black-bellied Plovers, Least Sandpipers, Sanderling, Lesser Yellowlegs and Ruddy Turnstones also have wintering ranges that extend north along the US Atlantic coast into the Study Area

but more commonly winter further south (Nettleship 2000, Macwhirter et al. 2002, Nebel and Cooper 2008, Tibbitts and Moskoff 2014, Poole et al. 2016).

2.2.3 Migration

Migration is the main period during which Arctic and Subarctic breeding shorebirds are present along the US Atlantic coast and potentially exposed to WEAs within the Study Area. The extent to which shorebirds use the US Atlantic coast during migration varies according to species and season. Lesser Yellowlegs, White-rumped Sandpipers and Pectoral Sandpipers are present along the US Atlantic coast mainly during fall migration and take inland routes, including through the midcontinent, in spring (Parmelee 1992, Farmer et al. 2013, Tibbitts and Moskoff 2014). Least Sandpipers, Red-Knot, Semipalmated Sandpiper and Whimbrel are present during both spring and fall migration but follow more coastal routes through the Study Area during the spring. During fall, these species, as well as White-rumped Sandpipers, often undertake transoceanic flights to South America departing from Atlantic coastal sites in both Canada and the US including from sites within the Study Area (Parmelee 1992, Skeel and Mallory 1996, Nebel and Cooper 2008, Hicklin and Gratto-Trevor 2010, Baker et al. 2013). Black-bellied Plovers, Semipalmated Plovers, Sanderling, Ruddy Turnstones and Dunlin (*hudsonia* subspecies) migrate along the US Atlantic coast during both spring and fall migration (Warnock and Gill 1996, Nettleship 2000, Macwhirter 2002, Nol and Blanken 2014, Poole et al. 2016).

Important shorebird stopover sites within the Study Area include Delaware Bay, the Delmarva Peninsula, and Cape Cod, Massachusetts (Warnock and Gill 1996, Nettleship 2000, Macwhirter et al. 2002, Nebel and Cooper 2008, Hicklin and Gratto-Trevor 2010, Baker et al 2013, Brown et al. 2017, Holberton et al. 2019). Apart from the transoceanic flights that several species undertake between North and South America during fall migration, little is known about the frequency and location of offshore versus nearshore movements of shorebirds within our Study Area in the US Atlantic Region (O'Connell et al. 2011, except see Loring et al. 2018, 2019).

2.2.4 Conservation Status

The *rufa* Red Knot (the subspecies of Red Knot that migrates along the Atlantic coast) was listed as "Threatened" under the ESA in 2014 (USFWS 2014) and is also listed as "Endangered" under Canada's Federal Species at Risk Act (SARA; Environment and Climate Change Canada 2016).

The remaining focal species are not currently listed under either the ESA or Canada's SARA. However, seven of them have been assessed as either a species of High Concern (Whimbrel, Ruddy Turnstone, Dunlin, Pectoral Sandpiper, Lesser Yellowlegs, Semipalmated Sandpiper) or Moderate Concern (Sanderling) by the US Shorebird Conservation Plan Partnership (USSCP Partnership 2016).

2.3 Digital VHF Transmitters

We tracked the movements of shorebirds during fall and spring migration using digital VHF transmitters ("nanotags", Lotek Wireless, Ontario, Canada). Study partners deployed different models of transmitters based on target species and study goals. Across all birds within the study, transmitter weight with attachment materials never exceeded 5% of an individual bird's body mass.

All transmitters were programmed to transmit signals on a shared frequency of 166.380 MHz from activation through the end of battery life. Burst intervals (time intervals between transmissions) were specific to each transmitter and ranged from approximately 4 to 25 seconds. The expected battery life varied by transmitter model and burst interval, ranging from 55 days to 688 days. Tag deployment metadata for each nano-tagged bird are provided in Appendix A.

2.4 Capture and Transmitter Deployment

Shorebirds were captured using multiple methods (e.g., cannon nets, shoulder mounted netguns, bow nets, or mist nets) that varied by site and target species. Age class was determined by plumage characteristics and molt patterns, with birds classified as either Hatch Year (HY), After Hatch Year (AHY) or Unknown (U). For some birds captured on the breeding grounds, sex was determined based on plumage characteristics or incubation behavior. Alternatively, molecular-based methods were used to determine sex from contour feather samples (Avian Biotech, Gainesville, FL) or blood samples (van der Velde et al. 2017). Nanotags were attached by clipping a small area of feathers from the synsacral region and gluing the tags to the feather stubble and skin with a cyanoacrylate gel adhesive (Fig. 3).

Figure 3. Photo of digital VHF transmitter mounted to synsacral region of a Red Knot.
Photo: Kaiti Titherington/USFWS.

2.5 Automated Radio Telemetry Stations

We tracked the signals of nano-tagged birds using the Motus Wildlife Tracking System (hereafter: Motus). The Motus network currently comprises over 800 automated radio telemetry stations from Arctic Canada to South America and over 20,000 nano-tagged individuals representing a variety of taxa of birds, bats and insects (Taylor et al. 2017, www.motus.org). Detection data from all tagged organisms and tracking stations in the Motus network are centrally managed by Bird Studies Canada and accessed from the Motus database using the program R (version 3.4.1, R Core Development Team 2017) and associated package 'Motus' (Brzustowski and Lepage 2019).

Our Study Area along the US Atlantic Coast was the site of a regional node of automated radio telemetry stations funded by BOEM (hereafter: BOEM stations) that was embedded within the broader Motus network (Fig. 4). BOEM stations typically consisted of a 12.2-m radio antenna mast supporting six, nine-element (3.3 m length) Yagi antennas mounted in a radial configuration at 60-degree intervals (Fig. 5). At some sites, BOEM stations consisted of up to four Yagi antennas or a single omni-directional antenna attached to existing structures. At each station, the antenna(s) were connected to ports on a receiving unit (Lotek SRX-600 or Lotek SRX-800, Lotek Wireless, Ontario, Canada) via coaxial cable (TWS-200). The receivers were programmed to automatically log several types of data including: tag ID number, date, time stamp, antenna (defined by monitoring station and bearing), and signal strength (approximately linear scale: 1 to 255). Each receiving station was operated 24 hours per day using one 140-watt solar panel and two 12-volt deep-cycle batteries.

Offshore detection range of each BOEM station varied with the height of the station above sea level (asl) and with altitude of the transmitting bird. The maximum estimated detection range of stations 12.2 m asl was approximately 20 km for birds flying at 25 m asl (lower limit of RSZ of offshore wind turbines) and approximately 40 km for birds flying at 250 m asl (upper limit of RSZ of offshore wind turbines). Birds flying at migratory altitudes (1,000 m asl) may be detected at ranges exceeding 80 km (Loring et al. 2019).

In 2014, we operated an array of eleven land-based BOEM stations at sites along the US Atlantic Coast, ranging from Cape Cod, MA to Long Island, NY. In 2015, we expanded the array to include five additional land-based telemetry stations in Massachusetts, Rhode Island, and New York. During 2016, we added 14 additional BOEM stations at high-priority sites ranging from Cape Cod, MA to Back Bay, VA. The expanded array of 30 land-based telemetry stations remained in operation through the fall of 2017. To date (October 2019), the majority of the BOEM stations are still in operation to support the Motus network. A detailed description of the locations, specifications, and operational dates of each receiving station appears in Appendix B.

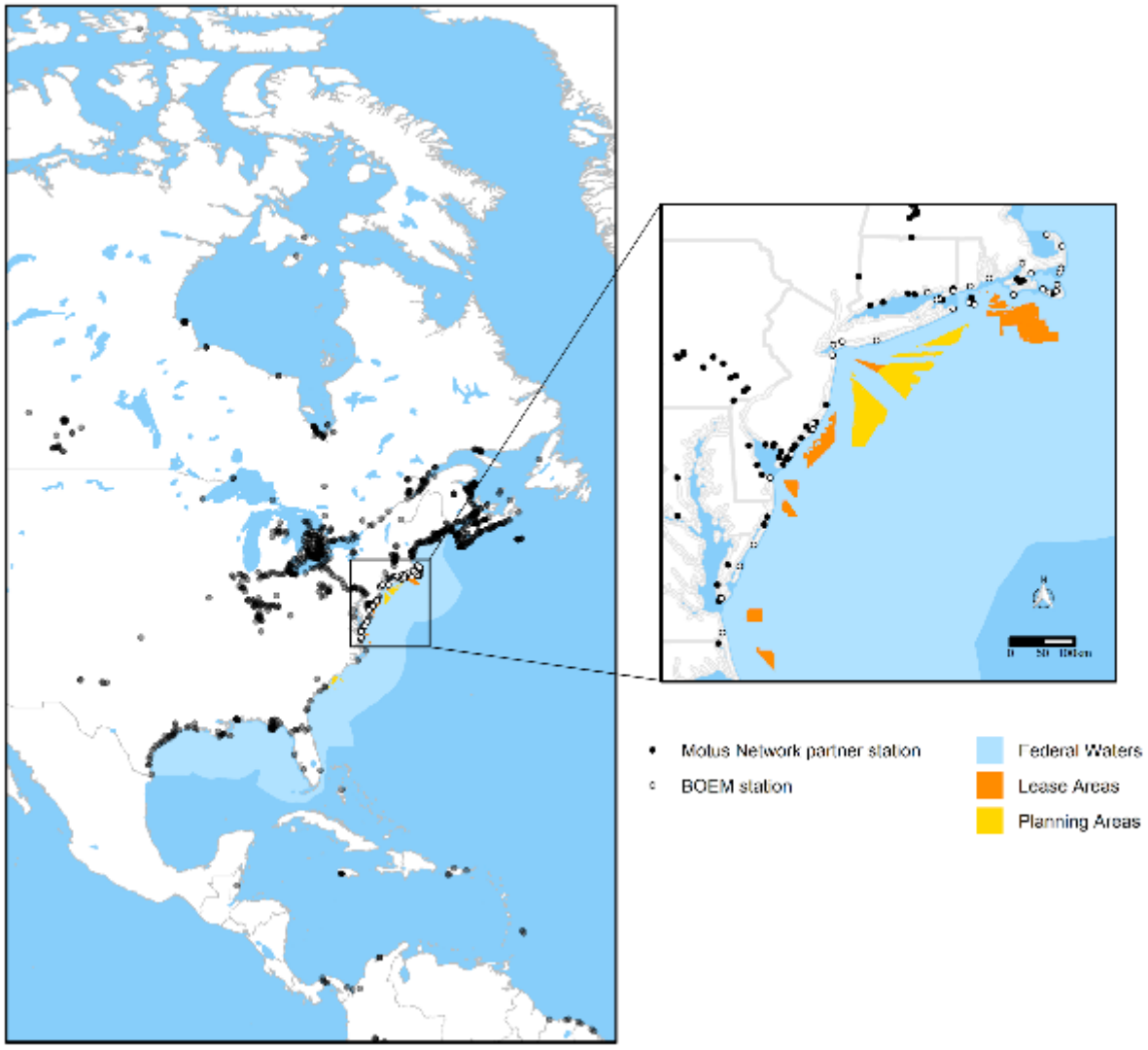

Figure 4. Map of automated radio telemetry stations operated during 2014 to 2017.
Left panel shows the larger Motus network, right panel shows the Study Area in the US Atlantic region. Black and white points show locations of telemetry stations operated for at least one year between 2014 and 2017. Federal waters of the U.S Atlantic are delineated by the light blue polygon (3 to 200 nautical miles). Within this boundary, all current (Feb 2019) BOEM Wind Energy Lease Areas and Wind Planning Areas are shown as orange and yellow polygons, respectively.

Figure 5. Automated radio telemetry station on Nantucket NWR (Great Point), Nantucket, MA. Station consisted of a radial Yagi antenna array atop a guyed, 12.2 m mast with a solar powered automated receiving unit at the base (photo: Matt Malin).

2.6 Post-processing of Telemetry Data

Detection data were downloaded from the Motus database and post-processed to remove false detections (Taylor et al. 2017). During post-processing, we removed any detections that fell outside the deployment period for each tag and any detections that occurred in spring the year after a tag was deployed because we expected tags to fall off during winter molting.

2.6.1 Dataset Used to Quantify Use of the Study Area Relative to the Broader Atlantic Coast

To obtain an estimate of the proportion of birds that used the Study Area relative to the broader Atlantic coast, we filtered the data from all tagged birds to include only birds that were detected at least 50 km away from where they were tagged and by at least one receiver station located within 30 km of the Atlantic coast (between Mingan QC, Canada and the Texas-Mexico border). We did this to minimize the influence of birds that lost tags or died before reaching the Atlantic coast, and to address issues with

detection probability across Motus Network, where most of the tracking stations are concentrated in the eastern U.S.

Any tags with ambiguous detections were removed from the dataset. We also removed detections with a standard deviation in transmitting frequency > 0.1 kHz. For this dataset we filtered data from all receivers using a consistent cutoff (minimum 7 consecutive bursts). We did this to avoid biasing detection probability towards BOEM stations which were all located within the Study Area. Detections from receiver stations that showed systematic issues (consistently high levels of false positives) during the post-processing of our dataset used to assess exposure to Federal waters within the Study Area (section 2.6.2) were also removed.

2.6.2 Dataset used to assess exposure to Federal Waters

To assess movements of birds within the Study Area and exposure to Federal Waters, we filtered the data from all tagged birds to include only birds with at least one detection by a BOEM station between February 1 and November 31. We excluded birds that were only detected by non-BOEM stations from the analysis to help address variation in detection probability among stations, as stations operated by other Motus projects and partners varied widely in configuration, maintenance, operation schedule, and availability of metadata. Additionally, we excluded detections that occurred between December 1 and January 31 because receiving stations in the Study Area were not maintained consistently during the winter leading to variable detection probabilities.

We removed 52 birds from the dataset that had ambiguous detections. Ambiguous detections occur when multiple tags with the same properties (ID code, burst interval) are active in the Motus network at the same time and cannot be distinguished from each other. We then filtered out detections with < 3 consecutive bursts and where the standard deviation in transmitting frequency was > 0.1 kHz (Mckinnon et al. 2019). Some receiving stations in the Motus network are prone to high rates of false positive detections (Loring et al. 2018; Anderson et al. 2019). We therefore used a stricter filter, removing detections with < 7 consecutive bursts, for detection data from the broader Motus network as well as one BOEM receiving station (JMBY) that was situated in a noisy urban location within New York, NY. Remaining false detections were identified by examining flight speeds between receiving stations and mapping flight paths. Flights were considered suspect if flight speed was > 42 m/s (Grönroos et al. 2012) or the flight path showed a large movement in a direction inconsistent with typical migration (e.g. a movement of 500 km north during southbound migration). We further examined the detections associated with these suspect flights for other indications that they were false (suspect detections occurring close in time with more reliable detections at a distant receiving station; short runs of consecutive bursts, no detections at nearby receiving stations). Through this process we found that some receiving stations were consistently associated with high rates of false positives during certain time periods and we therefore removed all detections at those stations during those periods.

2.7 Movement Models

In this study, we extended the modeling approach described in Loring et al. (2019) to estimate shorebird movements in the Atlantic OCS during spring and fall migration. The modeling approach in both studies

accounts for three-dimensional variation in signal strength, including multipath propagation, and estimates likely paths in continuous time, contingent on estimated behavioral states (e.g., on land vs. directed flight). The theoretical basis of the measurement model for received signal strength is described in Janaswamy et al. (2018), and both its extension to high-altitude flight and the state-based component are further described in McLaren et al. (*in prep*.). In brief, the current model accounts more fully for the vertical structure in signal strengths when compared with the Janaswamy et al. (2018) model (see Section 2.7.1) and applies constraints that are easier to derive from known flight characteristics of focal species. Importantly, our model can derive estimated locations and error bounds from detections at a single receiver station, whereas other radio telemetry location estimation techniques require detections from spatially separated receiving stations (Kays et al. 2011).

The model workflow proceeds in three steps, outlined in detail below and in Table 1. In the first two model steps (Fig. 6), we derived the most consistent estimated locations among plausible detections based on detection signal strength and behavior-based constraints. These constraints limited a bird's variation in horizontal and vertical speed during directed flight to within biologically relevant flight speeds and differentiated between local movements on or near land (at stopover areas) and directed non-stop flight (regional or migratory movements).

The localization components of the model (Steps 1 and 2) used here were a revised version of that used in Loring et al (2019), updated in several aspects:

(1) To focus on resolving directed flights into Federal Waters, we now allow for broader time-windows to maximize the chance of estimating locations from multiple antennas. Broader windows can enhance location accuracy by adding more information but reduce temporal resolution due to the bird's movement (see Section 2.7.2).

(2) In cases of long-range detections (>25 km), we constrained the model to specify high-altitude flight with minimum altitudes of 500 m. Detection ranges at lower altitudes are typically less than 20 km (see Taylor et al 2017). Long-range detections were identified through close-in-time detections at receivers separated by >50 km (see Section 2.7.4).

(3) To improve the likelihood of localization along receiver main beams and favor more frequent detections, we weighted the observations according to both the relative detection probability of a given bird to receiver bearing and the number of detections, detecting beams and receivers within the multi-antenna time window (see Section 2.7.2).

Because detections typically occurred at irregular intervals, the third model step (Section 2.7.6) interpolated the estimated locations to one-minute time intervals using a Brownian Bridge movement model (Horne et al. 2007).

Table 1. Workflow of localization estimation

Step	Action	Section	Method
1.0	Determine periods of non-stop flight	2.7.4	Based on thresholds for inter-station distance (default minimum, 15 km) and species-appropriate inferred flight speed[1]
1.1	Determine locations with multi-antenna detection sequences	2.7.2	Based on consistency of signal strength for each location and detecting beam within appropriate flight altitude bounds given species and flight mode
1.2	Update periods of non-stop flight	2.7.4	Based on locations from Step 1.1 in accordance with behavioral-based constraints (see Table 4)
1.3	Update locations within non-stop flight periods	2.7.5	Constrained by species-appropriate flight speed and minimizing discrepancy in location estimates and in accelerations (see Table 2)
2.0	Update periods of non-stop flight	2.7.4	Based on locations from Step 1.3 in accordance with behavioral-based constraints (see Table 4)
2.1	Determine locations from single-station detection sequences	2.7.3	Straight-line sequence within horizontal and vertical speed constraints (see Table 2)
2.2	Update periods of non-stop flight	2.7.4	Based on locations from Step 2.1 in accordance with behavioral-based constraints (see Table 4)
2.3	Update location estimates within non-stop flight periods	2.7.5	Constrained by species-appropriate flight speed and minimizing discrepancy in location estimates and in accelerations (see Table 2)
3	Interpolate to one-minute time step	2.7.6	Brownian Bridge model based on standard deviation in horizontal position, linear interpolation in vertical position

[1] See also Table 3 for minimum and range of horizontal speeds per species

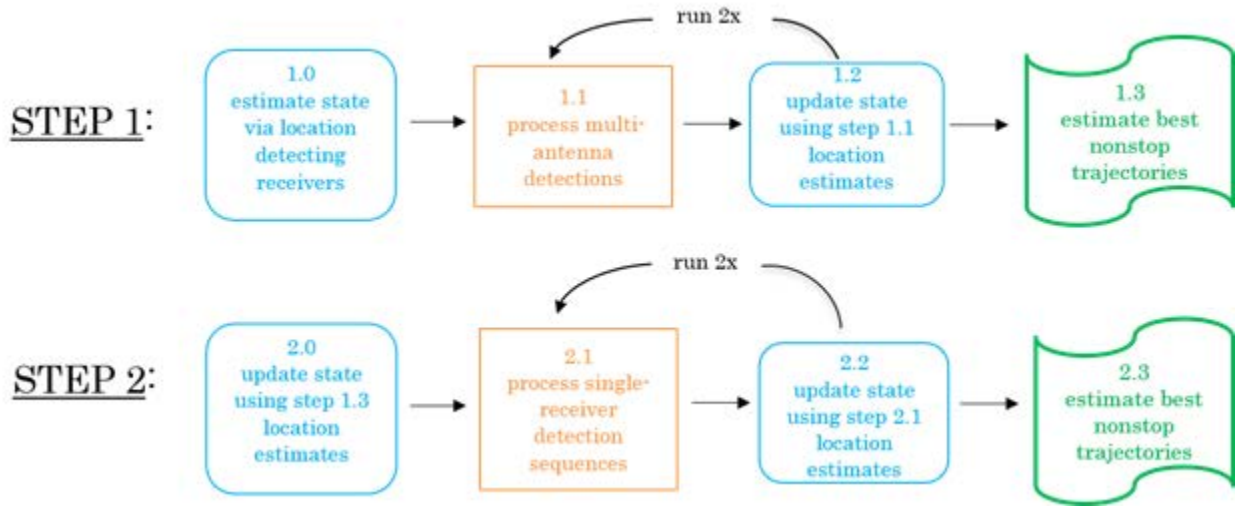

Figure 6. Schematic of the model flow for the first two model steps.

2.7.1 Formulation

For directional receiving antennas, such as the Yagi antennas deployed in this study, received signal strength (in dBm, normalized to a gain factor specific to the transmitter and receiver) varies with the two-dimensional and three-dimensional ranges (i.e., distance to receiver; *r* and *R*, respectively), radial angle ψ between receiver and transmitter, the height z of the transmitter (i.e., flight altitude of the bird), and height *H* of the receiving antennas. To account for altitude effects as well as ground-reflected signals (multipath), Janaswamy et al. (2018) incorporated the two-beam model and applied this model to the known radiation pattern of Yagi antennas. In this multipath formulation, the received signal is predicted to vary sinusoidally with flight altitude *z*, at least as long as the horizontal range *r* exceeds the vertical height *z* (Equation 1).

Equation 1:

$$\xi^2 = \xi^2(r, \psi|H) = g^2(\psi)\sin^2(k_0 H \cdot z/r)\,/(k_0 r)^2$$

Here g(ψ) governs the shape of the directional beam and k_0 (m^{-1}) represents the wavenumber in free-space (Janaswamy 2001). The sinusoidal dependence of flight altitude *z* on signal strength in Equation 1 illustrates how significant signal gain with height is possible, resulting in possible long-range (>50 km) detection of high-flying birds, and adding to the complexity of distinguishing flight altitudes based on signal strength.

For horizontal ranges much larger than the vertical range ($r>>z$), Equation 1 can be simplified and inverted to determine the transmitter (bird) height (*z*) above the ground as a function of horizontal range, *r*:

Equation 2:

$$z = z(r, \psi | \xi, H) = \frac{r}{k_0 H} \sin^{-1}\left(k_0 r \cdot \frac{\xi}{g(\psi)}\right)$$

This formulation (McLaren et al. *in prep.*) allows for efficient calculation and assessment of plausible locations in three dimensions while retaining the vertical structure of Equation (1).

2.7.2 Multi-antenna Detection Events

In the first model step, we derived estimated locations, and uncertainty in location, for all detections from separate receiving stations or separate antennas at a single receiving station within a time window of 180-900 seconds (hereafter, multi-antenna detection events). Broader time windows facilitated more accurate localization of directed flight and were later (Step 3) sub-interpolated to one-minute time windows to ensure that exposure to the Federal waters could be adequately assessed. Event time windows were initially set to a minimum time period between 180-300 seconds, and for high-altitude flight (above 500 m, see Section 2.7.4), between 300-600 seconds. These windows were then extended up to 900 seconds to include a single additional receiving station if the additional receiving station did not preclude the next sequence of detections from being classified as a multi-antenna detection event. For high-altitude non-stop flights (see Section 2.7.4), at least 3 receiving stations were included within 900 second windows.

To account for measurement and model errors, we used Equation 2 to evaluate the degree of correspondence among all received signals within the time window, considering all plausible horizontal ranges r and axial angles ψ. For each detection within the time window, we searched through 2,880 candidate horizontal locations (radial distances between 100 m and 50 km, and every 0.5°) to determine the consistency of each location given the other detections. For each within-window detected signal and candidate horizontal location (and corresponding vertical location, via Equation 2), the mean discrepancy in signal strength from all other detections was calculated (based on what their signal strength would be at the candidate location using Equation 1). Estimated locations that fell outside of the possible bounds on vertical location were excluded. Among the remaining locations (typically 500-100 candidate locations for each detection), we then chose the median location among those having the lowest 10% discrepancy in signal strength. This was repeated for each within-window detection event, and the discrepancy-mean of these best location estimates was chosen as the best overall ('mean') estimated location within the time window. Selecting the most representative value in the 10% most probable set of points was found to improve both model validation (Section 2.7.7) and the smoothness of non-stop flight trajectories, especially once these were constrained to within realistic flight speed bounds (see 2.7.4). Location means were also weighted by the relative probability of a given bearing (relative to the antenna's main beam) estimated from validation data using nonlinear least-squares (Section 2.7.7).

To assess exposure to Federal waters, uncertainty around this 'mean' location was quantified by the weighted standard error among the detection-specific 'best' detections, and the upper and lower quartile in vertical height. To ensure smoother optimization of trajectories at the end of each step (Section 2.7.4), we retained a broader altitudinal range (5% and 95% quantiles) in two cases: i) for high-altitude flight and ii) on initial detection of non-stop flight remote from capture sites (which often preceded high-altitude flight

over the Study Area). Dynamic flight constraints (Section 2.7.5) in both the horizontal and vertical planes were imposed using the 5-95% confidence intervals.

Table 2. Default state-dependent model constraints[1]

Behavioral state	Initial state classification via receiver locations[2]	Subsequent (iterative) classification	Duration first-step time window (s)	Second step time window (min)	Altitude range[3] (m)
Stopover movement	> 60 minutes below minimum horizontal speed	As below (i.e. not classified as a non-stop flight)	180-300, (to 600 if involves new station)	< 3 consecutive detections within 20 min	1-50
Non-stop flight	>30 minutes, ≥ 15 km travelled and within speed range	>30 minutes and overall speed within speed range	as above	≥ 3 consecutive detections within 20 min	100-3000
High-altitude non-stop flight	Detection distance ≥ 50 km and speed implying detection distance ≥ 25 km	Unchanged	300-600 (to 900 if involves new station)	As per above but within 30 min	500-6000
Final non-stop flight	Per state as above	Per state as above	N/A	As per above	Per state as above

[1] See also Table 3 for minimum and range of horizontal speeds per species

[2] Initial horizontal and speeds are set during the second step via neighboring estimates from the 1st step (using multi-antenna detection events), or when none exist, via location estimates from a static measurement model and detecting antenna beams.

[3] Altitude bounds were taken from the literature (e.g., Nisbet 1963, Richardson 1976, 1978, Williams & Williams 1990)

2.7.3 Single-receiver Detection Events

For detections not belonging to multi-antenna events, locations were estimated from sequences of single-antenna detections following one of two procedures: (1) numerical estimation of straight-line trajectories from a sequence of single-antenna detections or (2) estimation of the most likely location of a sequence of detections from a single-receiver (including multi-antenna sequences) based on received signal strengths and flight constraints. Specifically, (1) when three or more consecutive detections from (only) a single antenna ‘beam’ occurred within a span of 20 minutes (or 30 minutes for high-altitude non-stop flight), a straight-line trajectory was fit among candidate locations to minimize the discrepancy in signal strength

(log-transformed ξ squared) within the species-specific bounds for horizontal speed (see Section 2.7.5) using MATLAB routine 'fmincon' (see Section 2.7.4). An initial trajectory was used in the optimization procedure according to a linearized version of Equation 2 (or, equivalently, assuming, $z << r$). Additionally, among these 'sequential' single-beam detections, a constant vertical (climb speed) also was fit whenever initiation of non-stop flight was inferred (see Section 2.7.4) or if such a sequence occurred as final detections (the final 20 minutes). As with multiple-antenna detection events, location means were weighted by the relative probability of candidate bearings relative to the antenna's main beam.

Horizontal uncertainty was quantified for single-receiver detection events by an interpolation of the horizontal uncertainty between the closest simultaneous detections or of the closest simultaneous detection if only one occurred. Alternatively, (2) when fewer than three consecutive single-receiver detections occurred within 20 minutes, birds were presumed to be located along the main-beam (within 30 degrees of the main axis) and on the same side of the beam as the horizontally interpolated location from previous or following multi-antenna detection. As with multi-antenna location estimation, 2,880 candidate horizontal locations were tested for consistency with measured signal strength, the visible horizon and vertical bounds, and proximity to the interpolated location between any previous or subsequent location estimates derived from multi-antenna detections.

2.7.4 Determination of Non-stop and High-altitude Flight

Refining the movement trajectories of directed movements by birds through time and space required differentiation between stopover behavior and non-stop flight (Kranstauber et al. 2012; Jonsen 2016). The reasons for identifying non-stop flight events is two-fold: (1) previous or subsequent location and speed estimates should be used to facilitate estimation of current locations only if they are consistent with non-stop flight, and (2) using biologically reasonable bounds in altitude greatly improved model performance, given the potentially large range in flight altitudes and associated horizontal locations for any given signal strength (analogously to Poessel et al. 2018, Peron et al. 2019). Modeled flight altitudes were bounded during non-stop flight by 100-3,000 m and during high-altitude non-stop flight by 500-6,000 m (see Richardson 1974, Williams and Williams 1990). During flight stopover or staging periods, a minimum of 1 m and a maximum of 50 m was assumed (Dirksen et al. 2000, Langston and Pullan 2003). High-altitude non-stop flights were identified by close-in-time detections between receivers 50 or more km apart, such that the bird must have been more than 25 km away from one of the receivers (Section 2.8). Detection distances exceeding 25 km were identified by demonstrating that, if birds were midway between the two towers, flight speeds would exceed that maximum allowable for the species in question (Table 3). Classifying these cases as high-altitude (involving higher altitude bounds; see Table 2) helped resolve realistic trajectories for multiple cases of non-stop ocean-bound flights (which were typically to the S-SE, with no subsequent detections in the region).

Non-stop flight periods were determined iteratively in the model (Table 2), beginning by deriving proxy flight speeds based on inter-tower distances and the timing of subsequent detections. To reduce the risk of misidentifying simultaneous detection during stopover as non-stop flight, initial classification of non-stop flight during the first model step was restricted to detection events involving receivers separated by at least 15 km. Non-stop flight involved speed estimates within a biologically plausible range (Table 3), broadened to account for variability in proximity to detecting receivers, wind effects, and measurement imprecision. Non-stop flight periods were subsequently updated and refined using the improved location

estimates derived for multiple-antenna detections (step one) and single-receiver detections (step two). To prevent misclassification of brief stopovers between two non-stop flight bouts, any interim period implying less than 4 m/s for longer than two hours was considered a stopover as opposed to non-stop flight.

Within any (estimated) non-stop flight periods, biologically relevant non-stop flight paths were estimated separately for horizontal and vertical trajectories, as outlined below. This was performed using MATLAB's 'fmincon' routine using output from steps 1.1 and 2.1 for initial estimates and bounds on locations (McLaren et al. *in prep*.).

Horizontal trajectories were estimated by minimizing a weighted squared sum of (i) the Euclidian distance from the best within-event estimates and (ii) a measure of horizontal acceleration (Equation 3).

Equation 3:

$$A_h = f_s\left(\left(\frac{du_i}{dt_i}\right)^2 + \left(\frac{dv_i}{dt_i}\right)^2\right) + (1 - f_s)\left(\frac{ds_i}{dt_i}\right)^2$$

where the weights were the product of the number of within-event detections, detecting antennas and detecting receivers (scaled by exponents to favour multiple receiver events) represents the relative weight of discrepancy from within-event estimates (default 0.5). Horizontal acceleration was calculated as a weighted combination of the Eastward and Northward acceleration components and total horizontal acceleration (Equation 4) with f_s (default 0.5) representing the relative straightness in horizontal flight speed.

Equation 4:

$$\frac{ds_i}{dt_i} = \frac{d\left(\sqrt{{u_i}^2 + {v_i}^2}\right)}{dt_i}$$

The term $\alpha = 1/\text{median}\left(\frac{dS^2}{dt^2}\right)$ is a scaling factor to compare distance and acceleration measures.

Table 3. Ground speed ranges per species

Species	Ground speed[1] (m/s)	Minimal ground speed (m/s)	Maximal ground speed (m/s)	Minimal ground speed high altitude flight (m/s)	Maximal ground speed high altitude flight (m/s)
Black-bellied Plover, Red Knot, Semipalmated Plover, White-rumped Sandpiper, Whimbrel	20.00	10.00	30.00	12.00	35.00
Ruddy Turnstone	17.50	8.75	26.25	10.5	30.63
Lesser Yellowlegs, Dunlin, Pectoral Sandpiper, Semipalmated Sandpiper	15.00	7.50	22.50	9.00	26.25
Sanderling, Least Sandpiper	12.50	6.25	18.75	7.50	21.88

[1] Typical ground speeds were based on airspeeds listed in Alerstam et al 2007, matching species exactly, or for the species closest in morphology (size, wing-pointedness). Broad ranges were allowed to account for wind effects and model and measurement uncertainties.

2.7.5 Behavioral Flight Constraints

Location estimates during non-stop flight sequences were further refined, based on known characteristics of flight for each species, to ensure that flight trajectories were feasible, smooth and behaviorally consistent. Specifically, following initial location estimation of both multi-antenna and single-receiver detections, location estimates were adjusted, within the 5% and 95% bounds of the candidate locations, to ensure that: (i) vertical speeds (estimated changes in flight altitude between detections) were less than 1.5 m/s in magnitude (Hedenström and Alerstam 1994), (ii) horizontal speeds remained within bounds, while accounting for straightness of flight paths, wind conditions, and proximity to towers, and (iii) the total horizontal and vertical acceleration were minimized given constraints (i) and (ii). See Table 4 for parameter ranges used for each flight classification (i.e., non-stop, high-altitude, or final detected non-stop flight event). The uncertainty in each dimension was retained according to the standard deviations in the x and y components and both the interquartile range and the 5% to 95% quantiles in the vertical dimension among all candidate vertical locations.

Table 4. Default model options and optimization of non-stop flight periods (Steps 1.2, 2.2)

Setting	Initial estimate vertical speed (2nd step)[1]	Vertical speed range[1] (m/s)	Weight relative accuracy horizontal localization vs. straightness[2]	Weight relative accuracy vertical localization vs. acceleration[2]	Weight relative straightness vs. steadiness horizontal flight[2]	Max turning angle between detection events[3]
Non-stop flight	1.0 (0.5) m/s during first (subsequent) sequences	-1.5 - 1.5 m/s (-0.5 - 0.5) during first (subsequent) non-stop sequences	0.50	0.50	0.50	60°
Non-stop high-altitude flight	0.25 (0) m/s during first (subsequent) sequences	-1.5 - 1.5 m/s (-0.5 - 0.5) during first (subsequent) non-stop sequences	0.50	0.50	0.75	30°
Final non-stop flight period	0.5 (0.25) m/s during first (subsequent) sequences	0 - 1.5 m/s (-0.5 - 0.5) during first (subsequent) non-stop sequences	0.50	0.50	As per above	As per above

[1] Initial vertical speeds are zero unless otherwise stated; outside non-stop periods, altitudes are constrained by maximal descend and climb speeds (default -1.5 - 1.5 m/s; after Alerstam and Hedenström 1994)

[2] These quantities are scaled by median spatial and time scales to be comparable; see Section 2.7.4

[3] Horizontal angle between and among multi-antenna location estimates and single-receiver straight-line segments

2.7.6 Temporal Interpolation Using Brownian Bridge Movement Model

We spatiotemporally interpolated the irregular location estimates into one-minute time steps using a Brownian Bridge model (Horne et al. 2007). Modelled spatial locations were interpolated in three dimensions between all multi-antenna and single-receiver detections. Uncertainty of one-minute horizontal location estimates was quantified as the root-mean square of estimated variance in location from detections and time gaps between detections (via a maximum horizontal flight speed as listed in Table 3). Vertical uncertainty in one-minute time steps was linearly interpolated between all multi-antenna and single location estimates.

2.7.7 Calibration and Validation

Since Equation 1 is dependent on the transmitter and receiver properties, signal strength of the SRX-600 receiver (on a scale of 0-255) was calibrated using data from known locations:

$$\tanh^{-1}\left(\frac{Z}{255-Z}\right) = b \cdot \ln\left(\frac{\xi^2}{P_0} + 1\right)$$

where Z represents the SRX-600 receiver signal (1-255), *b* represents a rate of signal saturation and p_0 is a noise threshold (see Bai 2016 and Janaswamy et al. 2018).

To estimate these two coefficients, two 1.0 g nanotags were attached to a kite that was flown from the back of a motorboat. The motorboat was driven in transects within range of two land-based 12.2 m automated radio telemetry stations, each supporting six, 9-element Yagi antennas mounted in a radial configuration with main beams separated by 60°. The two stations were located 6.7 km apart on Monomoy NWR in Massachusetts.

The first (calibration) dataset comprised detections from flying the kite along main beams of the two automated radio telemetry stations. We flew the kite at two heights, 30 and 60 m above sea level (asl), to optimize our calibration estimates within rotor height, within the limitations of Federal Avian Administration regulations. We aligned the transmitting antennas of two nanotags horizontally and vertically (i.e. parallel and perpendicular to the water surface, respectively). This resulted in horizontal detection ranges from two automated radio telemetry stations up to 10 km (maximum distance of transect length) and, between the six antennas on each, all possible bearings between the transmitter and receiver. All detections were pooled and the data calibrated by fitting the coefficients p_0 and b in Equation 3 using non-least squares based on GPS location of the boat, the measured signal strength Z, and predicted signal strength (Equation 2).

Then, to validate the location model and coefficients, we used data from a second set of surveys where a nano-tagged kite flown at altitudes ranging from 10 to 30 m asl in a zig-zag pattern between the two automated radio telemetry stations on Monomoy NWR. This erratic pattern did not result in multi-antenna detections between towers (i.e. only between antennas from the same receiving tower) and therefore, could not be analyzed using traditional triangulation methods. To facilitate the kite's erratic movement, we used a shorter time window for fitting single-antenna sequences (5 minutes) and constrained modeled flight to altitudes within 10 to 40 m.

The median model error, i.e., horizontal distance between each known location of the nano-tagged kite and its corresponding model estimate, was 770 m (range 35 to 2,300 m; see Fig. 7). The model-estimated standard horizontal error (shown as colored polygon in Fig. 7) was considerably higher, with a median of 2,180 m (range 1,170 to 3,180 m). Therefore, in the model validation, 87% of model estimates fell within one standard error of the known locations and 99% within two standard errors.

Model-estimated altitudes are depicted in Fig. 7 (right panel), color-coded to time, with a median estimated kite altitude of 26 m (SD 2.5 m, range 23 to 33 m). During the survey, the altitude of the VHF-tagged kite was not accurately recorded because it varied with the wind, ranging between 20 and 30 m.

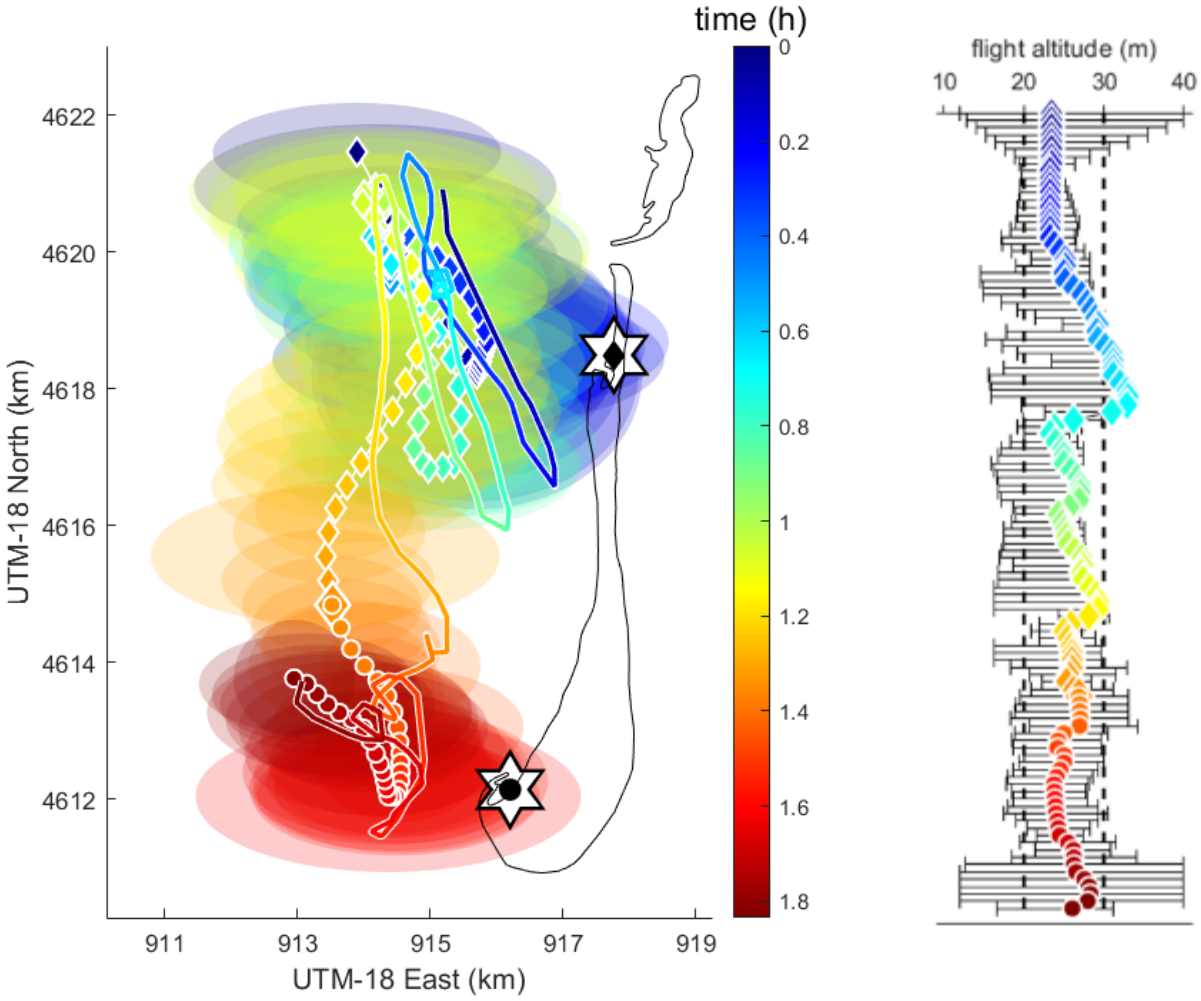

Figure 7. Results of model validation survey
Left panel: Model validation survey conducted during September 2014 adjacent to two BOEM automated radio telemetry stations (stars) on Monomoy NWR, MA, USA (land boundaries shown as black lines). Colored line shows GPS track of boat towing a kite with a nanotag attached to it flying at approximately 20 to 30 m above sea level (ASL). Colored symbols along the line show corresponding track estimated by the movement model, from detections at northern station (diamonds) and southern station (circles). Ellipses show model-estimated error (SD) corresponding to each location estimate. Right panel: Model-estimated altitudes (circles and diamonds) with color indicating time in hours, and bars representing standard error in altitude. Black dashes indicate the altitude range of kite during survey (20 to 30 m).

Most of the automated radio telemetry stations in the Study Area were BOEM stations equipped with SRX-600 receivers and gain set to 80. Additional global stations operated by partners in the Motus Network in the region (e.g. New Jersey, North Carolina) used Sensorgnome receivers (Taylor et al. 2017). Sensorgnome measurements are converted from received power to and reported in raw dBm units, which will vary with gain and other settings. To standardize Sensorgnome and SRX-600 signal strength data in order to make use of data collected from target birds at global stations, a gain of 80 was assumed and dBm units transformed to SRX-600 receiver Z units using a simple linear relationship (J. Brzustowski, personal communication):

$$Z = (40G_0 + 44 \cdot dBm + 4565)/11$$

2.8 Detection Probability of BOEM Automated Radio Telemetry Stations

To aid in interpretation of data collected by the telemetry array, we developed coverage maps to identify areas of low-to-high detection probability within the Study Area. First, we depicted the horizontal radiation pattern of a single antenna (Fig. 8), to illustrate the relationship between transmitter altitude and detection range of automated radio telemetry towers. There are two relationships to note here: 1) signal strength is inversely related to horizontal range *r*, i.e. a bird flying closer to an antenna at a given radial angle (ψ) will have a relatively stronger signal, and 2) as long as the flight altitude is less than the horizontal range (i.e., $z < r$), signal strength and altitude are positively related (i.e., the higher a bird, the stronger the received signal strength). This means that high flying birds can be detected at greater distances from receivers than low flying birds, due to both the increased signal strength propagation, as well as the farther detection horizon (given the curvature of the earth).

Second, we estimated the detection probability from a single receiving station as a function of radial angle using data from calibration surveys (Section 2.77). The receiving station had six antennas monitored sequentially with a 6.5 second dwell time per antenna, with a total scan time of 40 seconds. The detection rate per antenna within a 40 second total scan time was calculated by averaging the calibration data within each 40 second time window and calculating the range and bearing to each of the two receiving towers. Figure 9 depicts this within-cycle detection rate as a function of bearing to the receiver (solid line) and the angle of transmitter to receiver (dot-dashed line). Across the calibration surveys, the overall detection rate was approximately p = 0.5 (and highest along the main beam axis) and varied less strongly with the angle of transmitter to receiver.

Third, we calculated the detection probability of a single tower based on the radiation pattern and overall detection probability, as estimated from the calibration surveys described in Section 2.77. Fourth, we calculated each tower's probability of detecting a tagged target, given the target's altitude and signal strength value of corresponding detection. We used data from the calibration surveys to determine an overall detection rate of p = 0.5 (given target height = 30 m), where p = the proportion of test-tag locations that were detected by the towers. Across the calibration surveys, the overall detection rate was highest along the main beam axis, i.e., bearing close to zero degrees, and varied marginally with the angle

of transmitter to receiver. Next, we calculated the probability of detection by all antennas on a single tower. This probability varied depending on the location of the target within the radiation pattern, because side lobes from one antenna overlapped with the main beam and side lobes from other antennas. The probability of detection at any point in the radiation pattern = P, where P = 1 – (1-p)n, and n = the number of overlapping beams at that location (i.e. 6 beams for a six-antenna tower).

Lastly, we mapped the overlapping detection probabilities of the BOEM stations by year, given the target's altitude relative to upper and lower limit of the RSZ (25 m and 250 m, Figs. 10 to 12). We assumed the same detection rate, p = 0.5, across all heights. Towers from the global Motus network that detected our tagged birds provide extended coverage, which is not depicted here, due to variability in tower detections set up using different configurations. At higher flight altitudes, tower coverage overlaps due to increased detection range; in these cases, we display the maximum detection probability. Such overlapping ranges indicate where one target is likely to be detected simultaneously by multiple towers. Simultaneous detections provide more accurate estimates of altitude and spatial coordinates than what can be estimated from single detections. This information can help to provide guidelines for further research, based on the average flight height and distribution of focal species. Future studies should aim to maximize the number of overlapping tower ranges, to improve the altitude and location accuracy of their target estimates, given greater potential for simultaneous detections.

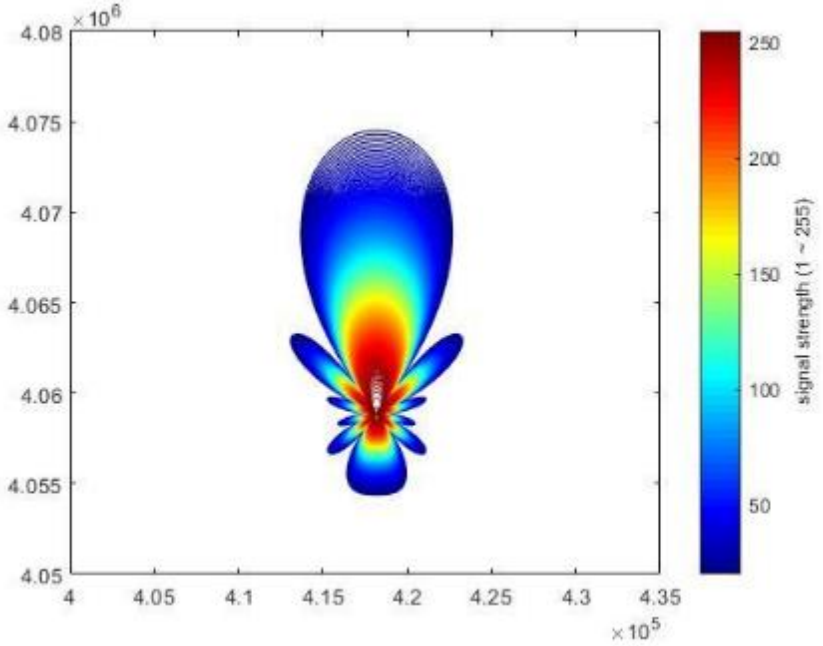

Figure 8. Two-dimensional radiation pattern of 9-element Yagi antenna.
Example main beam (pointed upwards) and side lobes (e.g., from backscatter) associated with a tower antenna, given a target's range of signal strengths (1-255, scale bar), height (100 m), and map resolution (100 m). Each line represents a signal strength, where the outermost value = 1 and the innermost value = 255. The heat map scaling indicates a higher density of signal strengths closer to the tower, where a bird is most likely to be detected at high signal strength values.

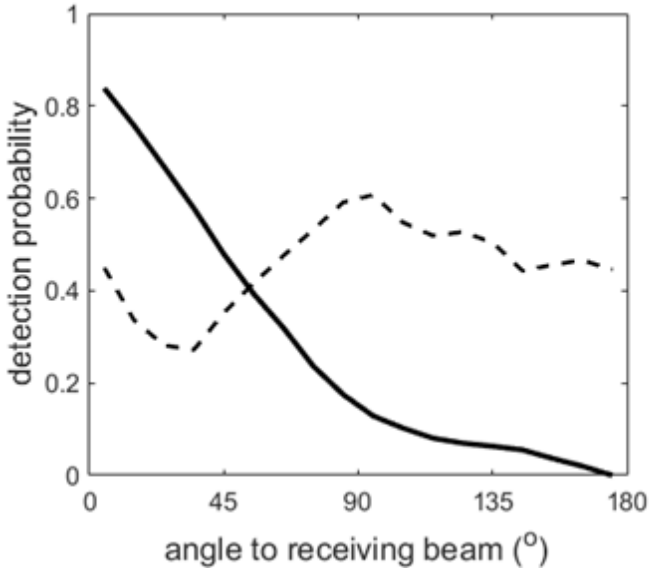

Figure 9. Detection probability of kite in relation to receiver location and transmitter alignment
Detection probability was calculated as proportion of received signals within each 40 second duty cycle, based on the kite's GPS location and the angles of kite to the main axis of the receiver antenna (solid line) and the angle of the transmitter antenna to the main receiver axis (dot-dashed line). Across the calibration surveys, the overall detection rate was approximately 0.5, highest for bearings along the main axis of receiving antennas (77% of detection events occurred from directions within 35° of the main axis), but varied less strongly with the angle of transmitter to receiver.

A.

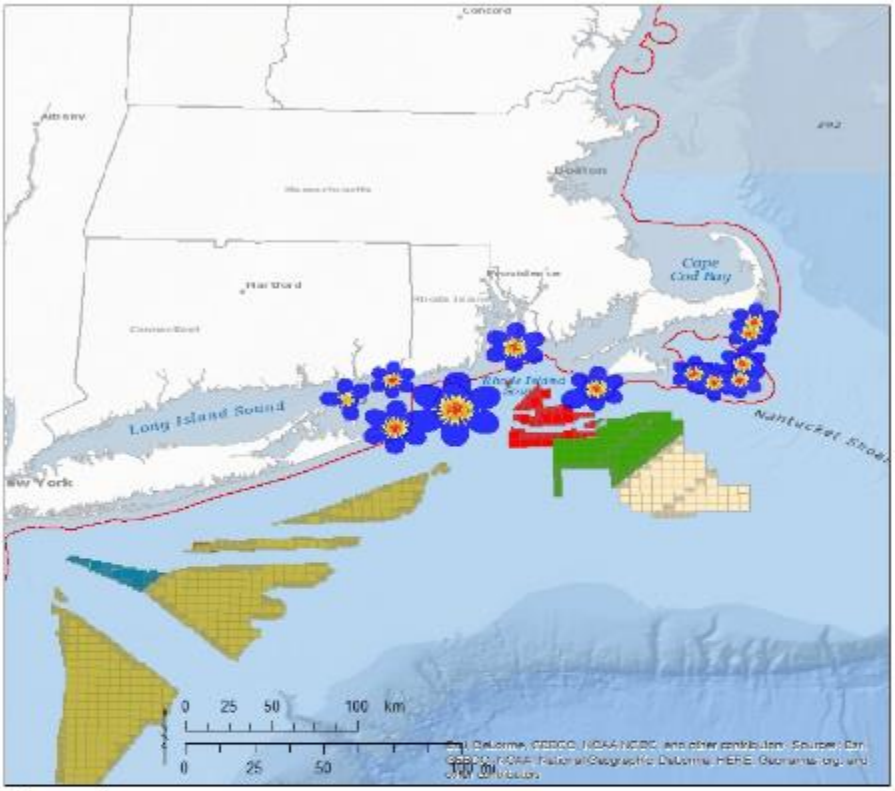

Legend

BOEM Wind Lease Areas

- RI/MA OCS-A 0486 and 0487
- MA OCS-A 0500 and 501
- NY OCS-A 0512
- NJ OCS-A 0498 and 0499
- DE OCS-A 0482 and 0519
- MD OCS-A 0490
- VA OCS-A 0483 and 0497

U.S. Federal Waters

- 3 nautical mile boundary

BOEM Wind Planning Areas

- Massachusetts PSN
- New York Bight Call Area
- New York Proposed Commercial Lease

Detection probability (flight altitude 25 m)

- < 0.5
- 0.5 - 0.6
- 0.6 - 0.7
- 0.7 - 0.8
- 0.8 - 0.9
- 0.9 - 1

B.

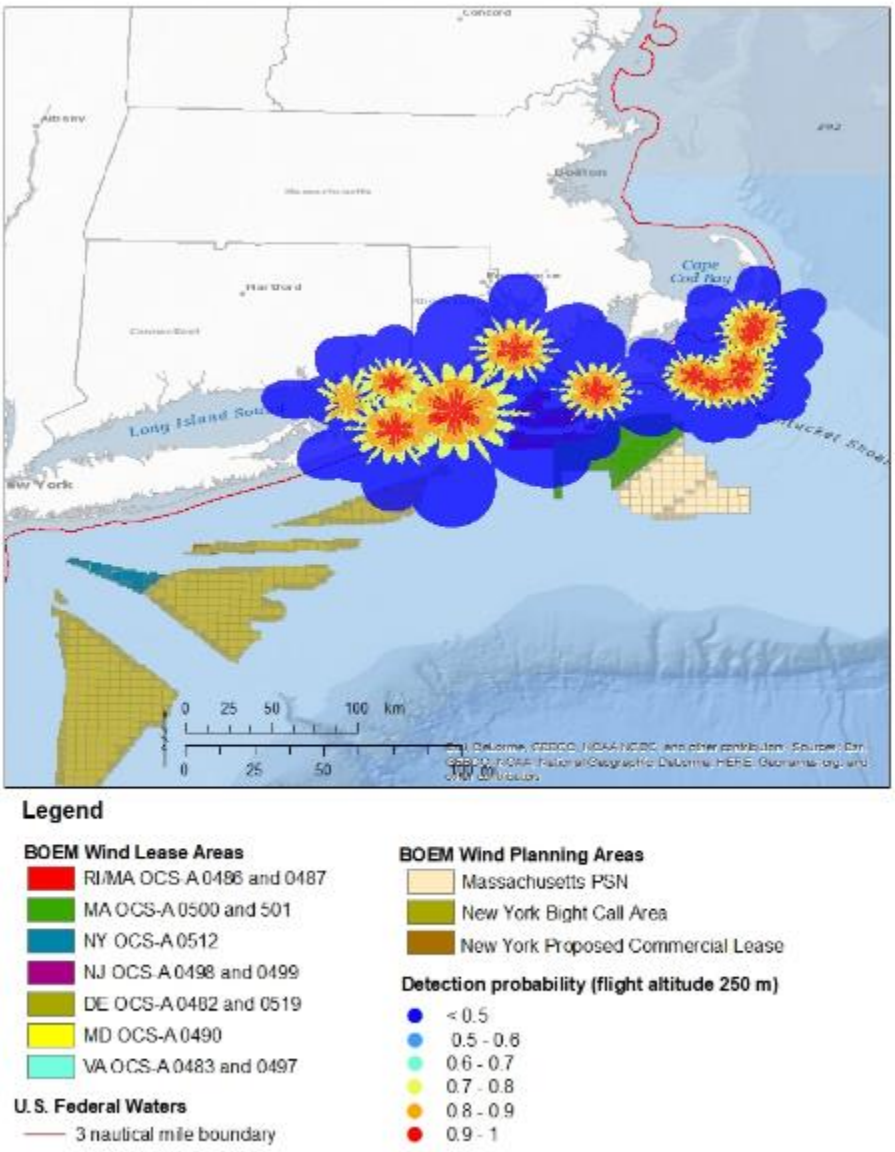

Figure 10. Coverage map from 2014 BOEM-funded tracking towers showing the probability of detecting a bird flying at (A) 25 m, and (B) 250 m

Coverage assumes signal strength value = 5. Higher signal strengths would be likely to show a similar probability distribution, but with contracted coverage consistent with Fig. 8. Overlapping tower ranges indicate the capacity for simultaneous detections to provide more accurate estimates of the target's altitude and spatial coordinates than what can be estimated from the single detections

A.

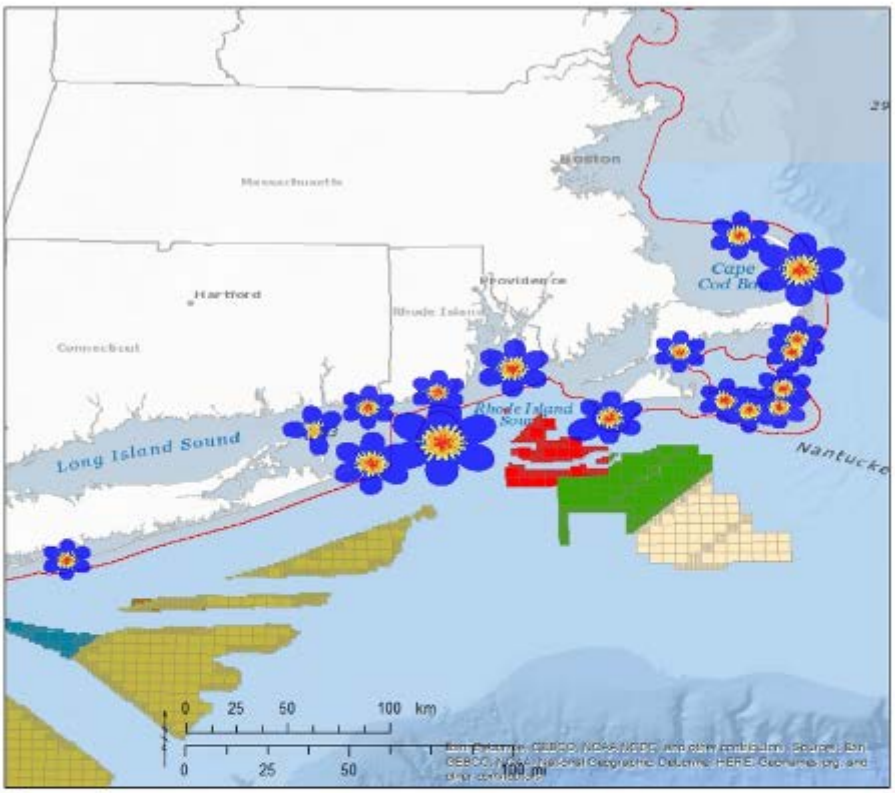

Legend

BOEM Wind Lease Areas
- RI/MA OCS-A 0486 and 0487
- MA OCS-A 0500 and 501
- NY OCS-A 0512
- NJ OCS-A 0498 and 0499
- DE OCS-A 0482 and 0519
- MD OCS-A 0490
- VA OCS-A 0483 and 0497

U.S. Federal Waters
- 3 nautical mile boundary

BOEM Wind Planning Areas
- Massachusetts PSN
- New York Bight Call Area
- New York Proposed Commercial Lease

Detection probability (flight altitude 25 m)
- < 0.5
- 0.5 - 0.6
- 0.6 - 0.7
- 0.7 - 0.8
- 0.8 - 0.9
- 0.9 - 1

B.

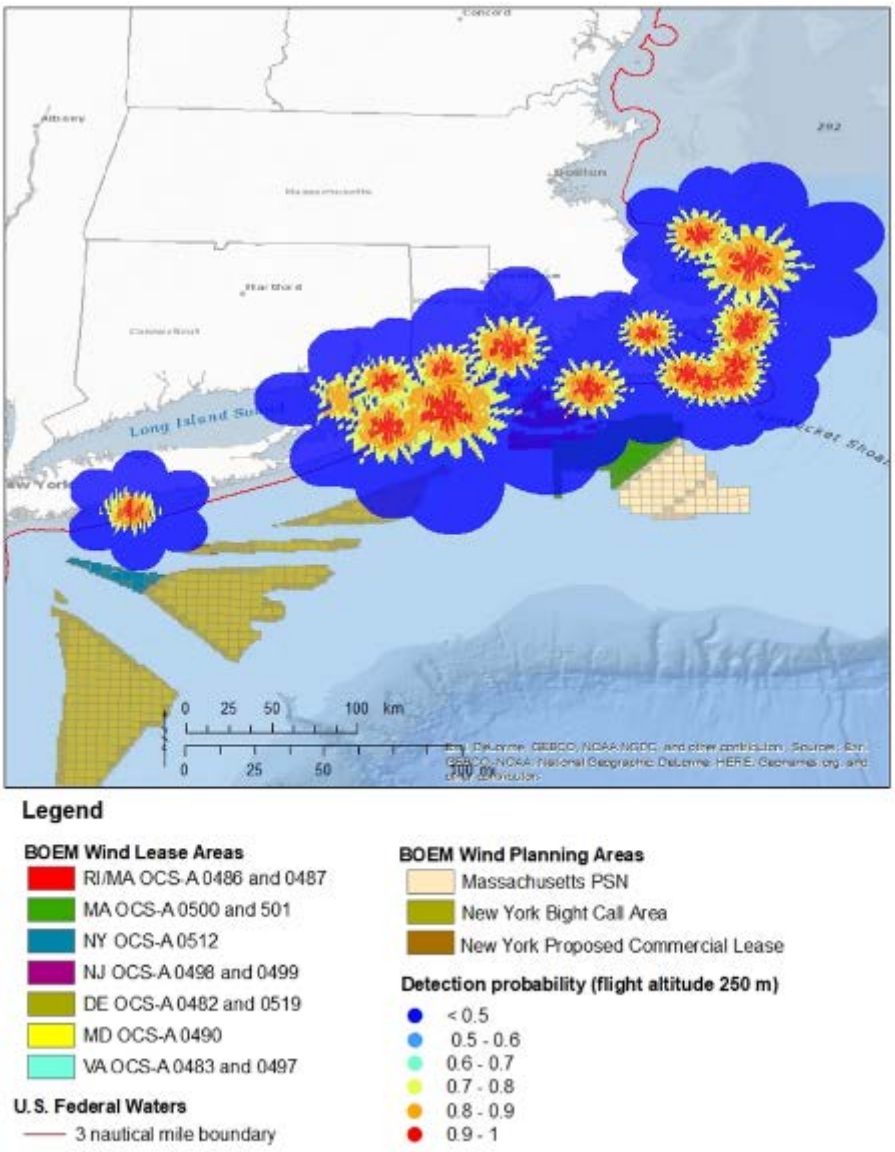

Figure 11. Coverage map from 2015 BOEM-funded tracking towers showing the probability of detecting a bird flying at (A) 25 m, and (B) 250 m.

Coverage assumes signal strength value = 5. Higher signal strengths would be likely to show a similar probability distribution, but with contracted coverage consistent with Fig. 8. Overlapping tower ranges indicate the capacity for simultaneous detections to provide more accurate estimates of the target's altitude and spatial coordinates than what can be estimated from the single detections.

A.

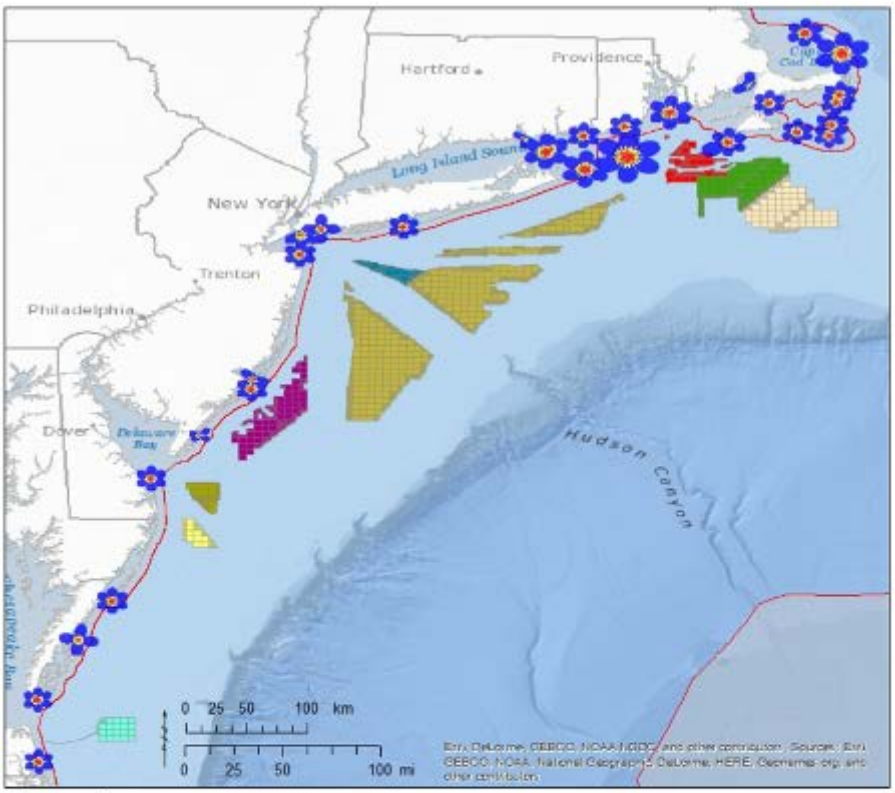

Legend

BOEM Wind Lease Areas
- RI/MA OCS-A 0486 and 0487
- MA OCS-A 0500 and 501
- NY OCS-A 0512
- NJ OCS-A 0498 and 0499
- DE OCS-A 0482 and 0519
- MD OCS-A 0490
- VA OCS-A 0483 and 0497

U.S. Federal Waters
- 3 - 200 nautical mile boundary

BOEM Wind Planning Areas
- Massachusetts PSN
- New York Bight Call Area
- New York Proposed Commercial Lease

Detection probability (flight altitude 25 m)
- < 0.5
- 0.5 - 0.6
- 0.6 - 0.7
- 0.7 - 0.8
- 0.8 - 0.9
- 0.9 - 1

B.

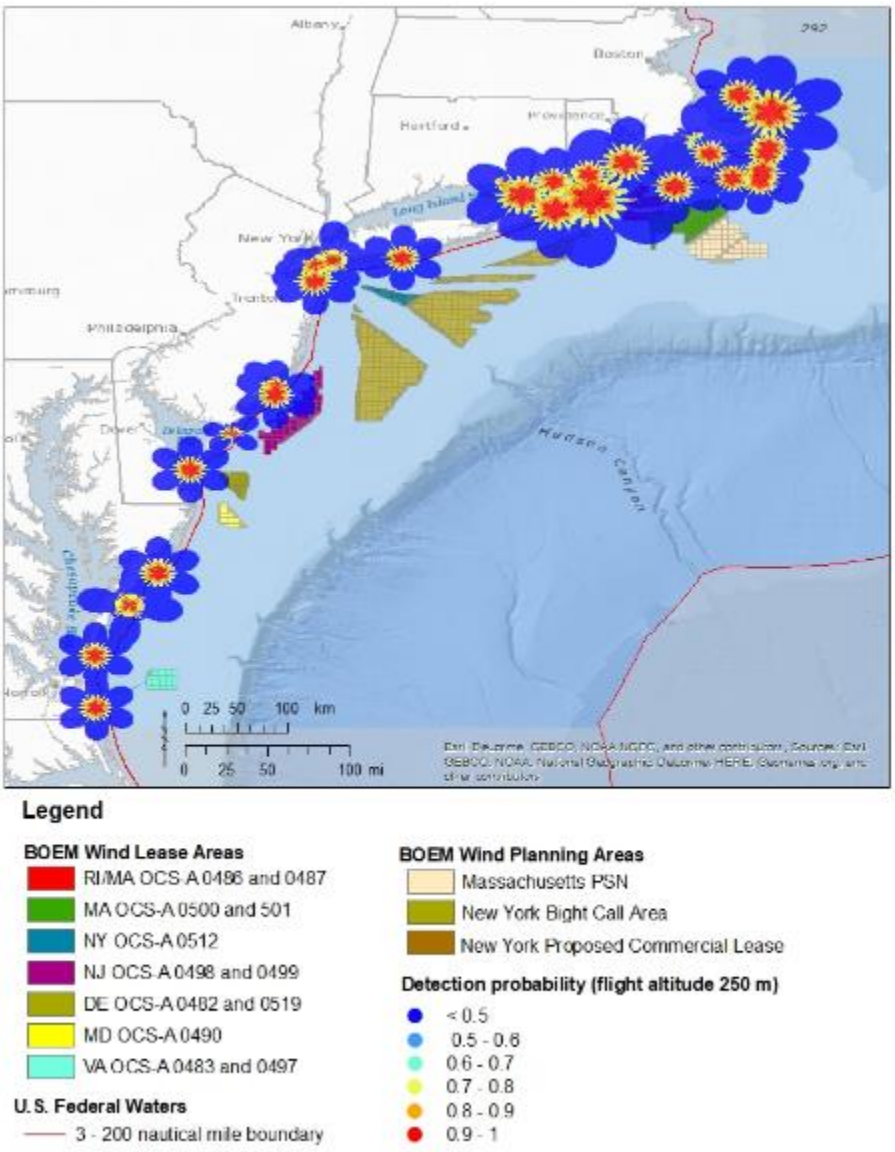

Figure 12. Coverage map from 2016-2017 BOEM-funded towers showing the probability of detecting a bird flying at (A) 25 m, and (B) 250 m.

Coverage assumes signal strength value = 5. Higher signal strengths would be likely to show a similar probability distribution, but with contracted coverage consistent with Fig. 8. Overlapping tower ranges indicate the capacity for simultaneous detections to provide more accurate estimates of the target's altitude and spatial coordinates than what can be estimated from the single detections.

2.9 Assessment of Movements and Occurrence in Federal Waters

To map the flight paths of shorebirds, we subset the data from the movement model to all 1-minute locations identified as 'non-stop flight', grouped flights by individual and flight event (continuous 1 minute location estimates), and plotted them using the "geom_path" function in the 'ggplot2' R package (Wickham 2016).

We assessed bird movements in the Study Area and occurrence in Federal waters using the mean location estimates (UTM Zone 18 N) interpolated to a one-minute time step. For the Atlantic OCS region, we obtained a GIS shapefile of the Submerged Lands Act boundary line, delineating the boundary between state waters (landward) and Federal waters (seaward). We clipped the shapefile to the boundaries of the Study Area (77^{o} W $\leq$ longitude $\leq$ 69^{o} W, 36^{o} N $\leq$ latitude $\leq$ 42.5^{o} N; Fig. 1). Interpolations generated from detections on long distance offshore flights were sometimes widely separated in time and space and as a result subjected to artificially low flight speed estimates and large locational error. To address uncertainty in model output, we considered locations as occurring within Federal waters when the mean estimated coordinates intersected the Federal water polygon during a flight identified by the movement model as 'non-stop'. These locations are referred to as "Federal water exposure events". Non-exposure events are locations that occurred within the Study Area but did not intersect the Federal water polygon during a non-stop flight.

2.10 Temporal and Meteorological Covariates

To examine movements relative to daylight, we used the R package 'maptools' (Bivand and Lewin-Koh 2016) to calculate local sunrise and sunset times for each modeled location estimate, interpolated to a 1-minute time step. Location estimates that occurred between the time of local sunrise and the time of local sunset were considered to have occurred during daytime hours. Conversely, location estimates that occurred between the time of local sunset and the time of local sunrise were considered to have occurred during nighttime hours.

To examine movements relative to meteorological covariates, we obtained satellite-derived North American Regional Reanalysis (NARR) environmental data for the Study Area (Atlantic coast and adjacent OCS from Cape Cod, Massachusetts to Back Bay, VA) in 3-hr time steps and approximately 32-km^2 spatial resolution (National Oceanic and Atmospheric Administration 2017). The specific meteorological covariates that we included were wind speed (m/s) and wind direction (the direction that the wind blows toward, in degrees clockwise from geographic north), both interpolated to estimated flight altitudes, and four additional meteorological covariates at surface level values: barometric pressure (Pascal [Pa]), precipitation accumulation (kg/m^2), air temperature (°C) and visibility (m).

These data were horizontally interpolated from their native Lambert conic grid to each location along the predicted trajectory (stored in the model in NAD83 UTM 18N coordinates), using a cubic spline based on the nearest 8 spatial locations, and linearly interpolated in time (MATLAB routines 'lambert1' and 'latln2val', respectively) for each individual at each 1-minute location estimate. The wind covariates were vertically interpolated to estimated flight altitudes by linear interpolation between the closest altitudes between fields at 10-m altitude and pressure levels of 1000, 950, 900, 850, 800, 750 and 700 mb, based

on the latter's current geopotential height (these vary with weather and range from approximately 100 m to 3000 m, respectively). Geospatially referenced location estimates and detection data for all birds, along with corresponding covariates, were submitted to BOEM as a supplement to this report (Appendix C).

2.11 Covariate Analysis of Exposure to Federal Waters

To assess timing and meteorological conditions of flights across Federal waters within the Study Area, we used model location estimates (1-minute time step) for each location that met the criteria for exposure to Federal waters described in Section 2.8. We first used histograms and summary statistics to compare the distribution of select meteorological conditions (visibility and precipitation) and time-of-day between Federal water exposure events compared to non-exposure events. For these comparisons, we assessed spring and fall migration seasons separately but pooled data across species. To assess variation by day of year, plotted separate histograms for each species because their migration timing varies (Parmelee 1992, Skeel and Mallory 1996, Warnock and Gill 1996, Nettleship 2000, Macwhirter et al. 2002, Nebel and Cooper 2008, Gratto-Trevor 2010, Baker et al 2013, Farmer et al. 2013, Hicklin and Nol and Blanken 2014, Tibbitts and Moskoff 2014, Poole et al 2016).

We then performed an integrated analysis of all covariates (temporal, demographic, and meteorological) to predict movements into Federal waters by species using a regression-based method, boosted GAMs (Generalized Additive Models). We fit these models using the R package 'mboost' and function "gamboost" (see also Buhlmann and Hothorn 2007). Due to wide variation in sample sizes of individuals tagged among species, we included in the boosted GAMs only species that had at least 10 individuals tracked in the Study Area per season.

We used the program R (version 3.4.1, R Core Development Team 2017) and associated packages to summarize and format location data for the Boosted GAMs. For the analysis of exposure to Federal waters, we used the packages 'plyr' (Wickham 2011) and 'lubridate' (Grolemund and Wickham 2011) to calculate the mean of each covariate to the nearest 3-hr bin (i.e. 0:00 hrs, 03:00 hrs, 06:00 hrs, 09:00 hrs, 12:00 hrs, 15:00 hrs, 18:00 hrs, 21:00 hrs) in local Eastern Standard Time (EST). For circular variables ('time of day' in hours EST and 'wind direction' in degrees relative to true north), we calculated the mean based on the circular distribution (R package 'Circular', Agostinelli and Lund 2017).

To fit responses of exposure to Federal waters as influencing discrete events, we used a binomial logistic regression formulation as the basis of the boosted GAMs. In this formulation, probability of exposure is incorporated as an 'inverse logit-link', with responses to each covariate presented as partial contributions to the likelihood (logit-transformed odds ratio) of an exposure event occurring, i.e. the higher the contribution, the increased predicted likelihood of an exposure event. Responses represent the contribution of a given covariate to the likelihood of exposure, quantified by logit-transformed odds ratio of exposure. The boosted GAM method also is advantageous because it fits non-linear and independent responses (based on spline functions) to each covariate and only the most influential covariates are chosen. Therefore, the model performs both model fitting and predictor selection simultaneously, i.e., covariates with little to no influence on exposure to offshore waters are automatically excluded.

The boosted approach iteratively sums simple regressions based on single-covariate "learner" functions, each chosen to minimize an equivalent loss function based on binomial predictors (see Buhlmann and Hothorn 2007). The additive approach estimates the relative influence of each covariate as the number of boosts, choosing that covariate to minimize the current loss. Model parameters were chosen to reduce possible bias and overfitting (Buhlmann and Hothorn 2007). The fit was incremented using small step sizes or "shrinkage" (set to the default 0.25) of each iterative sub-model to the fit and also was terminated before convergence (i.e., before the fit was maximized; see e.g. Maloney et al. 2012). To confirm that the number of iterations used was reasonable, we assessed the cross-validated risk using function "cvrisk" using 8 separate 'folds' (independently sampled fits). This resulted in 1,000 boosts per analysis.

Learner functions for fitting responses were tailored to the nature of each covariate. Responses to the categorical covariates ('species' and 'age' in fall and 'species' in spring) were fit using linear learner functions (resulting in fixed effects for each category). Responses to each individual were treated as random intercepts and responses to all the meteorological covariates were fit using boosted cubic p-splines. We also included interactions between 'age' and 'date' in fall and 'species' and 'date' in spring. Responses to the periodic covariates ('hour of day' and 'wind direction') were set to be cyclical. To assess the significance of the predicted covariate responses, we performed bootstrap analysis (using function "confint" with 1000 model fits) to produce 95% confidence intervals for each covariate response.

2.12 Distribution of Flight Altitudes in Federal Waters

We used the input data for boosted GAM models (3-hour time step, as described in Section 2.11) to summarize the altitude of flights in Federal waters during spring and fall migration by day versus night. Flight segments that primarily occurred between the hours of sunrise and sunset were classified as "day", whereas flight segments that primarily occurred between the hours of sunset were classified as "night". All results are reported relative to the RSZ of offshore wind turbines (25-250 m).

2.13 Departure Bearings from the Study Area

We analyzed flight headings of the last non-stop flight trajectory of each bird departing from the Study Area assess the flight direction of birds departing from the detection range of the BOEM telemetry array. For all birds included in the covariate analysis of exposure to Federal waters, we used the R package 'Circular', (Agostinelli and Lund 2017) to calculate circular mean departure headings (in degrees relative to true N) and mean resultant length (ρ, a measure of dispersion of a sample of directional measurements). The mean resultant length, ρ, is a statistic between 0 and 1, where 0 indicates a large spread in directional data and 1 indicates that data are concentrated in a single direction (Cremers and Klugkist 2018).

3 Results

3.1 Tagging Summary

Between 2014 and 2017, study partners deployed nanotags on 3,955 shorebirds of 17 species: American Golden-Plover (*Pluvialis dominica*), Black-bellied Plover, Dunlin, Least Sandpiper, Lesser Yellowlegs, Pectoral Sandpiper, Purple Sandpiper (*Calidris maritima*), Red Knot, Red Phalarope (*Phalaropus fulicarius*), Red-necked Phalarope (*Phalaropus lobatus*), Ruddy Turnstone, Sanderling, Short-billed Dowitcher (*Limnodromus griseus*), Semipalmated Plover, Semipalmated Sandpiper, Whimbrel, and White-rumped Sandpiper.

3.2 Use of the Study Area Relative to the Broader Atlantic Coast

We assessed shorebird use of the Study Area relative to the broader Atlantic coast using data from individuals that were detected by automated radio telemetry stations located at least 50 km from where they were tagged and within 30 km of the coastline from Mingan QC, Canada to the north and the Texas-Mexico border to the south (Fig 13, orange and purple tracks). We used this dataset to assess shorebird use of the Study Area to minimize the influence of birds that lost tags or died before reaching the Atlantic coast, and to address issues with detection probability across Motus Network, where most of the tracking stations are concentrated in the eastern U.S and Canada. Of these individuals (n = 1,363), 65% were detected in the Study Area (Fig. 13, orange tracks). The estimated proportion of shorebirds using the Study Area varied by species. Use of the Study Area was highest among Red Knots, Ruddy Turnstones and Pectoral Sandpipers (Table 5). The two species with the largest sample sizes, Red Knots and Semipalmated Sandpipers, showed divergent use of the Study Area. The majority (86%) of Red Knots were detected within the Study Area, compared to approximately half (53%) of Semipalmated Sandpipers. During fall, the remaining Semipalmated Sandpipers (~47%) departed from the Atlantic coast north of the Study Area, primarily from Atlantic Canada (Fig. 13).

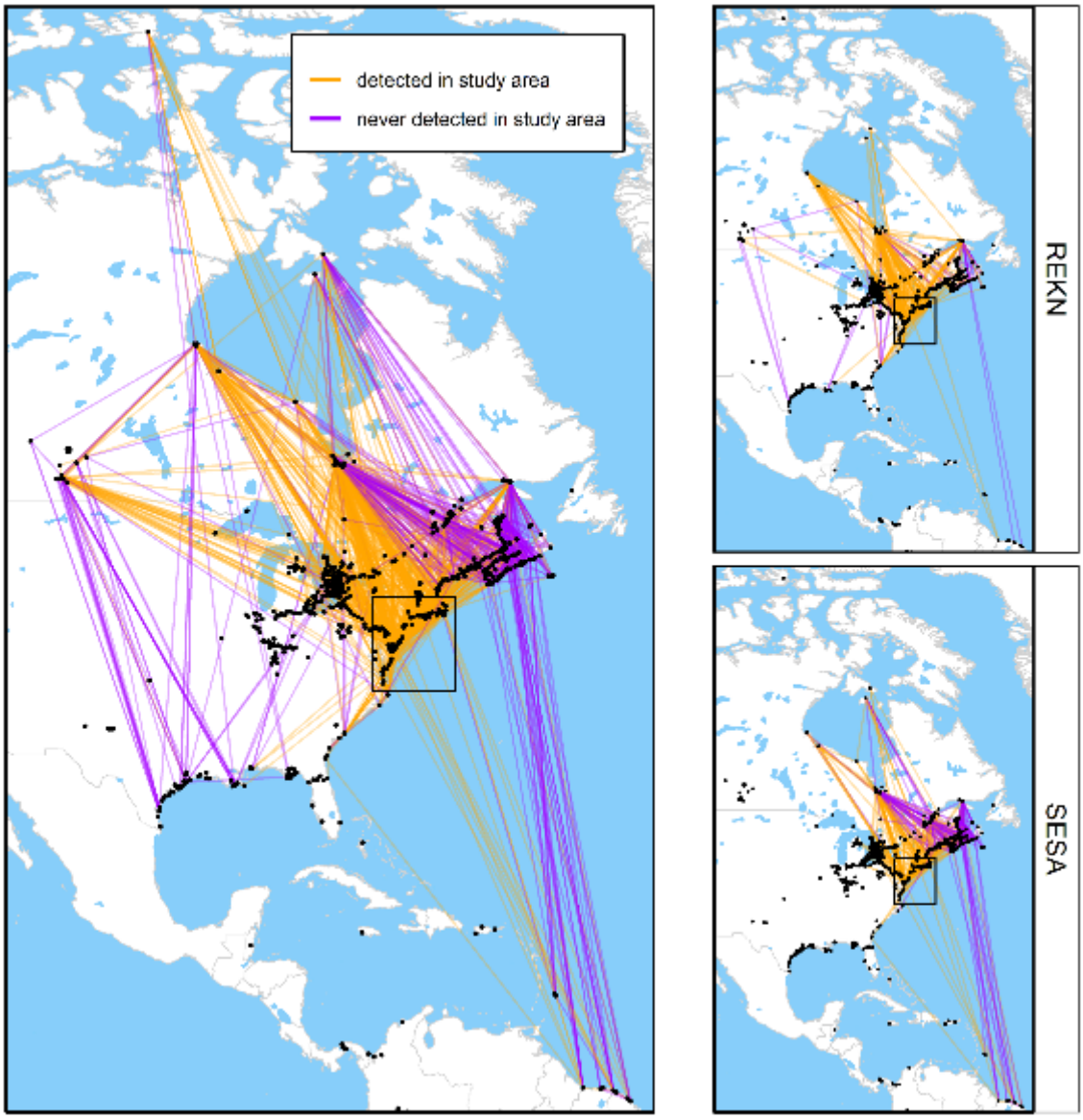

Figure 13. Comparison of the detection patterns of shorebirds that were not detected in the Study Area to those that were detected in the Study Area, 2014 to 2017.

Maps show tracks of shorebirds that were detected at least 50 km from their tagging site and also detected within 30 km of the coastline from Mingan QC, Canada to the north and the Texas-Mexico border to the south. Left panel shows tracks for all species, right panels shows Red Knot (REKN) and Semipalmated Sandpiper (SESA) tracks only. The Study Area is indicated by a black rectangle and telemetry receiving stations (BOEM stations and Motus network partner stations) are shown as black dots.

Table 5. Estimated proportion of shorebirds that departed or arrived on the coast between Mingan QC, Canada and the Texas-Mexico border that were detected within the Study Area, 2014 to 2017.

Species	Individuals tagged (*n*)	Individuals (*n*) detected at least 50 km from their tagging site and detected on the Atlantic coast	Individuals (*n*) detected in the Study Area	Estimated proportion of individuals using the Study Area
Black-bellied Plover	47	11	3	0.27
Dunlin	104	8	5	0.63
Least Sandpiper	76	27	20	0.74
Lesser Yellowlegs	11	7	2	0.29
Pectoral Sandpiper	46	8	7	0.88
Red Knot	1,175	390	336	0.86
Ruddy Turnstone	172	67	66	0.99
Sanderling	326	129	87	0.67
Semipalmated Plover	273	124	46	0.37
Semipalmated Sandpiper	1,381	490	262	0.53
Whimbrel	33	8	1	0.13
White-rumped Sandpiper	265	91	53	0.58
American Golden-Plover	4	1	0	0.00
Red-necked Phalarope	4	1	0	0.00
Short-billed Dowitcher	1	1	0	0.00
Purple Sandpiper	1	0	0	0.00
Red Phalarope	36	0	0	0.00
Total	**3,955**	**1,363**	**888**	**0.65**

3.3 Assessment of Exposure to Federal Waters

3.3.1 Summary of Data Used in Analysis of Exposure to Federal Waters

Of the 3,955 shorebirds tagged, 594 individuals of 12 species (Black-bellied Plover, Dunlin, Least Sandpiper, Lesser Yellowlegs, Pectoral Sandpiper, Semipalmated Plover, Whimbrel, White-rumped Sandpiper, Red Knot, Ruddy Turnstone, Sanderling, and Semipalmated Sandpiper) met the criteria for inclusion in our analysis of exposure to Federal waters (Table 6). The dataset used to assess exposure to Federal waters was limited to individuals detected by at least one BOEM receiver station that were tracked during at least one non-stop flight in the Study Area. This included four species with data in the Study Area during both spring and fall migration: Red Knot, Ruddy Turnstone, Sanderling, and Semipalmated Sandpiper. Only fall movement data were available for the remaining eight species. For a few Red Knots (n = 14) and Semipalmated Sandpipers (n = 4), there were data from both spring and fall

migration movements from the same individuals. The amount of available metadata on age and sex of individuals varied by species (Table 7).

Table 6. Number of shorebirds of each species tagged by project partners between 2014 and 2017 compared with the number that met the criteria to be included in the dataset used to assess exposure to Federal waters (shown in brackets). Species totals are shown in bold.

Species[1]	Capture Site	2014	2015	2016	2017	Total
AMGP	Southampton Island, NU, Canada	-	1 (0)	2 (0)	1 (0)	**4 (0)**
BBPL	Bathurst Island, NU, Canada	-	8 (0)	12 (3)	-	20 (3)
	Coats Island, NU, Canada	-	4 (0)	3 (0)	-	7 (0)
	Mingan Archipelago, QC, Canada	-	1 (0)	-	-	1 (0)
	Saint Lawrence River, QC, Canada	1 (0)	-	-	-	1 (0)
	Southampton Island, NU, Canada	2 (0)	3 (1)	6 (0)	7 (0)	18 (1)
						47 (4)
DUNL	Churchill, MB, Canada	9 (0)	26 (0)	16 (0)	19 (0)	70 (0)
	Coats Island, NU, Canada	-	1 (0)	-	-	1 (0)
	James Bay, ON, Canada	2 (0)	20 (1)	-	-	22 (1)
	Mingan Archipelago, QC, Canada	8 (0)	-	-	-	8 (0)
	Southampton Island, NU, Canada	-	-	-	3 (0)	3 (0)
						104 (1)
LESA	Churchill, MB, Canada	-	1 (0)	-	-	1 (0)
	James Bay, ON, Canada	3 (0)	-	33 (11)	29 (10)	65 (21)
	Miscou Island, NB, Canada	-	-	10 (2)	-	10 (2)
						76 (23)
LEYE	James Bay, ON, Canada	-	-	8 (1)	3 (1)	**11 (2)**
PESA	James Bay, ON, Canada	-	-	15 (3)	31 (6)	**46 (9)**
PUSA	Southampton Island, NU, Canada	-	1 (0)	-	-	**1 (0)**
REKN	Brazil	-	-	-	10 (0)	10 (0)

Species[1]	Capture Site	2014	2015	2016	2017	Total
	Cape Cod, MA, USA	21 (11)	39 (23)	99 (42)	-	159 (76)
	Charleston, SC, USA	-	-	-	20 (6)	20 (6)
	Delaware Bay, NJ, USA	96 (16)	104 (4)	178 (34)	137 (31)	515 (85)
	Gulf of Mexico, LA, USA	-	-	18 (0)	1 (0)	19 (0)
	Gulf of Mexico, TX, USA	-	11 (0)	10 (0)	-	21 (0)
	James Bay, ON, Canada	1 (0)	6 (1)	9 (2)	-	16 (3)
	Mingan Archipelago, QC, Canada	16 (0)	122 (0)	248 (0)	29 (0)	415 (0)
						1,175 (170)
REPH	Bathurst Island, NU, Canada	-	6 (0)	5 (0)	-	11 (0)
	Coats Island, NU, Canada	-	-	5 (0)	-	5 (0)
	Southampton Island, NU, Canada	-	-	4 (0)	16 (0)	20 (0)
						36 (0)
RNPH	Chaplin, SK, Canada	-	-	-	1 (0)	1 (0)
	Coats Island, NU, Canada	-	-	2 (0)	-	2 (0)
	James Bay, ON, Canada	-	-	1 (0)	-	1 (0)
						4 (0)
RUTU	Cape Cod, MA, USA	-	-	7 (4)	-	7 (4)
	Coats Island, NU, Canada	-	3 (1)	3 (0)	-	6 (1)
	Delaware Bay, NJ, USA	-	46 (4)	86 (5)	-	132 (9)
	James Bay, ON, Canada	-	-	4 (4)	-	4 (4)
	Mingan Archipelago, QC, Canada	1 (0)	-	-	14 (0)	15 (0)
	Southampton Island, NU, Canada	-	3 (2)	3 (2)	2 (0)	8 (4)
						172 (22)
SAND	Bathurst Island, NU, Canada	-	5 (1)	29 (10)	-	34 (11)
	Chaplin, SK, Canada	-	38 (3)	40 (7)	39 (16)	117 (26)
	Delaware Bay, NJ, USA	-	-	50 (16)	-	50 (16)
	Gulf of Maine, ME, USA	-	4 (3)	-	-	4 (3)
	Gulf of Mexico, LA, USA	-	-	11 (0)	19 (1)	30 (1)
	Gulf of Mexico, TX, USA	-	24 (0)	26 (1)	40 (3)	90 (4)
	James Bay, ON, Canada	-	1 (0)	-	-	1 (0)

Species[1]	Capture Site	2014	2015	2016	2017	Total
						326 (61)
SBDO	Miscou Island, NB, Canada	-	-	1 (0)	-	**1 (0)**
SEPL	Churchill, MB, Canada	-	42 (4)	29 (5)	31 (9)	102 (18)
	Coats Island, NU, Canada	-	-	2 (0)	-	2 (0)
	Gulf of Maine, ME, USA	-	4 (0)	-	-	4 (0)
	James Bay, ON, Canada	-	-	24 (11)	42 (10)	66 (21)
	Miscou Island, NB, Canada	-	-	27 (1)	49 (3)	76 (4)
	Polar Bear Provincial Park, ON, Canada	-	-	8 (3)	2 (0)	10 (3)
	Southampton Island, NU, Canada	-	1 (1)	4 (0)	8 (0)	13 (1)
						273 (47)
SESA	Bay of Fundy, NB/NS, Canada	105 (1)	-	-	-	105 (1)
	Coats Island, NU, Canada	29 (2)	18 (1)	14 (5)	-	61 (8)
	Delaware Bay, NJ, USA	-	60 (11)	95 (16)	84 (26)	239 (53)
	Gulf of Maine, ME, USA	30 (8)	49 (11)	30 (7)	-	109 (26)
	Jamaica Bay, NY, USA	-	-	5 (1)	19 (1)	24 (2)
	James Bay, ON, Canada	80 (8)	80 (18)	36 (8)	50 (12)	246 (46)
	Miscou Island, NB, Canada	-	-	38 (1)	56 (1)	94 (2)
	Mingan Archipelago, QC, Canada	23 (0)	13 (0)	48 (1)	24 (3)	108 (4)
	Plymouth Bay, MA, USA	-	13 (5)	29 (21)	30 (15)	72 (41)
	Saint Lawrence River, QC, Canada	2 (0)	8 (1)	32 (1)	42 (7)	84 (9)
	Southampton Island, NU, Canada	-	-	1 (0)	-	1 (0)
	Suriname	-	-	131 (1)	107 (0)	238 (1)
						1,381 (193)
WHIM	Miscou Island, NB, Canada	-	2 (0)	3 (0)	-	5 (0)
	Mingan Archipelago, QC, Canada	-	-	-	10 (0)	10 (0)
	Polar Bear Provincial Park, ON, Canada	-	-	10 (0)	8 (1)	18 (1)
						33 (1)
WRSA	Bathurst Island, NU, Canada	-	1 (0)	6 (2)	-	7 (2)

Species[1]	Capture Site	2014	2015	2016	2017	Total
	Coats Island, NU, Canada	-	2 (0)	-	-	2 (0)
	James Bay, ON, Canada	58 (5)	50 (21)	27 (12)	58 (19)	193 (57)
	Miscou Island, NB, Canada	-	-	13 (0)	-	13 (0)
	Southampton Island, NU, Canada	9 (0)	12 (2)	14 (0)	15 (0)	50 (2)
						265 (61)

[1] Species codes: AMGP - American Golden-Plover, BBPL - Black-bellied Plover, DUNL - Dunlin, LESA - Least Sandpiper, LEYE - Lesser Yellowlegs, PESA - Pectoral Sandpiper, PUSA - Purple Sandpiper, REKN - Red Knot, REPH - Red Phalarope, RNPH - Red-necked Phalarope, RUTU - Ruddy Turnstone, SAND - Sanderling; SBDO - Short-billed Dowitcher, SEPL - Semipalmated Plover, SESA - Semipalmated Sandpiper, WHIM - Whimbrel, WRSA - White-rumped Sandpiper.

Table 7. Distribution of age and sex classifications, by species and season, among shorebirds included in analysis of exposure to Federal waters.

Species	Season	Age			Sex		
		HY	AHY	U	F	M	U
Red Knot	Spring	-	38	-	-	-	38
	Fall	16	127	10	5	13	135
Ruddy Turnstone	Spring	-	5	-	1	4	-
	Fall	2	15	-	9	6	2
Sanderling	Spring	-	1	-	-	-	1
	Fall	3	57	-	-	-	60
Semipalmated Sandpiper	Spring	-	26	1	-	-	27
	Fall	64	106	2	2	8	162
Black-bellied Plover	Fall	-	4	-	2	2	-
Semipalmated Plover	Fall	14	32	1	10	12	25
Pectoral Sandpiper	Fall	5	4	-	3	2	4
White-rumped Sandpiper	Fall	2	59	-	4	-	57
Least Sandpiper	Fall	17	4	2	-	-	23
Dunlin	Fall	1	-	-	-	-	1
Lesser Yellowlegs	Fall	2	-	-	-	-	2
Whimbrel	Fall	-	1	-	-	-	1

[1]Age codes: HY - Hatch Year, AHY - After Hatch Year
[2]Sex codes: F - Female, M - Male, U – Unknown

3.3.2 Summary of Movements in the Study Area

Movement patterns in the Study Area varied by species and season but showed some consistency throughout (Figs. 14 - 25). During fall, movements and departures into Federal waters were concentrated at the northern end of the Study Area between Cape Cod, MA and eastern Long Island Sound, NY, as well as coastal New Jersey and the Delaware Bay region. More dispersed movement patterns throughout the Study Area were most apparent among Sanderlings (Fig. 16). The final estimated locations of 41% (*n* = 541) of individuals were over Federal waters in the fall. Offshore departures during fall were most apparent among White-rumped Sandpipers, where most individuals transited the Study Area during non-stop flights to the southeast, with 72% last detected over Federal waters (Fig. 17).

All Red Knots and Semipalmated Sandpipers tagged during spring migration were tagged at sites along the US Atlantic coast. Movements of Red Knots (Fig. 14) and Semipalmated Sandpipers (Fig 15) tracked during spring were concentrated near tagging sites in the Delaware Bay and western Long Island, with some regional movements detected between staging areas. Several individuals from both species crossed Federal waters during regional flights between staging and stopover sites located throughout the Study Area before departing northward towards the breeding grounds (Figs. 14 and 15).

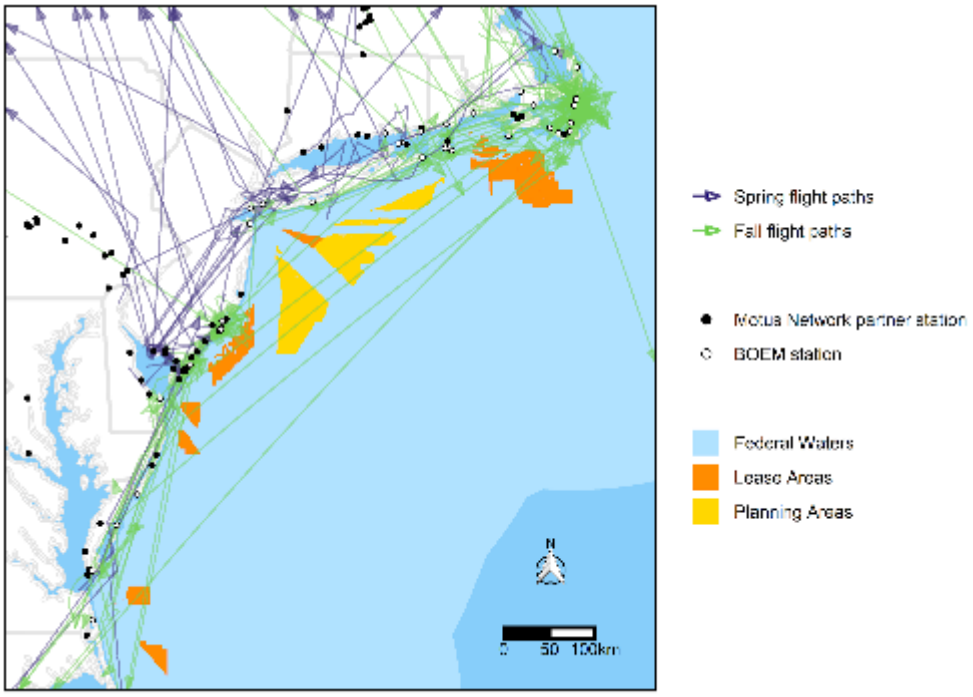

Figure 14. Modeled flight paths of Red Knots crossing the Study Area during spring migration (*n* = 31) and fall migration (*n* = 146) in 2014 to 2017.
Arrows indicate direction and location of the last detection in the Study Area for each individual.

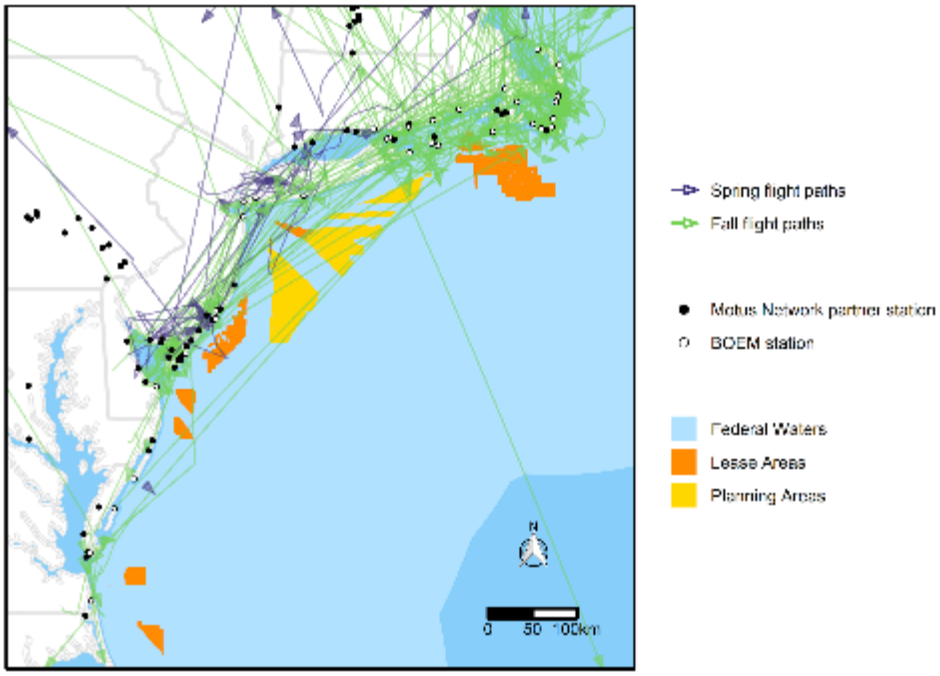

Figure 15. Modeled flight paths of Semipalmated Sandpipers crossing the Study Area during spring migration (*n* = 25) and fall migration (*n* = 170) in 2014 to 2017.
Arrows indicate direction and location of the last detection in the Study Area for each individual.

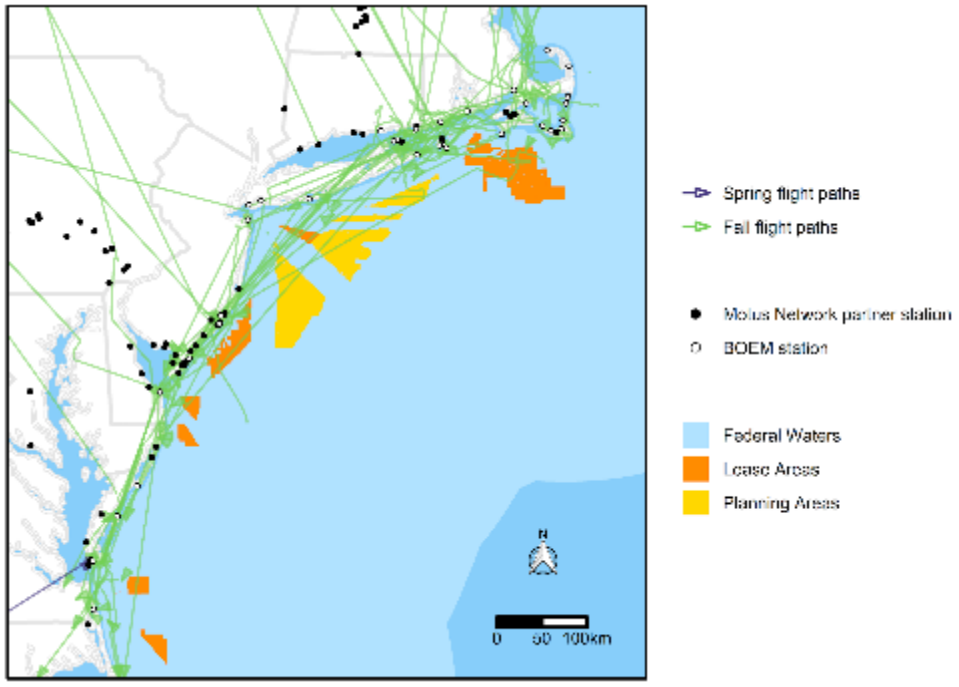

Figure 16. Modeled flight paths of Sanderling crossing the Study Area during spring migration (*n* = 1) and fall migration (*n* = 60) in 2015 to 2017.
Arrows indicate direction and location of the last detection in the Study Area for each individual.

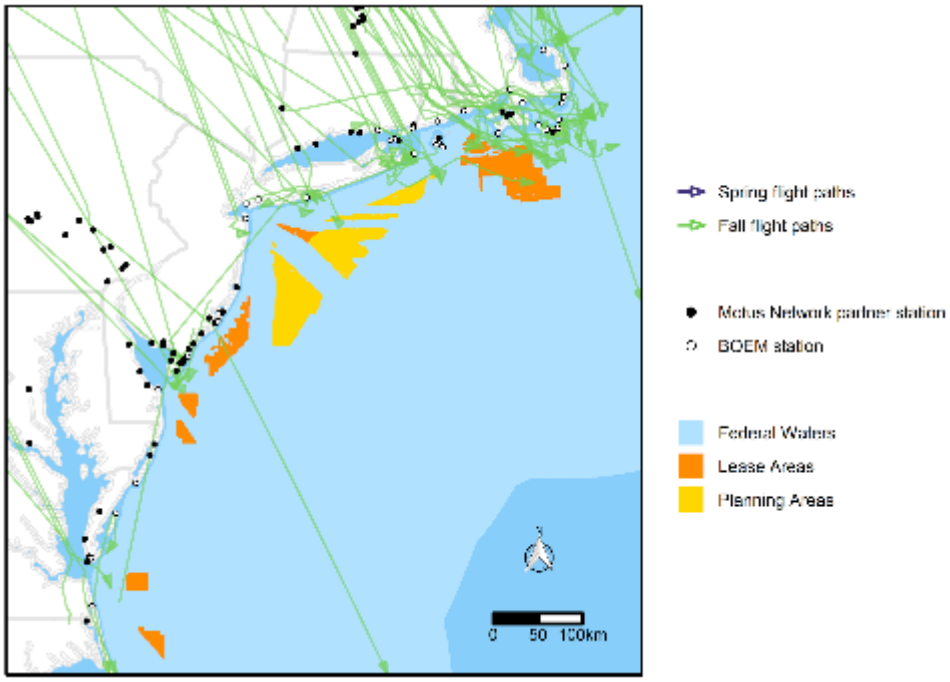

Figure 17. Modeled flight paths of White-rumped Sandpipers crossing the Study Area during fall migration (*n* = 61) in 2014 to 2017.
Arrows indicate direction and location of the last detection in the Study Area for each individual.

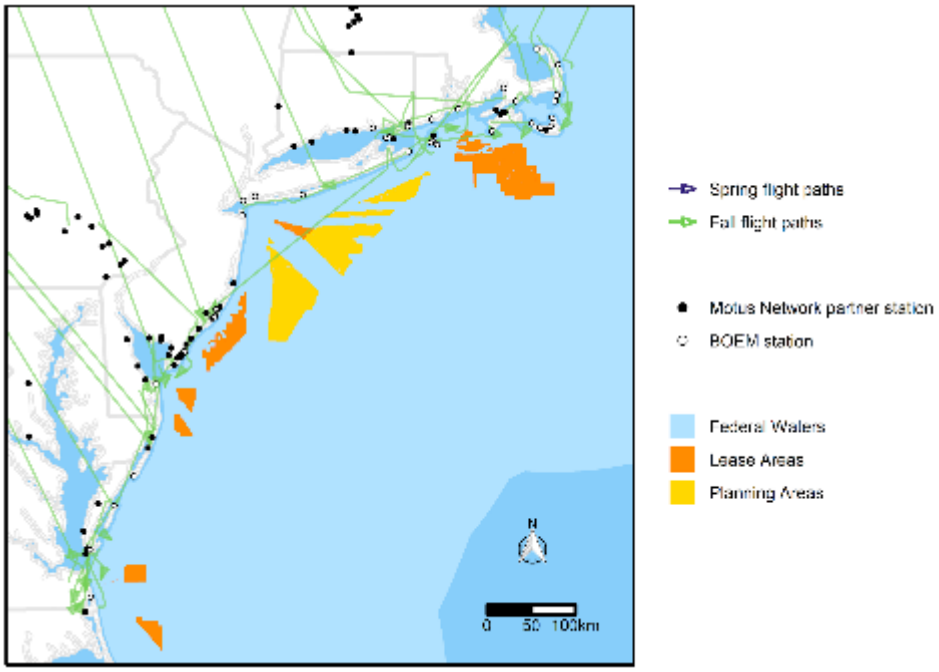

Figure 18. Modeled flight paths of Least Sandpipers (*n* = 23) crossing the Study Area during fall migration in 2016 to 2017.
Arrows indicate direction and location of the last detection in the Study Area for each individual.

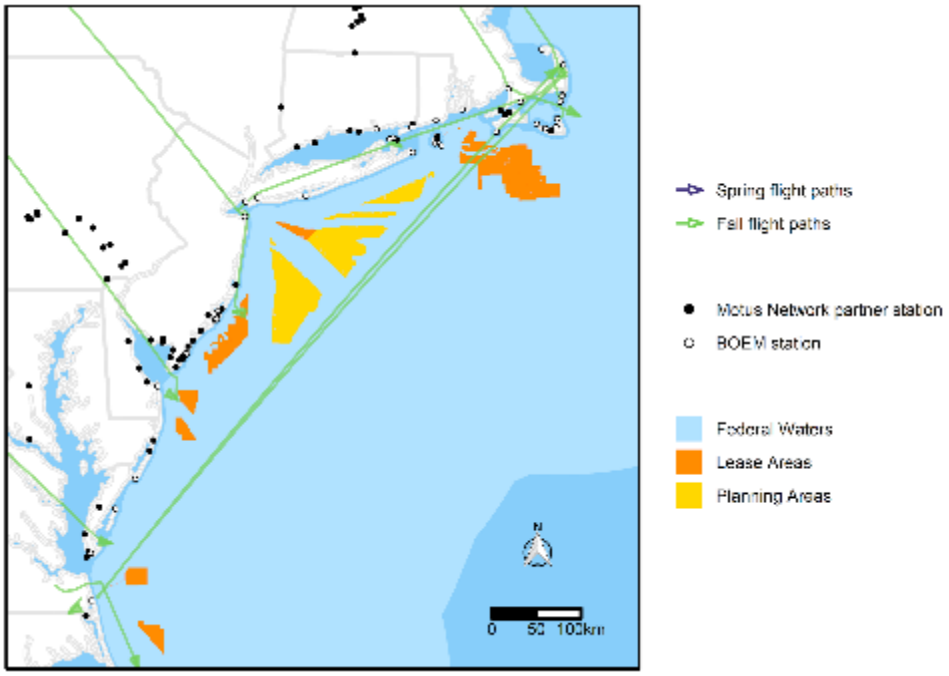

Figure 19. Modeled flight paths of Pectoral Sandpipers (*n* = 9) crossing the Study Area during fall migration in 2016 to 2017.
Arrows indicate direction and location of the last detection in the Study Area for each individual.

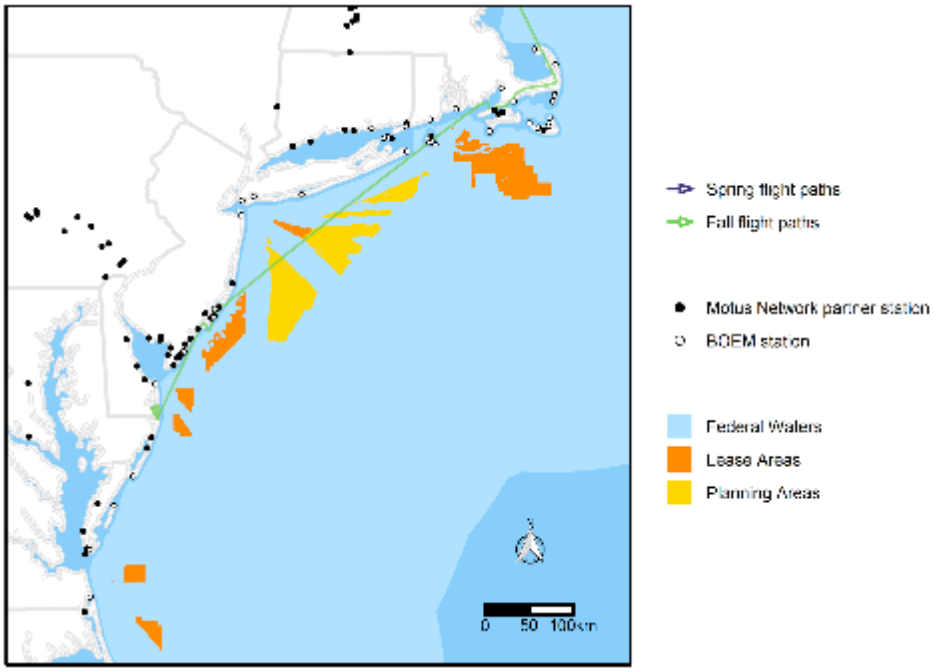

Figure 20. Modeled flight paths of Dunlin (*n* = 1) crossing the Study Area during fall migration in 2015.

Arrows indicate direction and location of the last detection in the Study Area for each individual.

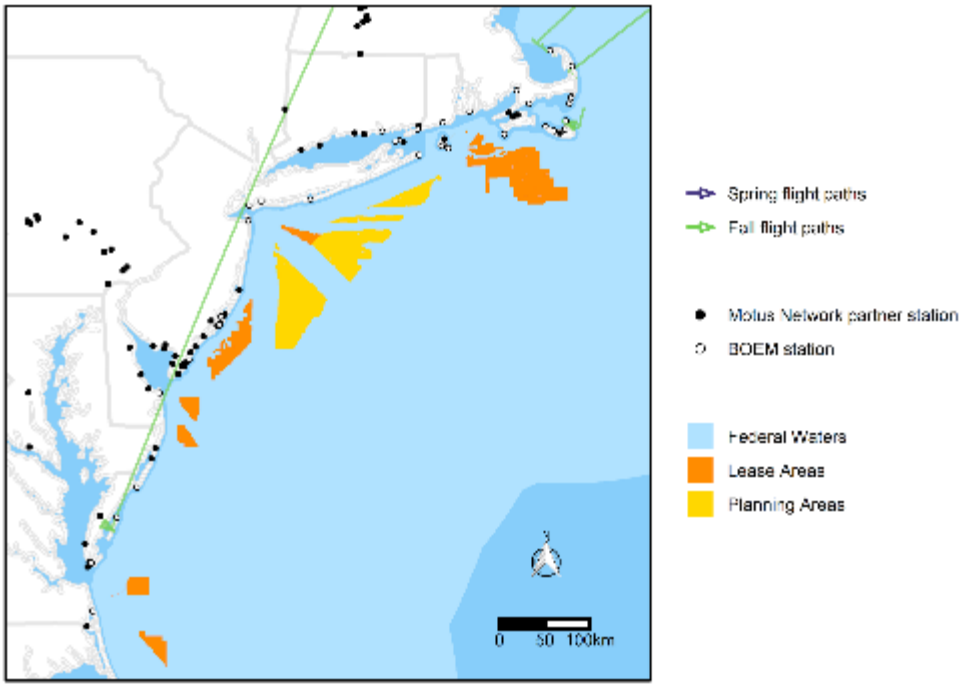

Figure 21. Modeled flight paths of Black-bellied Plovers (*n* = 4) crossing the Study Area during fall migration in 2015 to 2016.

Arrows indicate direction and location of the last detection in the Study Area for each individual.

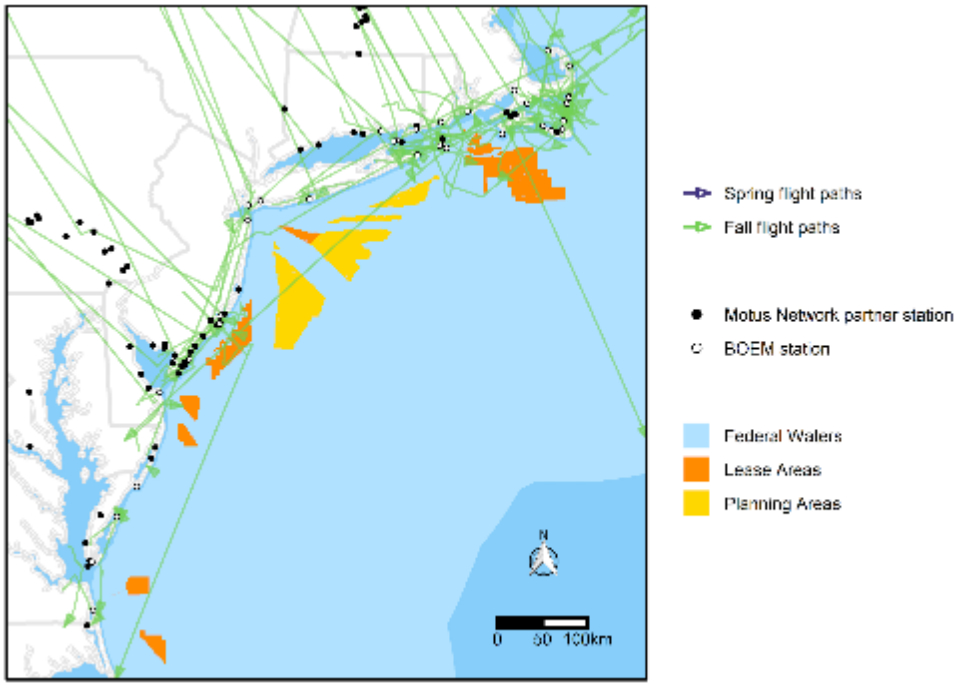

Figure 22. Modeled flight paths of Semipalmated Plovers crossing the Study Area during fall migration (*n* = 47) in 2015 to 2017.
Arrows indicate direction and location of the last detection in the Study Area for each individual.

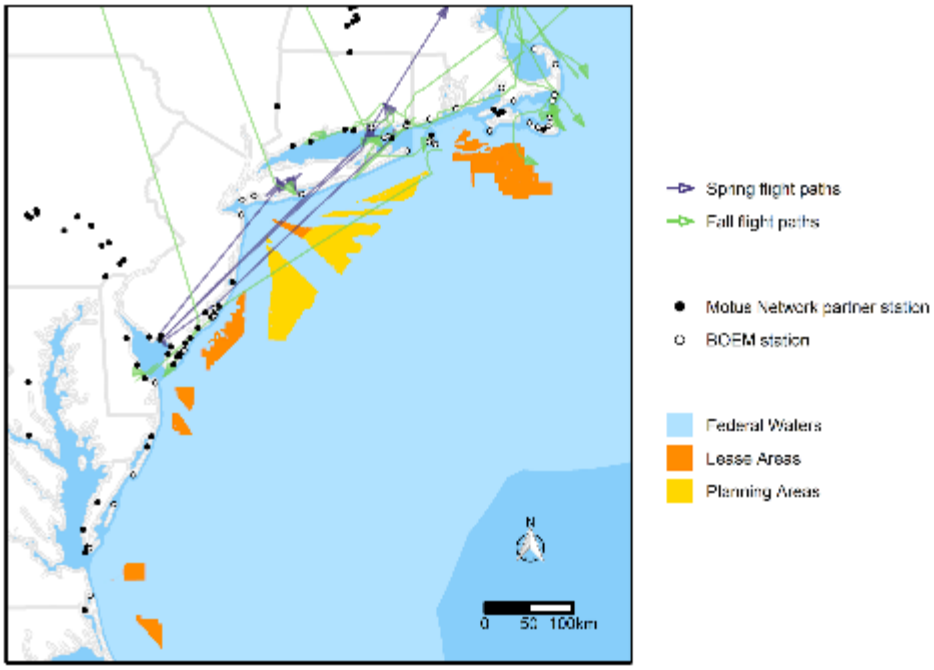

Figure 23. Modeled flight paths of Ruddy Turnstone crossing the Study Area during spring migration (*n* = 5) and fall migration (*n* = 17) in 2015 to 2016.
Arrows indicate direction and location of the last detection in the Study Area for each individual.

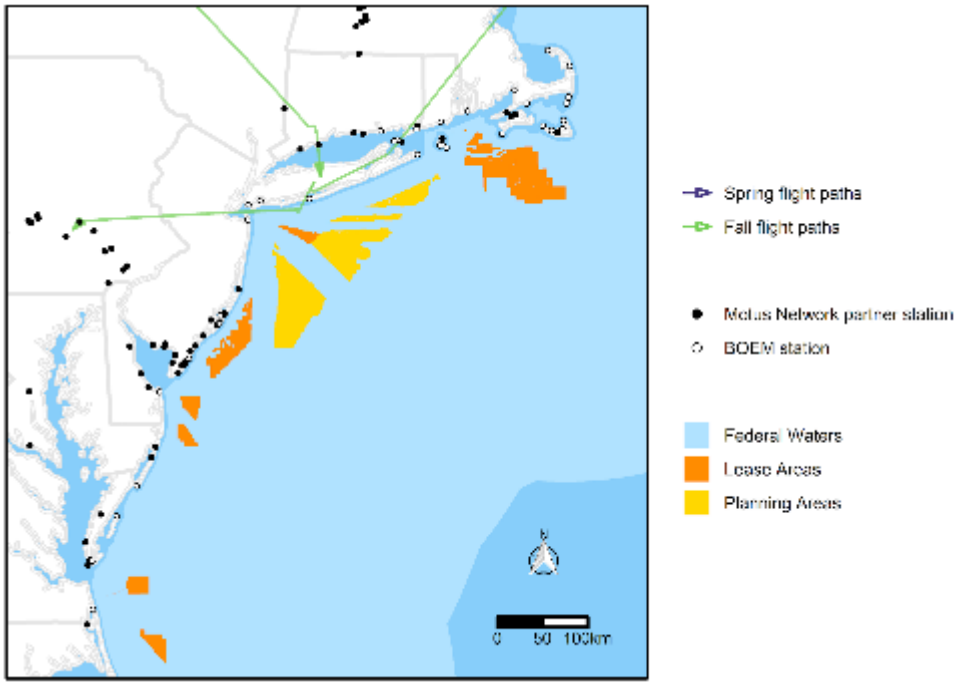

Figure 24. Modeled flight paths of Lesser Yellowlegs (*n* = 2) crossing the Study Area during fall migration in 2016 to 2017.
Arrows indicate direction and location of the last detection in the Study Area for each individual.

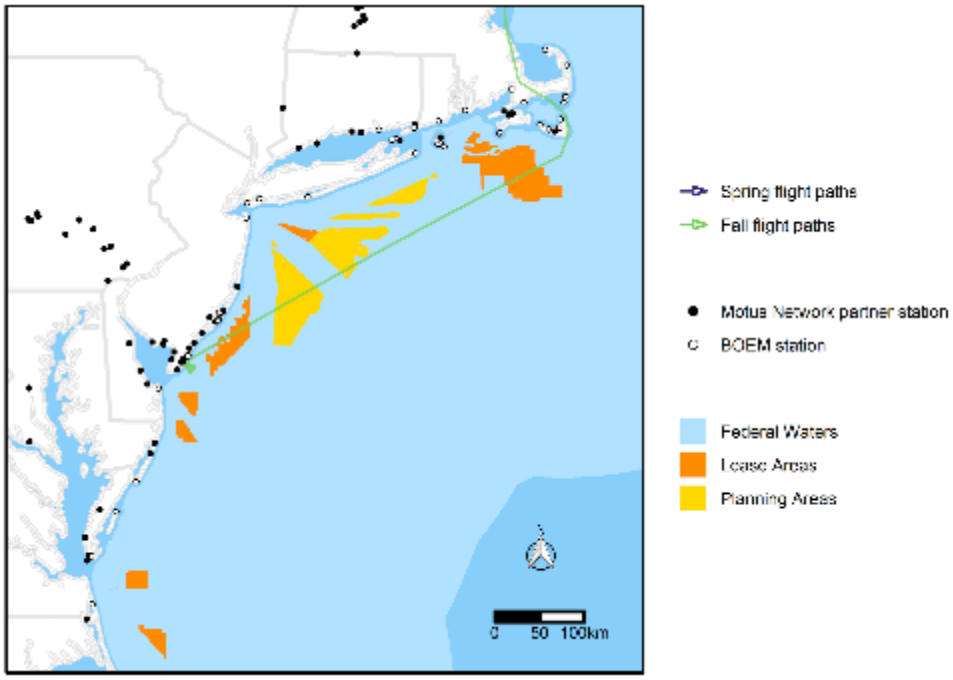

Figure 25. Modeled flight paths of Whimbrel (*n* = 1) crossing the Study Area during fall migration in 2017.

Arrows indicate direction and location of the last detection in the Study Area for each individual.

3.3.3 Exposure to Federal Waters

In the fall, 81% (436 of 541) of shorebirds that met the criteria to be included in our analysis of exposure to Federal waters had tracks that intersected with Federal waters. Estimated exposure to Federal waters varied by species (Table 8). Among species with observations from more than 10 individuals tracked during fall, estimated number of individuals exposed to Federal waters ranged from 51% (Least Sandpiper) to 87% (White-rumped Sandpiper).

In the spring, 31% (19 of 62) of shorebirds that met the criteria to be included in our analysis of exposure had tracks that intersected with Federal waters. The lower estimated exposure rate during spring compared to the fall is likely in large part because all but one of the birds included in our spring analysis had already arrived on the US Atlantic coast before being tagged (Table 6). Among species with observations from more than 10 individuals tracked during spring (Red Knot and Semipalmated Sandpiper), estimated exposure to Federal was similar (26% and 28% of individuals, respectively).

Table 8. Estimated proportion of shorebirds exposed to Federal waters (FW) between 2014 and 2017 during spring and fall migration. Seasonal totals shown in bold.

Species	Season	Total # of individuals	# of individuals exposed to FW	Proportion exposed to FW
Black-bellied Plover	Fall	4	3	0.75
Dunlin	Fall	1	1	1.00
Least Sandpiper	Fall	23	12	0.52
Lesser Yellowlegs	Fall	2	1	0.50
Pectoral Sandpiper	Fall	9	7	0.78
Red Knot	Fall	146	118	0.81
Ruddy Turnstone	Fall	17	14	0.82
Sanderling	Fall	60	48	0.80
Semipalmated Plover	Fall	47	33	0.70
Semipalmated Sandpiper	Fall	170	145	0.85
Whimbrel	Fall	1	1	1.00
White-rumped Sandpiper	Fall	61	53	0.87
	Fall (total)	**541**	**436**	**0.81**
Red Knot	Spring	31	8	0.26
Ruddy Turnstone	Spring	5	4	0.80
Sanderling	Spring	1	0	0.00
Semipalmated Sandpiper	Spring	25	7	0.28
	Spring (total)	**62**	**19**	**0.31**

3.3.4 Temporal and Meteorological Variation in Exposure to Federal Waters

During both the spring and the fall, most estimated exposure events occurred during high visibility conditions (> 19 km, Fig. 26). In the spring, more estimated exposure events occurred during periods of reduced visibility (0 - 10 km) compared to non-exposure events (Fig. 26). In the fall, the opposite pattern occurred, with more estimated exposure events occurring during periods of high visibility (> 19 km) compared to non-exposure events (Fig. 26). Precipitation during estimated exposure events and non-exposure events was similar and generally low (< 3 kg/m², Fig. 27). During both spring and fall, non-exposure events were distributed relatively evenly by hour of day. In contrast, more estimated exposure events occurred during late afternoon and nocturnal hours compared to other times of day (Fig. 28).

Across all species, estimated exposure events ranged from May 10th to June 4th in the spring and July 3rd to Nov 29th in the fall. Peaks in the dates of estimated exposure to Federal waters varied by species, but generally most estimated exposure events occurred either at the beginning and/or end of the date ranges

that each species was detected in the Study Area during each migration season (Fig. 29). The most common pattern was a peak in exposure at the beginning of each species detection range in the Study Area during the fall (e.g. Red Knot, Least Sandpiper, Sanderling, Fig. 29). Patterns in the spring were less clear likely because data was available for fewer individuals and species (Table 8).

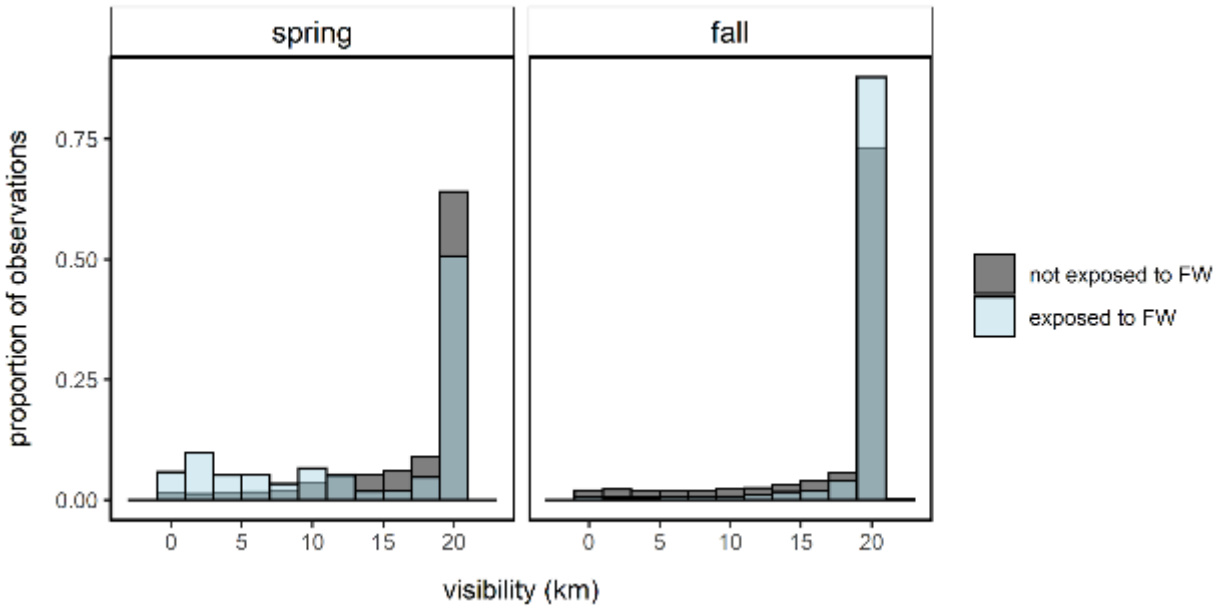

Figure 26. Distribution of visibility (m) during Federal water (FW) exposure events compared to non-exposure events in the spring and fall from 2014 to 2017 with data from all shorebirds pooled by species.

Light blue shows the distribution of visibility during exposure events, grey shows the distribution during non-exposure events and dark blue shows the overlap of the distributions. The y-axis indicates the proportion of observations falling within each bin (binwidth = 2 km) with each observation corresponding to a modeled location estimates (1-minute temporal resolution).

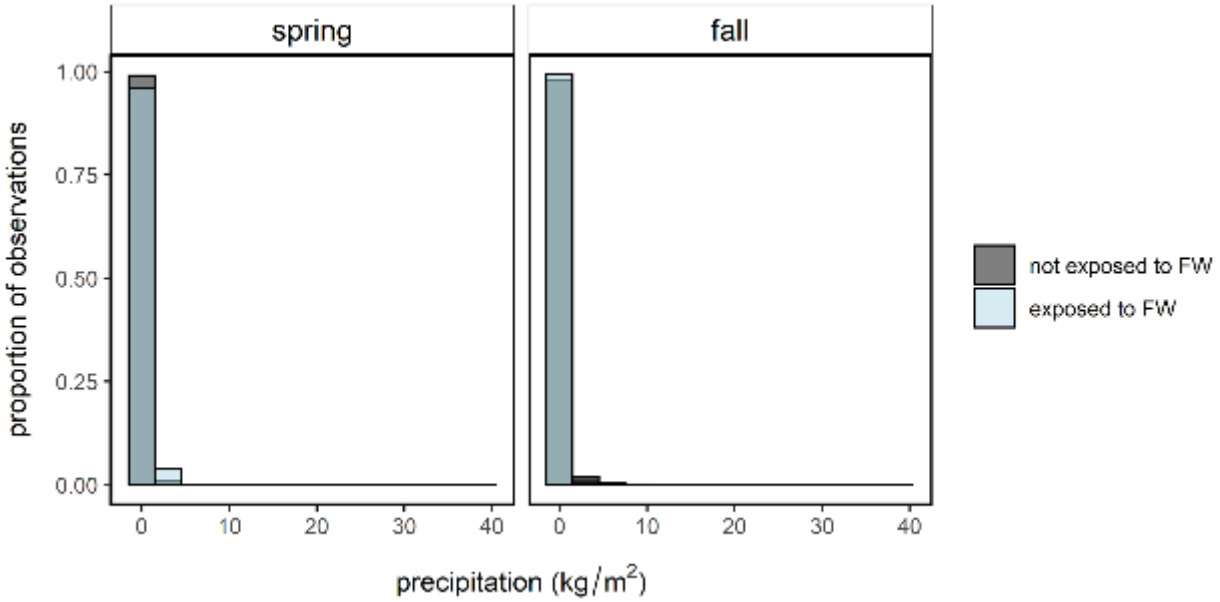

Figure 27. Distribution of precipitation (kg/m²) during Federal water (FW) exposure events compared to non-exposure events in the spring and fall from 2014 to 2017 with data from all shorebirds pooled by species.

Light blue shows the distribution of precipitation during exposure events, grey shows the distribution during non-exposure events and dark blue shows the overlap of the distributions. The y-axis indicates the proportion of observations falling within each bin (binwidth = 3 kg/m²) with each observation corresponding to a modeled location estimates (1-minute temporal resolution).

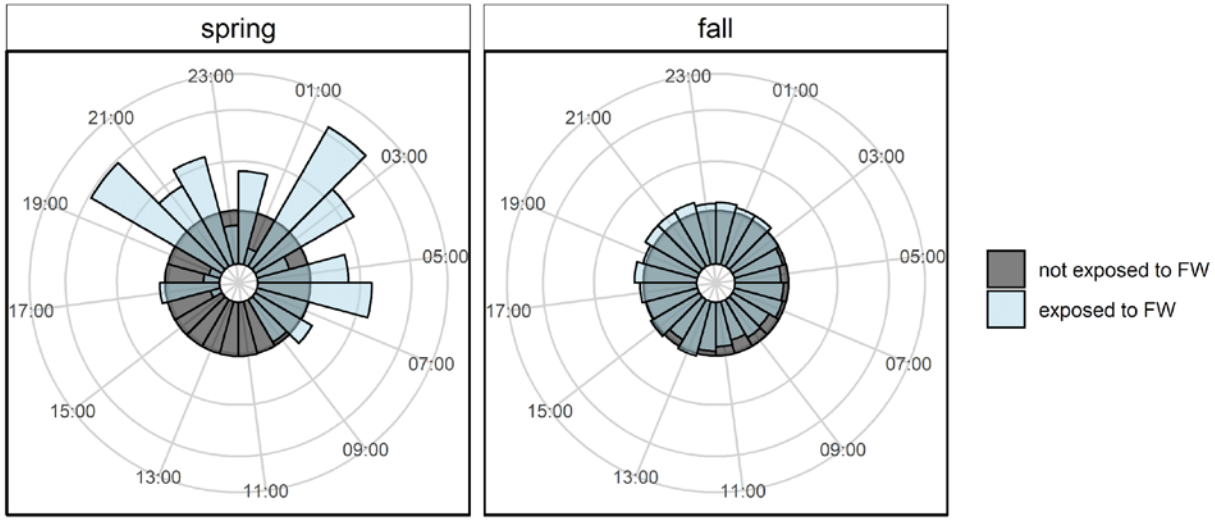

Figure 28. Diel variation (hrs, EST) during Federal water (FW) exposure events compared to non-exposure events in the spring and fall from 2014 to 2017 with data from all shorebirds pooled by species.

Light blue shows the distribution of time of day during exposure events, grey shows the distribution during non-exposure events and dark blue shows the overlap of the distributions. The length of the bars indicates the proportion of observations falling within each bin (binwidth = 1 hour) with each observation corresponding to a modeled location estimates (1-minute temporal resolution).

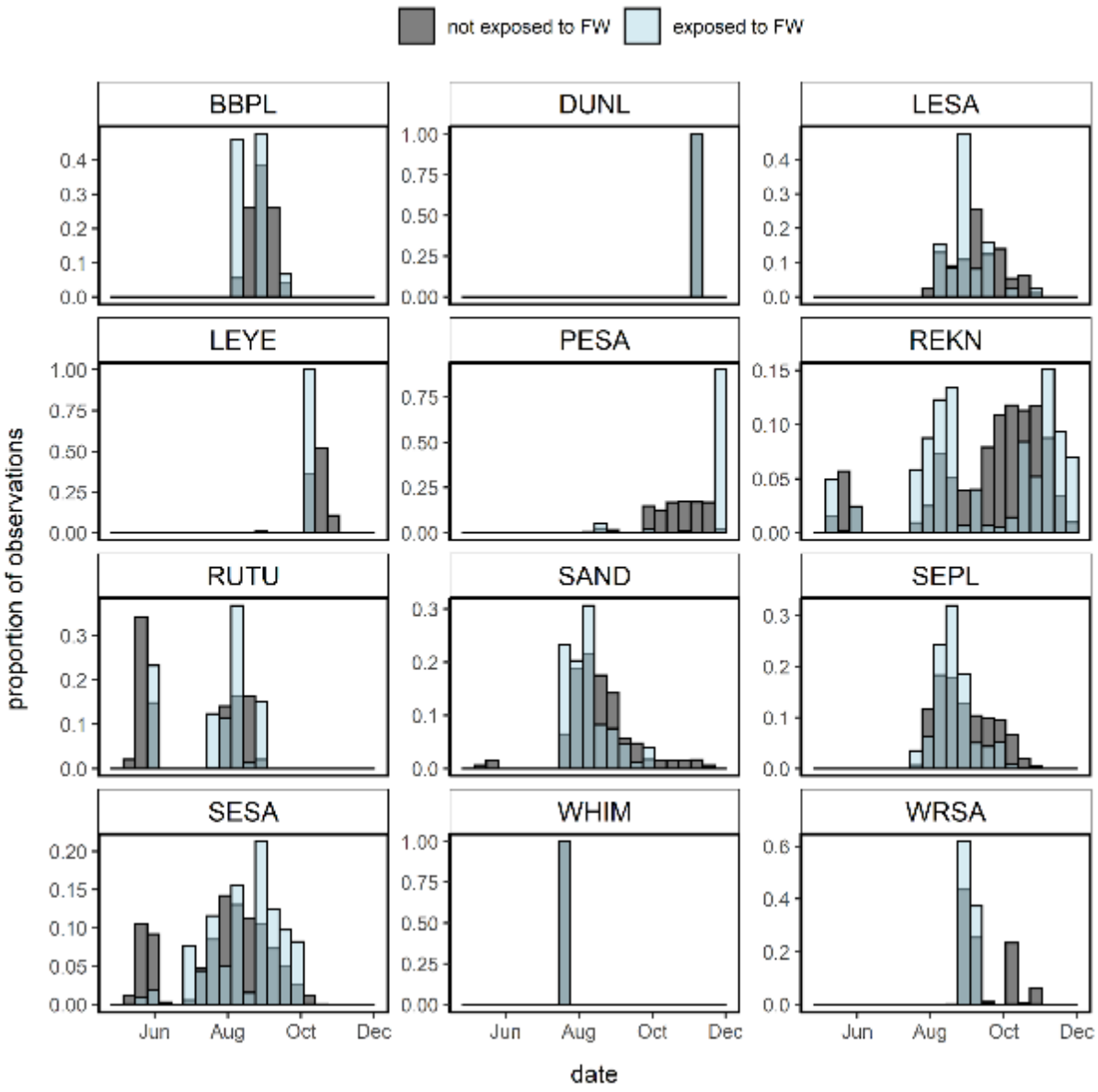

Figure 29. Distribution of calendar date of Federal water exposure events compared to non-exposure events in the spring and fall from 2014 to 2017.

Light blue shows the distribution of dates during exposure events, grey shows the distribution during non-exposure events and dark blue shows the overlap of the distributions. The y-axis indicates the proportion of observations falling within each bin (binwidth = 10 days) with each observation corresponding to a modeled location estimates (1-minute temporal resolution). Species codes: BBPL - Black-bellied Plover, DUNL - Dunlin, LESA - Least Sandpiper, LEYE - Lesser Yellowlegs, PESA - Pectoral Sandpiper, REKN - Red Knot, RUTU - Ruddy Turnstone, SAND - Sanderling, SEPL - Semipalmated Plover, SESA - Semipalmated Sandpiper, WHIM - Whimbrel, WRSA - White-rumped Sandpiper.

3.4 Integrated Covariate Analysis of Exposure to Federal Waters

3.4.1 Spring Migration

Two species (Red Knot and Semipalmated Sandpiper) had sufficient tracking data during spring migration ($n \geq 10$ individuals tracked in Study Area) to be included in the Boosted GAM analysis of exposure to Federal waters. During the spring migration period, wind speed at flight altitudes had the strongest influence on occurrence in Federal Waters, both in terms of selection among boosts (Table 9) and the magnitude of predicted response (Fig. 30). Date (Fig. 31) and wind direction (Fig. 32) were also predictive of exposure to Federal waters during spring migration. Exposure was highest in moderately strong winds (~10 m/s; Fig. 30) blowing to the north (onshore; Fig. 32) in May and early June (Fig. 31). The small sample size in spring (n = 40 3-hour periods of non-stop flight over Federal waters) resulted in large uncertainty in the confidence intervals particularly among covariates with lesser influence: precipitation (Fig. 33), visibility (Fig. 34), and atmospheric pressure (Fig. 35).

Table 9. Description and selection frequencies of covariates in binomial Boosted GAM analysis of exposure of shorebirds to Federal waters in spring.

Covariate (units)	Fitting function	Selection Frequency
Wind speed (m/s)	p-spline	0.52
Date (Julian)	p-spline	0.18
Wind direction (° true N)	cyclical p-spline	0.14
Precipitation (kg/m^2)	p-spline	0.08
Visibility (m)	p-spline	0.07
Atmospheric pressure (Pa)	p-spline	0.01
Air temperature (°C)	P-spline	0.00
Hour of day (EST)	Cyclical p-spline	0.00
Species	Categorical (REKN, SESA)	0.00
Date (Julian) * Species	Interaction term	0.00
Bird ID	Random intercept	0.00

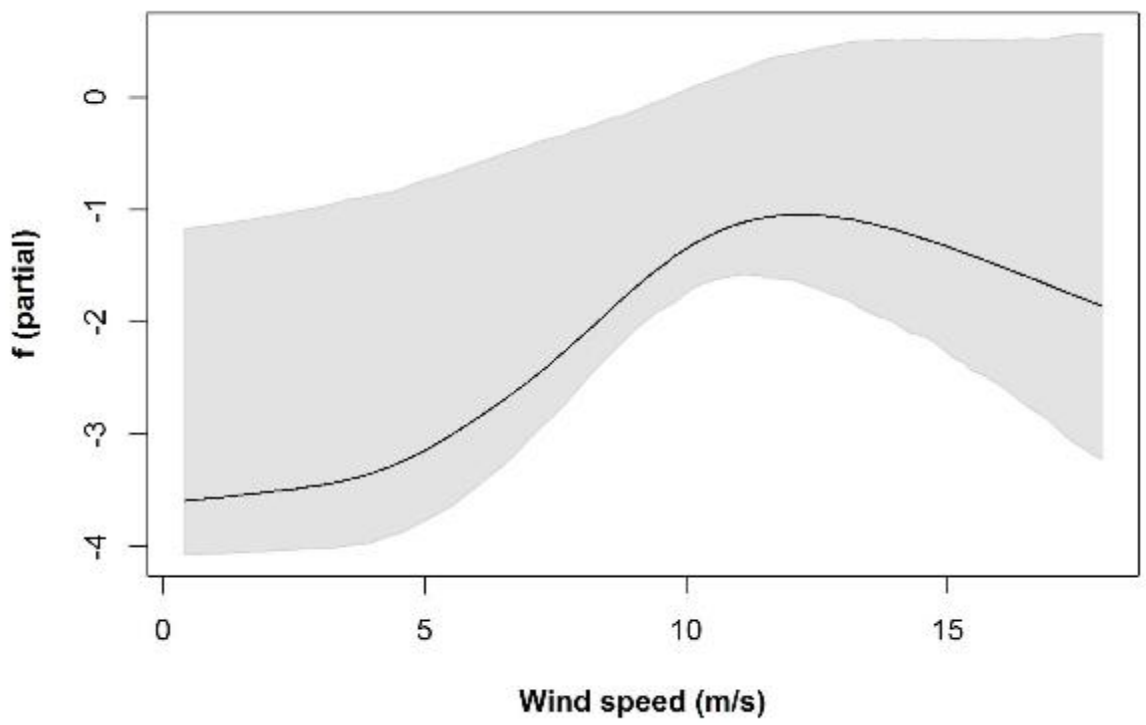

Figure 30. Boosted GAM prediction for the partial contribution of the wind speed covariate (x-axis, in m/s) to the likelihood (logit-transformed odds ratio) of exposure to Federal waters among shorebirds tracked during spring migration.

The gray-shaded area represents the 95% confidence interval for the response based on 1,000 bootstrapped models.

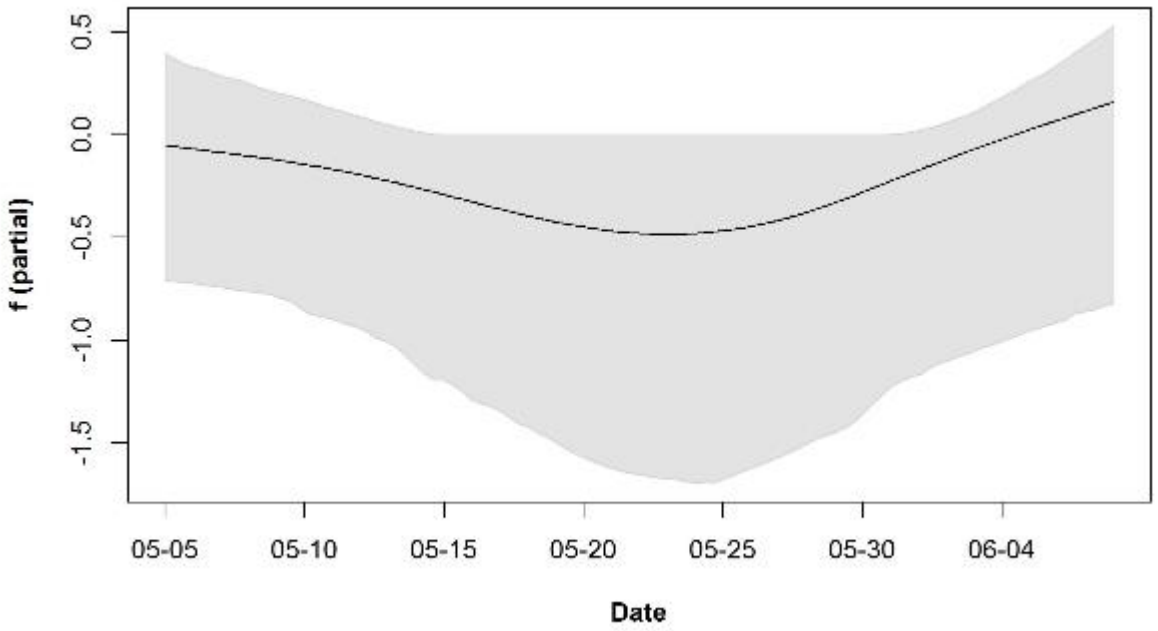

Figure 31. Boosted GAM prediction for the partial contribution of the date covariate (x-axis) to the likelihood (logit-transformed odds ratio) of exposure to Federal waters among shorebirds tracked during spring migration.

The gray-shaded area represents the 95% confidence interval for the response based on 1,000 bootstrapped models.

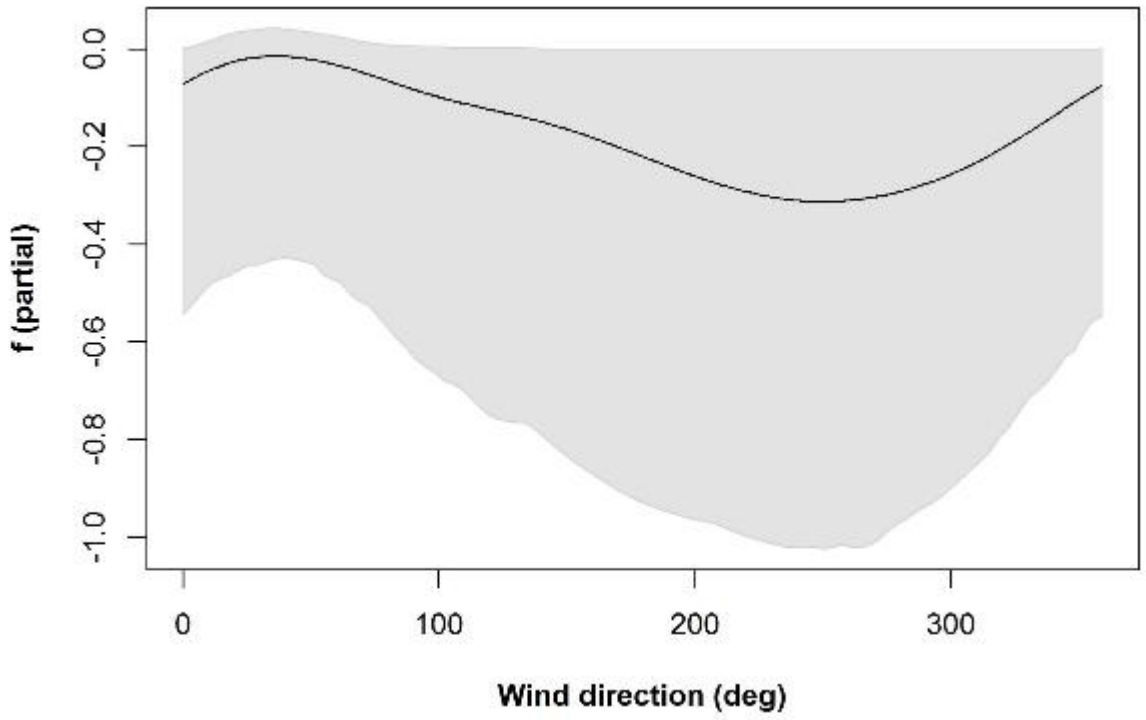

Figure 32. Boosted GAM prediction for the partial contribution of the wind direction covariate (x-axis, in degrees relative to true N) to the likelihood (logit-transformed odds ratio) of exposure to Federal waters among shorebirds tracked during spring migration.
The gray-shaded area represents the 95% confidence interval for the response based on 1,000 bootstrapped models.

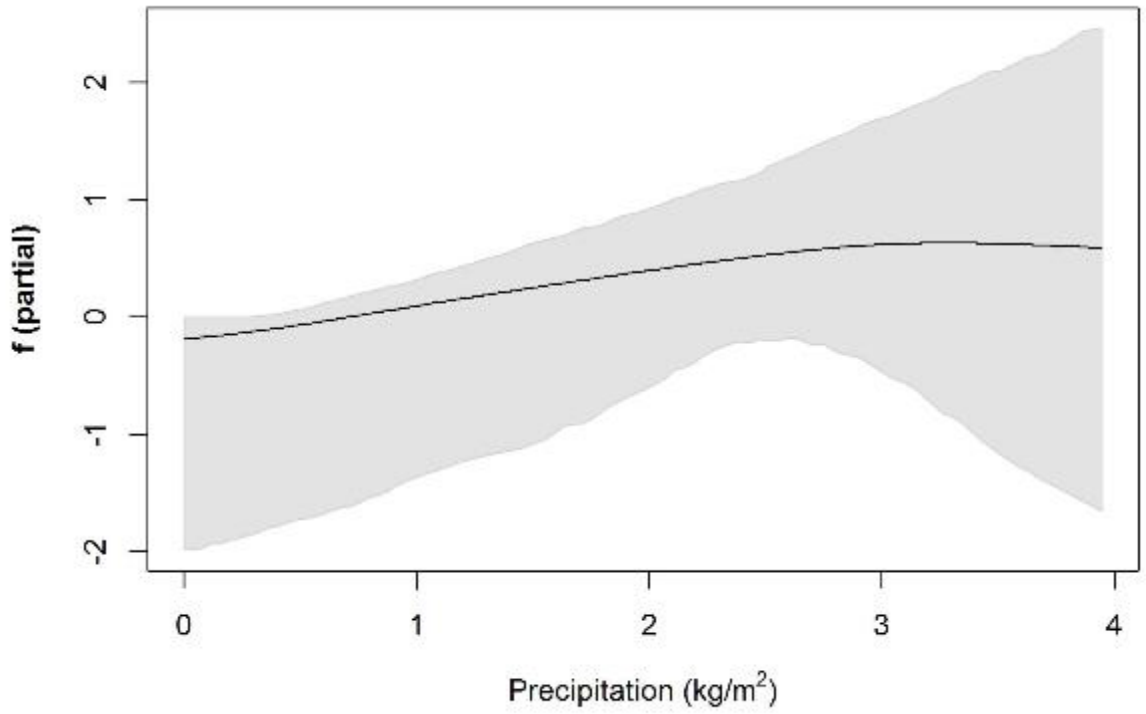

Figure 33. Boosted GAM prediction for the partial contribution of the precipitation accumulation covariate (x-axis, in kg/m^2) to the likelihood (logit-transformed odds ratio) of exposure to Federal waters among shorebirds tracked during spring migration.
The gray-shaded area represents the 95% confidence interval for the response based on 1,000 bootstrapped models.

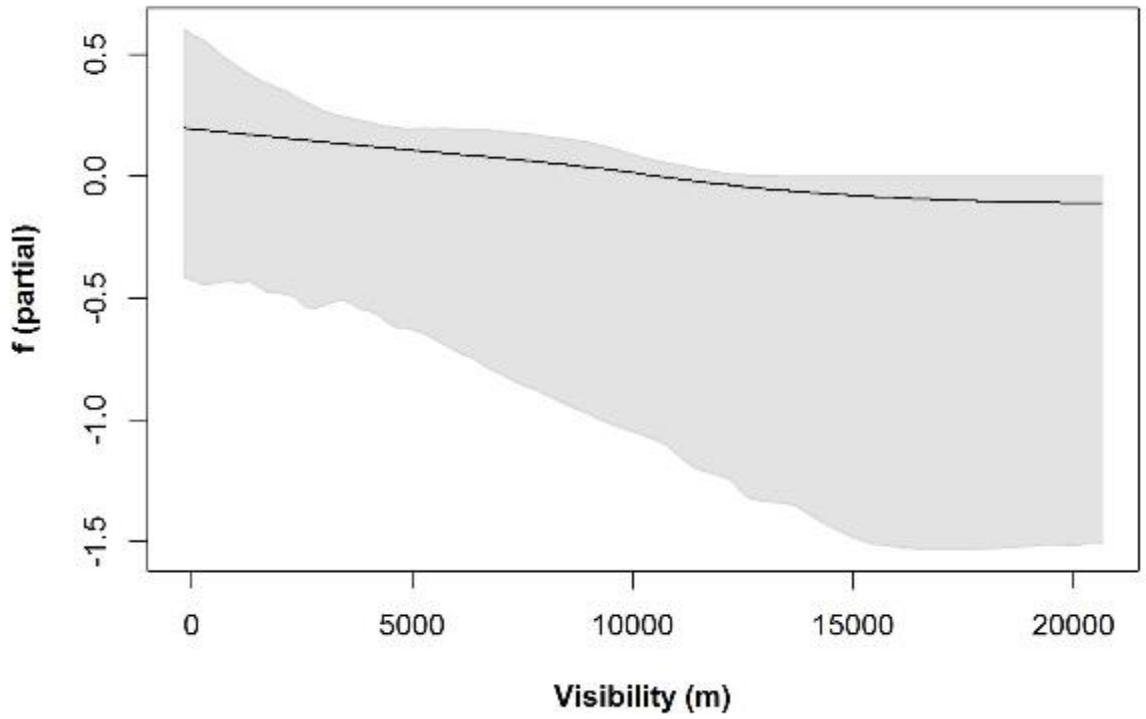

Figure 34. Boosted GAM prediction for the partial contribution of the visibility covariate (x-axis, in m) to the likelihood (logit-transformed odds ratio) of exposure to Federal waters among shorebirds tracked during spring migration.

The gray-shaded area represents the 95% confidence interval for the response based on 1,000 bootstrapped models.

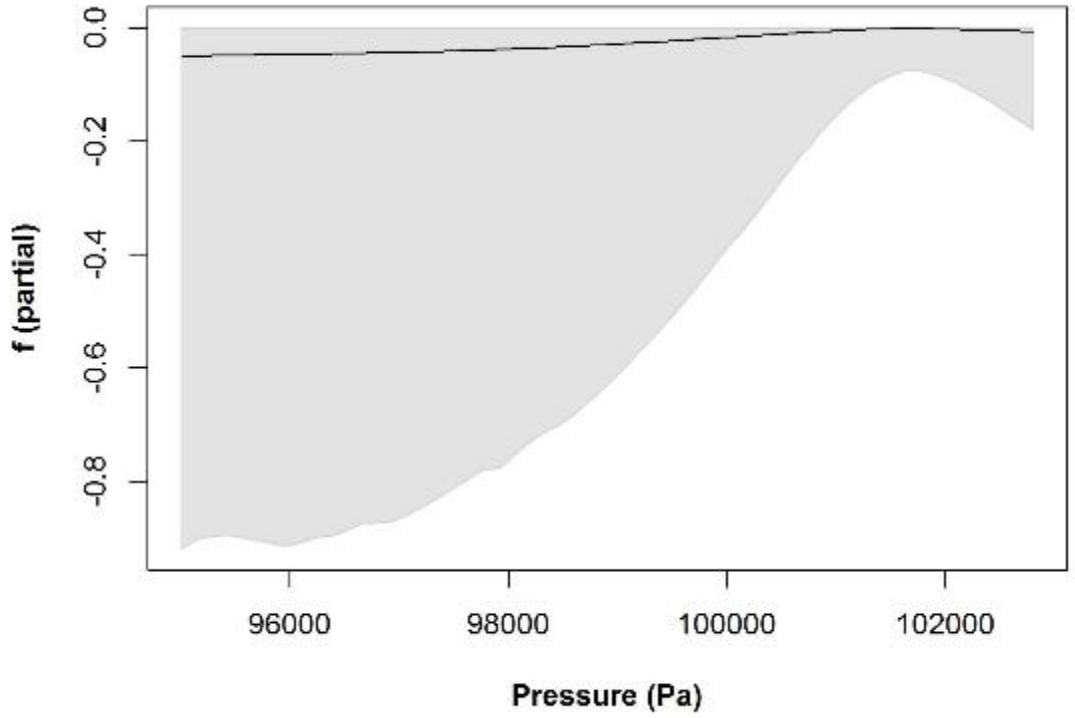

Figure 35. Boosted GAM prediction for the partial contribution of the atmospheric pressure covariate (x-axis, in Pa) to the likelihood (logit-transformed odds ratio) of exposure to Federal waters among shorebirds tracked during spring migration.
The gray-shaded area represents the 95% confidence interval for the response based on 1,000 bootstrapped models.

3.4.2 Fall Migration

Seven species (Least Sandpiper, Red Knot, Ruddy Turnstone, Sanderling, Semipalmated Plover, Semipalmated Sandpiper, and White-rumped Sandpiper) had sufficient tracking data during spring migration ($n \geq 10$ individuals tracked in Study Area) to be included in the Boosted GAM analysis of exposure to Federal waters. During the fall migration period, the species covariate had the strongest influence on occurrence in Federal waters, both in terms of selection among boosts (Table 10) and the magnitude of predicted response (Fig. 36). Relative to other species tracked, White-rumped Sandpipers had the highest predicted occurrence in Federal waters versus in coastal areas, indicating that most made direct flights through the Study Area into offshore waters, rather than spending time at staging areas along the coast. Red Knots had the lowest predicted occurrence in Federal waters, indicating that they spent more time at coastal sites within the Study Area relative to other species tracked. Wind direction (Fig. 37), date (Fig. 38), and atmospheric pressure (Fig. 39) were also predictive of exposure to Federal waters. Estimated exposure to Federal waters was highest during July, decreased into October and increased slightly in November (Fig. 38). Exposure was highest when winds were blowing to the south-southeast (offshore; Fig. 37) and atmospheric pressure was high (Fig. 39).

Table 10. Description and selection frequencies of covariates in binomial Boosted GAM analysis of exposure of shorebirds to Federal waters in fall.

Covariate (units)	Fitting function	Selection Frequency
Species	Categorical	0.33
Wind direction (° true N)	cyclical p-spline	0.31
Date (Julian)	p-spline	0.24
Atmospheric pressure (Pa)	p-spline	0.13
Wind speed (m/s)	p-spline	0.00
Precipitation (kg/m^2)	p-spline	0.00
Visibility (m)	p-spline	0.00
Air temperature (°C)	P-spline	0.00
Hour of day (EST)	Cyclical p-spline	0.00
Age	Categorical (HY, AHY, U)	0.00
Date (Julian) * Age	Interaction term	0.00
Bird ID	Random intercept	0.00

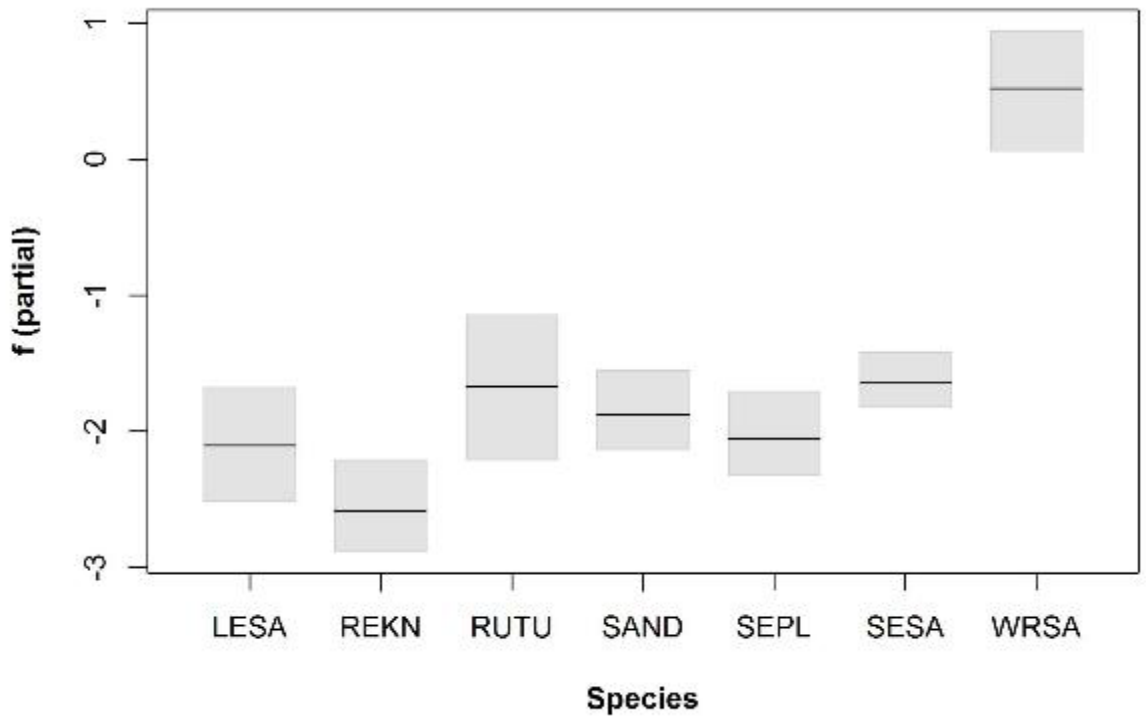

Figure 36. Boosted GAM prediction for the partial contribution of the species covariate (x-axis) to the likelihood (logit-transformed odds ratio) of exposure to Federal waters among shorebirds tracked during fall migration.

The gray-shaded area represents the 95% confidence interval for the response based on 1,000 bootstrapped models.

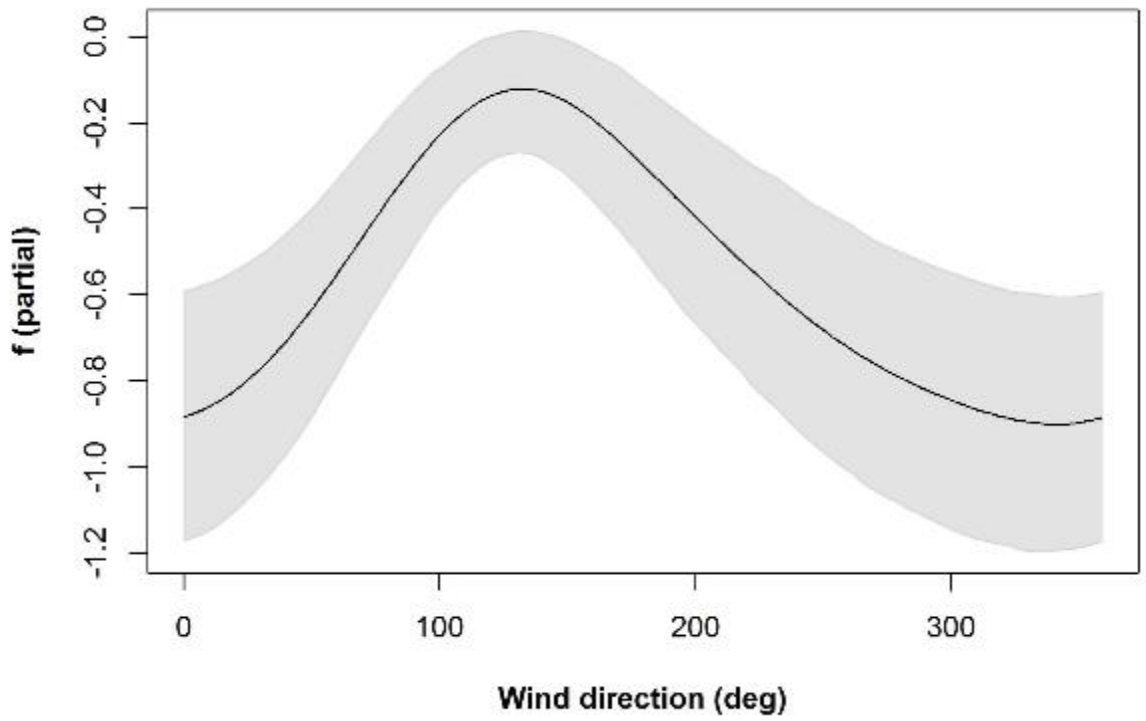

Figure 37. Boosted GAM prediction for the partial contribution of the wind direction covariate (x-axis, in ° true N) to the likelihood (logit-transformed odds ratio) of exposure to Federal waters among shorebirds tracked during fall migration.

The gray-shaded area represents the 95% confidence interval for the response based on 1,000 bootstrapped models.

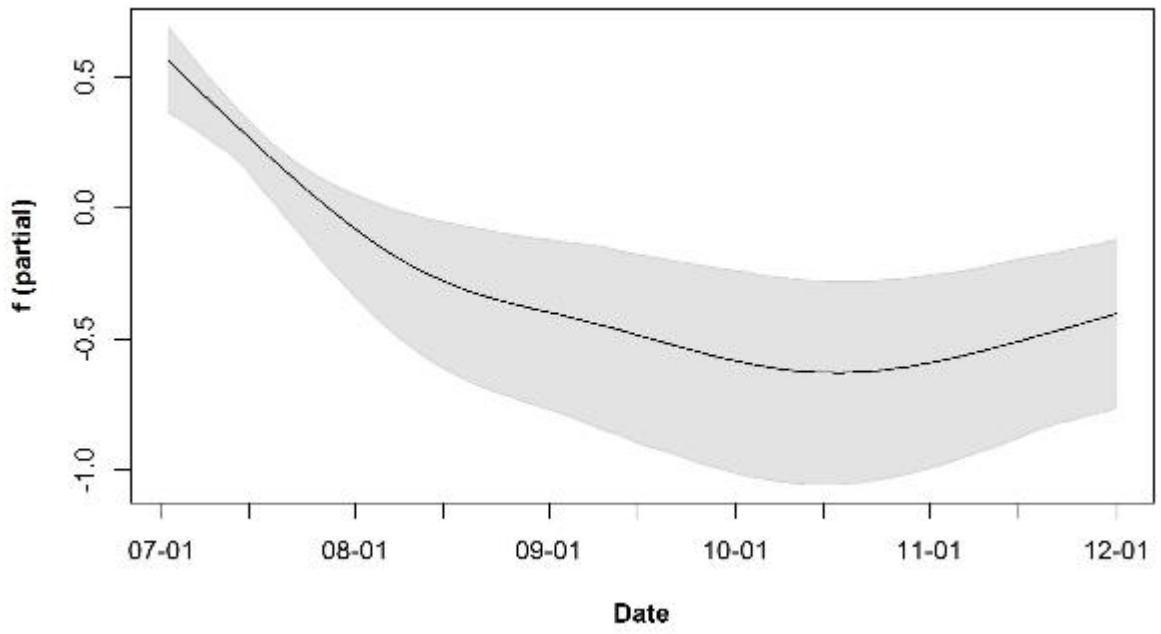

Figure 38. Boosted GAM prediction for the partial contribution of the date covariate (x-axis) to the likelihood (logit-transformed odds ratio) of exposure to Federal waters among shorebirds tracked during fall migration.

The gray-shaded area represents the 95% confidence interval for the response based on 1,000 bootstrapped models.

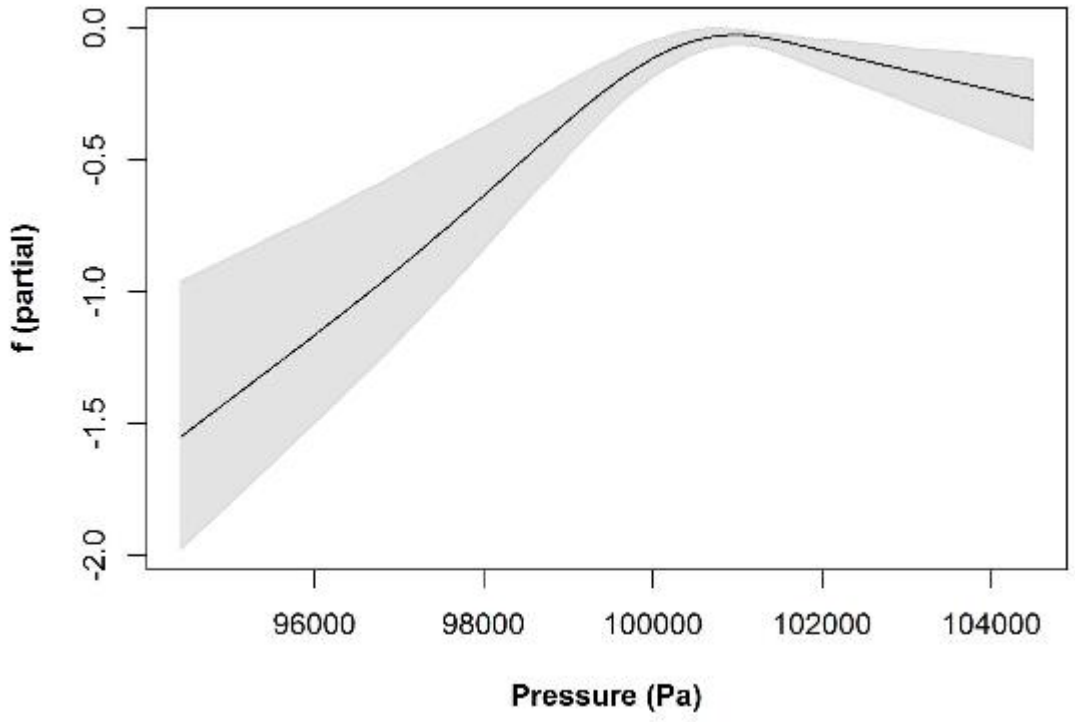

Figure 39. Boosted GAM prediction for the partial contribution of the atmospheric pressure covariate (x-axis, in Pa) to the likelihood (logit-transformed odds ratio) of exposure to Federal waters among shorebirds tracked during fall migration.
The gray-shaded area represents the 95% confidence interval for the response based on 1,000 bootstrapped models.

3.5 Distribution of Flight Altitudes Over Federal Waters

We summarized flight altitudes of the 436 individuals in fall and 19 individuals in spring that were included in the covariate analysis of exposure to Federal waters (Table 8). During non-stop flights over Federal waters, flight altitudes varied greatly (28 - 2,940 m asl) but mostly occurred above the upper-limit of the RSZ (250 m asl). Overall mean flight altitudes were 914 m during spring and 545 m during fall (Table 11). Nonetheless, frequency of predicted occurrence within the RSZ was non-trivial, with 24% of mean flight altitudes occurring within the RSZ during spring and 36% during fall. Frequency of occurrence in the RSZ during night and day was similar during the fall but markedly different in spring (40% during the day and none at night); however, the sample sizes were much smaller in spring than in fall (Table 11).

Figures 40 and 41 show altitude distributions, and uncertainty within altitude bins for spring and fall, during day and night. Even considering the broad ranges of uncertainty, the RSZ overlapped with an

average of 11% of each altitude range during spring and 14% of each altitude range during fall (Table 11).

Table 11. Model-estimated flight altitudes (m) of shorebirds during non-stop flights over Federal waters in spring and fall, and during the day and night, with sample size (number of 3-hour time intervals) and percentage of estimated occurrence within the rotor swept zone (25-250 m) among mean altitudes and altitude ranges (5-95%).

Season	Time of Day	Mean Altitude (5-95% Range)	Sample Size (*n*)	Mean Altitude in RSZ (%)	Altitude Range in RSZ (%)
Spring	All	914 (53-2,495)	25	24	11
	Day	616 (53-1,251)	15	40	18
	Night	1,361 (685-2,940)	10	0	1
Fall	All	545 (28-1,510)	691	36	14
	Day	561 (28-1,580)	419	36	13
	Night	521 (28-1,440)	272	36	14

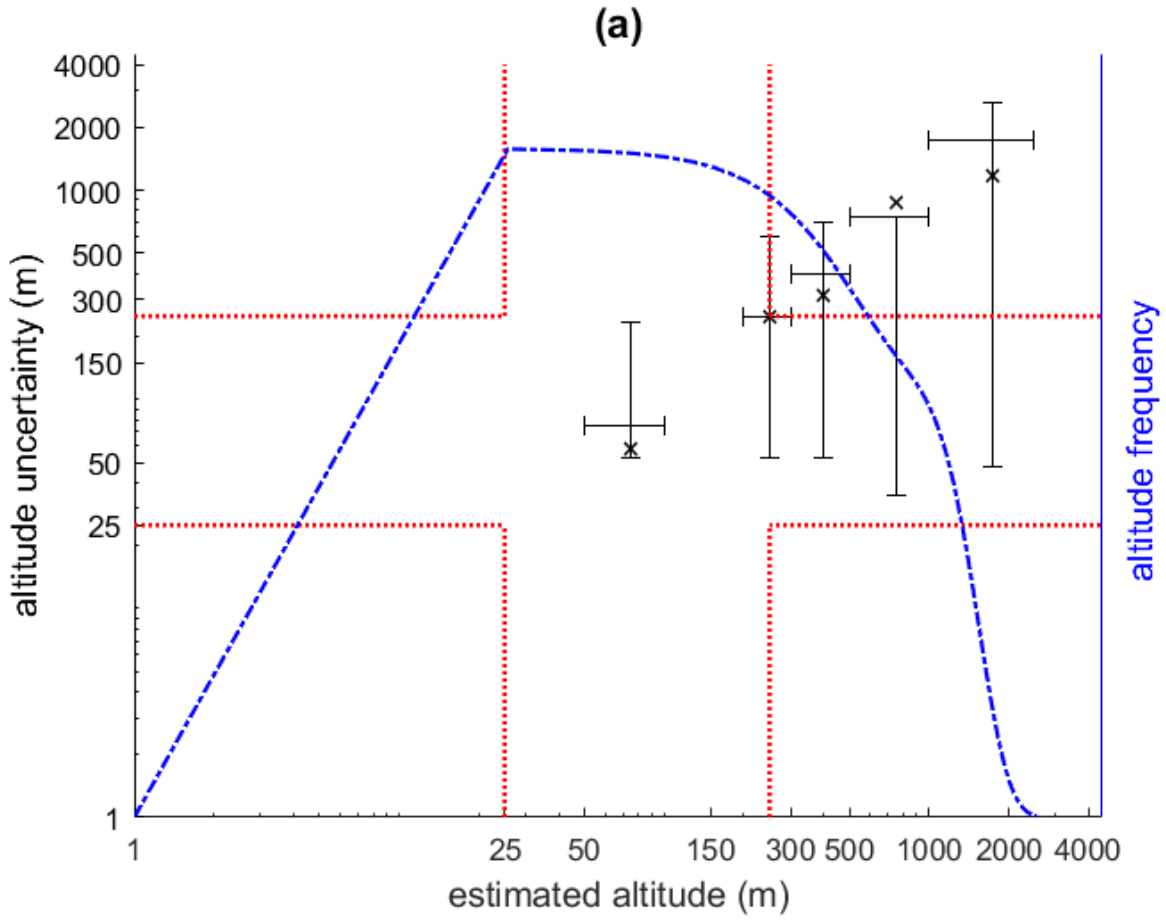
(a)
4000
2000
1000
500
300
150
50
25
1
altitude uncertainty (m)
1
25
50
150
300
500
1000
2000
4000
estimated altitude (m)
altitude frequency

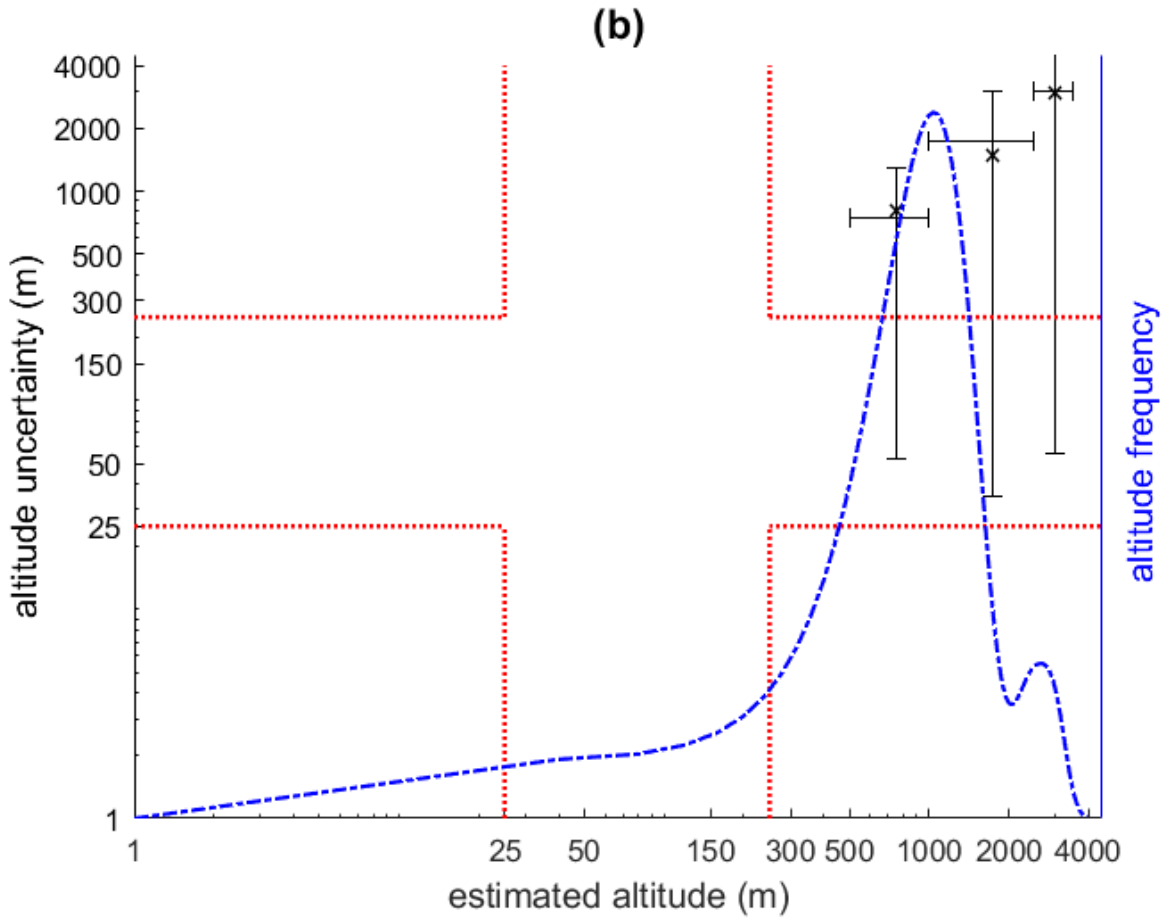

Figure 40. Uncertainty in (left y-axis) and relative frequency of (right y-axis) predicted flight altitudes of shorebirds in the spring during exposure to Federal waters during (a) day and (b) night.

The horizontal bars represent ranges within altitudinal bins (beginning from 2, 25, 50, 100, 200, 300, 500, 1000, 2500 - 3500 m) and vertical bars represent the model-estimated range of flight altitudes falling within those bins, with the mean within-bin altitude shown as a black cross. The blue dashed line represents the frequency distribution of altitudes (m) among all 3-hour intervals during estimated exposure to Federal waters. The red dot-dashed line delineates the bounds of the altitude range of the RSZ (25 to 250 m asl).

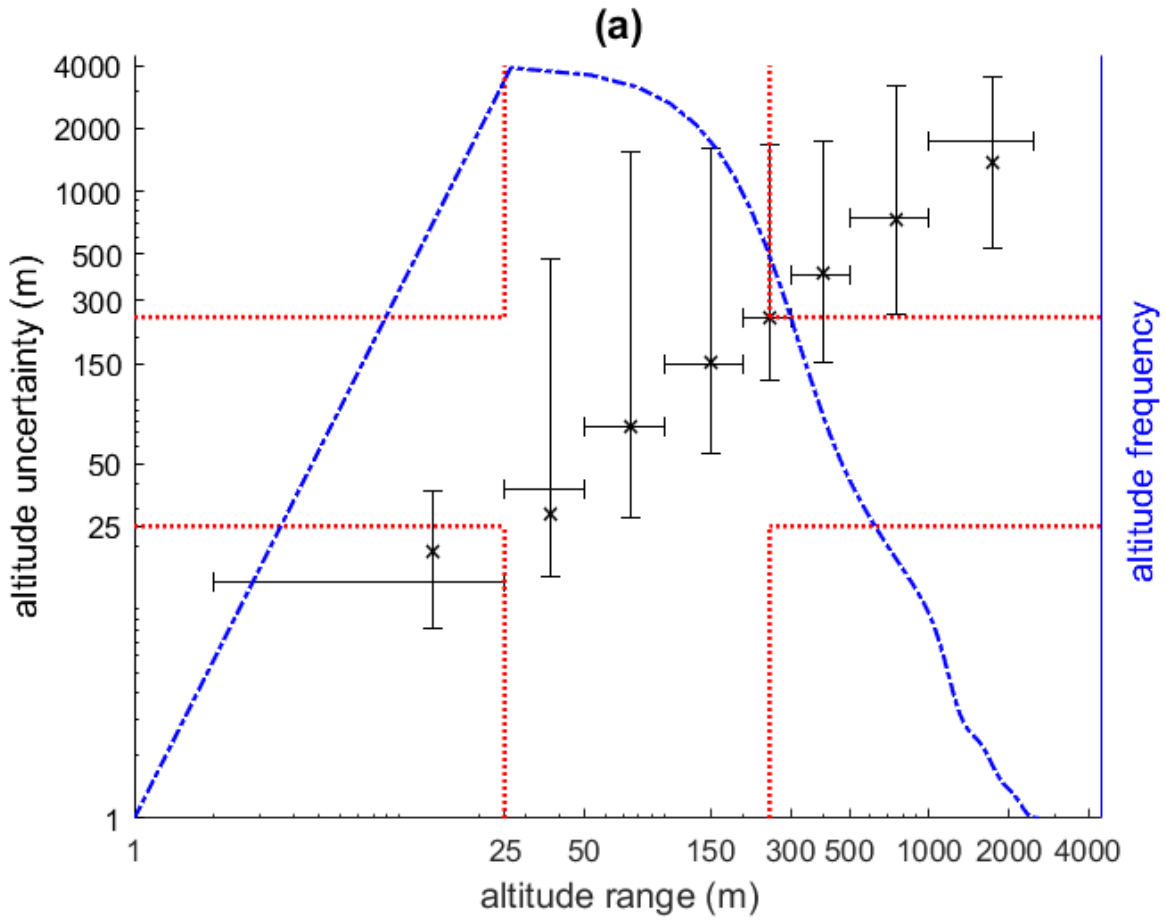
(a)
4000
2000
1000
500
300
150
50
25
1
altitude uncertainty (m)
1
25
50
150
300
500
1000
2000
4000
altitude range (m)
altitude frequency

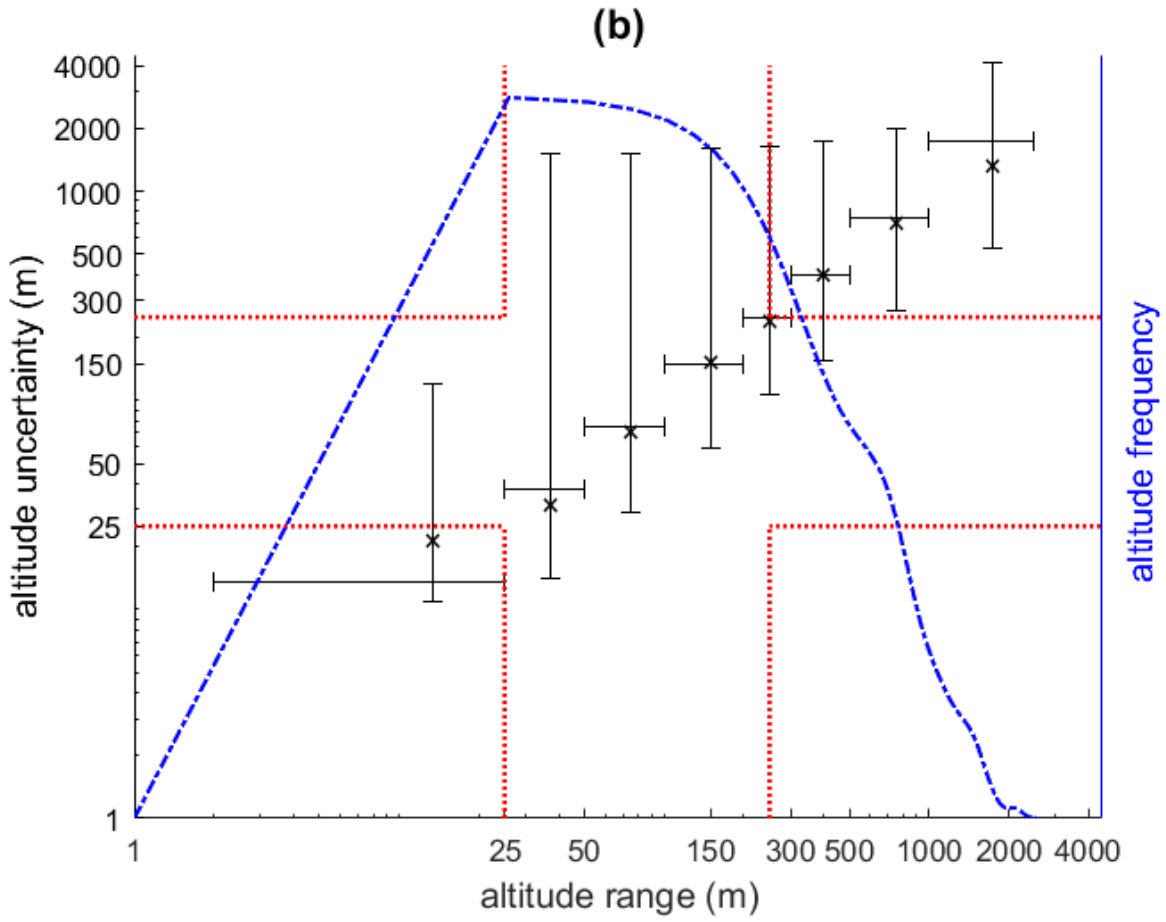

Figure 41. Uncertainty in (left y-axis) and relative frequency of (right y-axis) predicted flight altitudes of shorebirds in the fall during exposure to Federal waters during (a) day and (b) night.

The horizontal bars represent ranges within altitudinal bins (beginning from 2, 25, 50, 100, 200, 300, 500, 1000, 2500 - 3500 m) and vertical bars represent the model-estimated range of flight altitudes falling within those bins, with the mean within-bin altitude shown as a black cross. The blue dashed line represents the frequency distribution of altitudes (m) among all 3-hour intervals during estimated exposure to Federal waters. The red dot-dashed line delineates the bounds of the altitude range of the RSZ (25 to 250 m asl).

3.6 Departure Bearings from the Study Area

During spring migration, Red Knots primarily departed from the Study Area to the north (mean 3° true N) whereas Semipalmated Sandpipers departed to the northeast (mean 42° true N). The spread (ρ) of departure directions during spring migration was slightly higher for Red Knots ($\rho = 0.44$) relative to Semipalmated Sandpipers ($\rho = 0.54$, Table 12, Fig. 42).

Species tracked during fall migration primarily departed from the Study Area to the south-southeast (mean 160° to 180° true N). Mean departure directions of Least Sandpipers and White-rumped Sandpipers were primarily southeast (offshore). Sanderlings primarily departed to the southwest (mean 208° true N), indicating a prevalence of nearshore flights along the mid-Atlantic coast and Bight. Directional headings of fall migratory departure flights were most concentrated among White-rumped Sandpipers ($\rho = 0.75$) and Ruddy Turnstones ($\rho = 0.70$). Red Knots had the largest spread in directional departure headings during fall migration ($\rho = 0.14$), indicating a wide range variability including coastal to offshore departure flights (Table 13, Fig. 43).

Table 12. Heading (in ° relative to true N) and mean resultant length (ρ) of spring migratory departure flights from Study Area by species and number of birds tracked (*n*).

Species	*n*	Heading (° true N)	ρ
Red Knot	31	3	0.54
Semipalmated Sandpiper	25	42	0.44

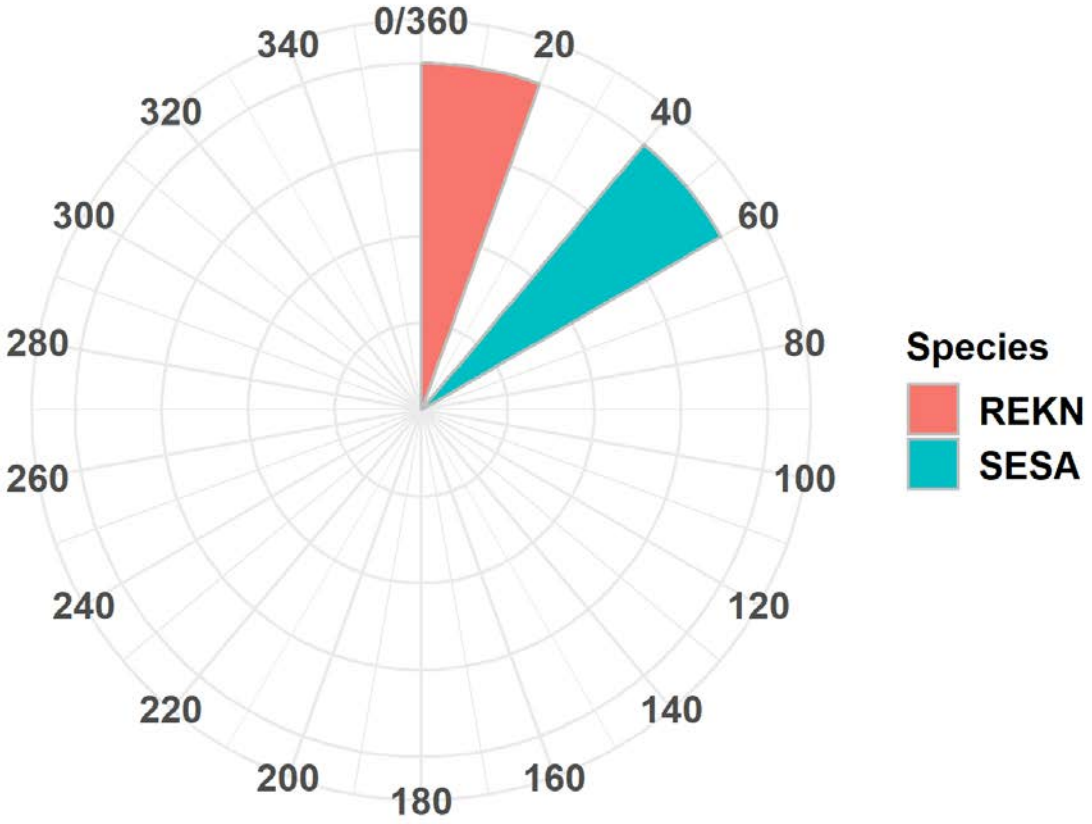

Figure 42. Circular mean heading (in ° relative to true N) of spring migratory departure flights from the Study Area by species.
Red Knot (REKN; *n* = 31) and Semipalmated Sandpiper (SESA; *n* = 25).

Table 13. Heading (in ° relative to true N) and mean resultant length (ρ) of fall migratory departure flights from Study Area by species and number of birds tracked (*n*).

Species	*n*	Heading (° true N)	ρ
Least Sandpiper	23	160	0.58
Red Knot	146	164	0.14
Ruddy Turnstone	17	176	0.70
Sanderling	60	208	0.58
Semipalmated Plover	47	162	0.31
Semipalmated Sandpiper	170	170	0.45
White-rumped Sandpiper	61	155	0.75

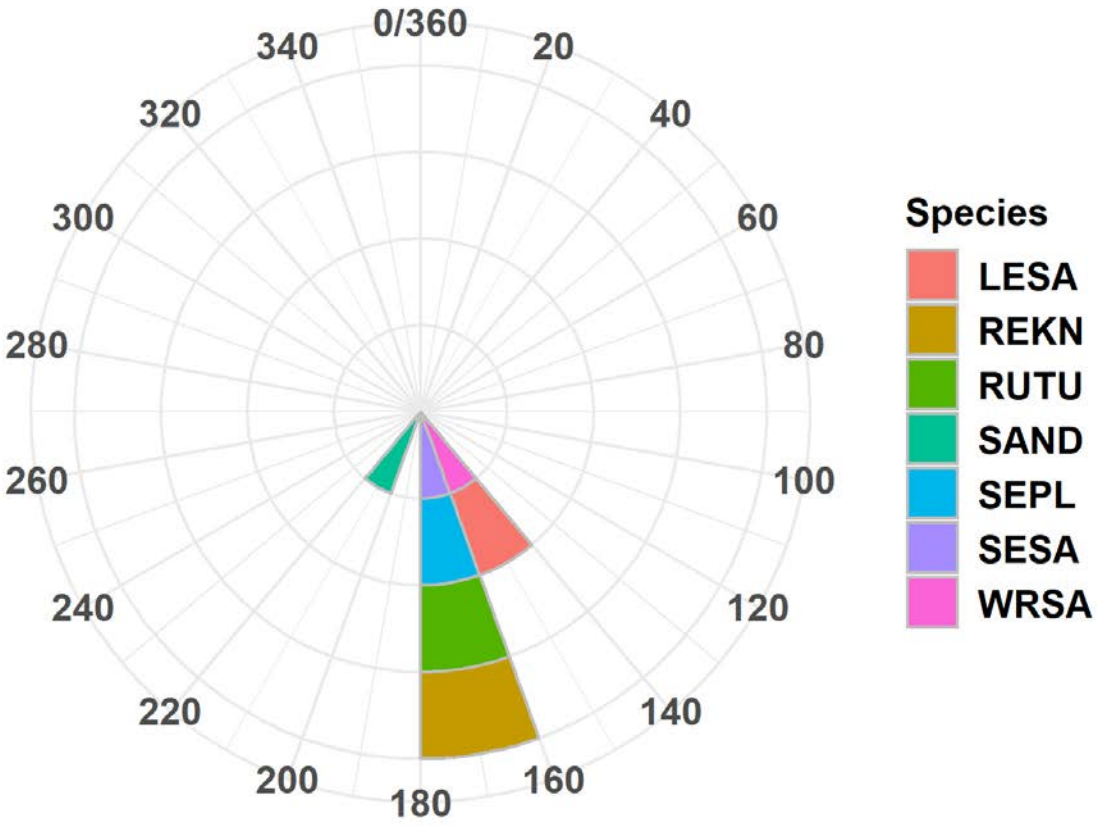

Figure 43. Circular mean heading (in ° relative to true N) of fall migratory departure flights from the Study Area by species.

Least Sandpiper (LESA; *n* = 23), Red Knot (REKN; *n* = 146), Ruddy Turnstone (RUTU, *n* = 17), Sanderling (SAND, *n* = 60), Semipalmated Plover (SEPL; *n* = 47) Semipalmated Sandpiper (SESA; *n* = 170) and White-rumped Sandpiper (WRSA, *n* = 61).

4 Discussion

4.1 Collaboration with Motus Network

In this study, we analyzed data from twelve species of shorebirds tagged by partners in the Motus Wildlife Tracking System, a collaborative automated radio telemetry network, to address information gaps on the movements of shorebirds in the US Atlantic region. Collaborating with the Motus network offered a unique opportunity to synthesize individual movement data from thousands of shorebirds across a large portion of the migratory range, greatly expanding the sample sizes and geographic scale over what had been possible in previous shorebird tracking efforts. These shorebird movement data are particularly relevant to BOEM's avian risk assessments in the US Atlantic OCS because most of the populations represented are in steep decline and use migratory routes that cross the Atlantic Ocean. In particular, the *rufa* Red Knot, which had one of the largest sample sizes in the dataset, is a high priority for BOEM assessments due to its threatened status under the ESA.

In the present study, we refined three-dimensional movement models developed in previous BOEM studies to estimate flight paths and altitudes of shorebirds tracked through a portion of the US Atlantic region where an array of automated radio telemetry stations was established by the USFWS and BOEM for tracking movements of shorebirds and seabirds over adjacent Federal waters (>5.5 km from coast) of the Atlantic OCS (Loring et al 2018, Loring et al. 2019). By applying these models to the large dataset of shorebirds tagged by partners in the Motus network, our overarching objective was to synthesize information on movement patterns of shorebirds in the US mid-Atlantic region, and describe variation by species, age and sex. We explored whether date, time and weather conditions could predict offshore movements of shorebirds into Federal waters of the US Atlantic OCS, where BOEM offshore WEAs are located. Through this assessment, we provide baseline information on shorebird occurrence and behavior in the US Atlantic; information that can inform future assessments of collision risk to shorebirds from development of offshore wind facilities in the US Atlantic OCS.

4.2 Limitations of Data

Collaboration with the Motus network provided access to tracking data from thousands of shorebirds tagged by partners across the Western Hemisphere. However, the opportunistic nature of this analysis meant that our interpretation of movements in the US Atlantic was complicated by several factors, including: 1) uneven tagging effort across time, space, and species; 2) issues with detection probability associated with loss of transmitters fitted with temporary attachment methods (cyanoacrylate gel adhesive); 3) incomplete coverage from tracking stations along the US Atlantic coast due to limited detection ranges; and 5) intermittent spatial and temporal gaps in operation at individual stations due to power loss or other maintenance issues.

We addressed issues associated with uneven sampling effort and tag loss by using a subset of data to estimate use of the Study Area in the US mid-Atlantic region (spanning from Cape Cod, MA to Back Bay, VA), relative to the broader Atlantic Coast. The subset was limited to birds that were detected at least 50 km away from where they were tagged by at least one receiving station located along the Atlantic

coast of North America, between Mingan, QC, Canada in the northeast and Texas, USA in the southwest. To further address variation in numbers of individuals per species tracked per year, we limited the integrated covariate analysis of exposure to Federal waters to species within the subset that had data from at least 10 individuals tracked per season.

Tracking birds at the scale of the US Atlantic coast, including offshore areas, pushes the limits of VHF tracking technology. Incomplete spatial and temporal coverage can greatly complicate interpretation of movements. We defined a Study Area in the US mid-Atlantic region, within which we worked to ensure more complete coverage, and limited our detailed analyses of movements in Federal waters to within the bounds of this Study Area. The Study Area contained towers funded by BOEM and operated by the USFWS that were designed to track offshore flights of shorebirds and seabirds for this and other BOEM studies (Loring et al. 2018, Loring et al. 2019). These BOEM automated radio telemetry stations were positioned strategically at coastal sites, spanning from Cape Cod, MA in the north to Back Bay, VA in the south, with direct line-of-sight to offshore areas of the US mid-Atlantic Bight. Each tower was 10.2 m tall and had six, high range directional antennas arranged radially to track movements of birds in all directions. This design attempted to maximize the detection range and directionality, but nevertheless had limited coverage for tracking movements into offshore areas of the US Atlantic OCS beyond 20 km from land, resulting in large gaps in detection coverage where many BOEM WEAs are located.

Gaps in detection coverage also occurred due to occasional maintenance or power issues at individual stations that caused receivers to go offline temporarily. We attempted to minimize these issues by checking each station at least monthly during the field seasons (approximately May through November each year). Our final analysis excluded data collected during winter months, when stations were not maintained on a regular basis.

Due the various issues with detection probability resulting from tag loss, limited offshore detection ranges and offline stations, the tracking array likely missed flights that occurred within the Study Area. Therefore, estimates of occurrence within the Atlantic OCS reported here should be considered minimum estimates. However, results from the study, when interpreted in the context of these limitations, provide novel baseline information on the regional movement patterns of shorebirds in the US mid-Atlantic region, including timing and meteorological conditions predictive of offshore flights into Federal waters. In addition, we report new information on the flight paths and altitudes of shorebirds tracked with automated radio telemetry which could be explored in greater detail in future studies as tagging technology advances.

4.3 Summary of Movements

Of the 3,955 shorebirds tagged by Motus network partners, one-third of tagged individuals were detected at least 50 km away from where they were tagged and by at least one receiving station located along the Atlantic coast of North America, between Mingan, QC, Canada in the northeast and Texas, USA in the southwest. The remaining two-thirds used alternate migration routes, had lost or malfunctioning tags, or otherwise were not detected by the Motus network. Among the Atlantic coast migrants, 65% were detected within the Study Area with substantial differences across species. This indicates that the US mid-Atlantic region is frequently used by Arctic and Subarctic breeding shorebirds that stage and migrate

along the Atlantic flyway. This is consistent with what is currently known about shorebird migration routes (Rodewald 2015) and use of important staging sites located within the Study Area including Delaware Bay, the Delmarva Peninsula, and Cape Cod, MA (Warnock and Gill 1996, Nettleship 2000, Macwhirter et al. 2002, Nebel and Cooper 2008, Hicklin and Gratto-Trevor 2010, Baker et al 2013, Brown et al. 2017, Holberton et al. 2019).

Visual interpretation of our shorebird movement data suggested that individuals using the most easterly and westerly migration routes often bypassed the Study Area. Because several shorebird species show east-west structure to populations, these patterns of use of the Study Area could have important implications for the risk faced by subpopulations. For example, during fall migration, some Red Knots using the Mingan Islands stopover in Quebec, Canada, did not subsequently make use of the Study Area. The Mingan stopover is used primarily by the extreme long-distance migrant *rufa* knots who will migrate to Tierra del Fuego, the population considered to be of greatest conservation concern (Niles et al. 2008). However, during spring migration, this long-distance population is likely to pass through the Atlantic OCS during migratory flights from wintering areas in South America to staging areas in Delaware Bay, using migration routes that could intersect with WEAs in the US mid-Atlantic region (Baker et al. 2004, Niles et al. 2010). In contrast, the shorter-distance migrant knots (that will winter in the United States and the Caribbean) are believed to travel routes that lie west of the Mingan Islands, stopping along the Atlantic coast of the US. This subpopulation is known to undertake feather molt within the Study Area and may exhibit a greater tendency for local or regional movements during fall migration, due to their prolonged stay (Loring et al. 2018).

Semipalmated Sandpipers provide another example of the importance of considering subpopulations within risk assessments. During migration, approximately half of Semipalmated Sandpipers departed offshore from Atlantic Canada on a southeast trajectory over the Atlantic Ocean in the fall, bypassing the Study Area. The other half of the tagged sample of Semipalmated Sandpipers staged and migrated through the Study Area, and likely belonged to the declining eastern population (Andres et al. 2012; Brown et al. 2017; Gratto-Trevor et al. 2012a, b; Smith et al. 2012). However, we observed a substantial number of movements of birds from the mid-continent to the coast and vice versa, demonstrating that shorebirds can and do undertake migrations that defy conventional flyway concepts (Gratto-Trevor et al. 1994). More detailed information on population connectivity and use of the US Atlantic OCS by at-risk species of shorebirds is warranted to assess potential population-level impacts from development of offshore WEAs throughout the migratory range.

Overall, nearly 600 shorebirds representing 12 different species met the criteria for inclusion in the analysis of movements within Study Area. During fall migration, movements were concentrated within and among staging areas on Cape Cod, MA, Long Island, NY, and Delaware Bay. During both spring and fall migration, shorebirds crossed Federal waters during arrival and departure flights from the Study Area, and during movements between staging sites. When these regional offshore movements cross Federal waters, it may increase relative collision risk by increasing the passage rates of individual shorebirds through one or more WEAs during a single migratory season.

4.4 Timing and Weather Conditions of Offshore Flights with Implications for Collision Risk

To describe seasonal timing and weather conditions associated with shorebird movements into the Atlantic OCS, we first generated summary statistics of temporal and meteorological covariates associated with flights over Federal waters. During fall migration, flights over Federal waters ranged from early July through late November, with variation in peak dates by species. Across all species, offshore flights during fall were associated with fair weather conditions, including high visibility (> 19 km) and little to no precipitation. Boosted GAM models applied to a subset of seven species with sufficient sample sizes of individuals in the Study Area ($n \geq 10$; Least Sandpiper, Red Knot, Ruddy Turnstone, Sanderling, Semipalmated Plover, Semipalmated Sandpiper, and White-rumped Sandpiper) indicated that the species covariate had the strongest influence on predicted exposure to Federal waters during fall migration. The influence of the species covariate was largely a result of the binomial model structure that compared the amount time that individuals spent in coastal and nearshore (< 5.5 km from the coast) areas of the Study Area (coded as non-events) versus the amount of time they spent in Federal waters (coded as events). Within this structure, the model estimated that White-rumped Sandpipers had higher exposure to Federal waters relative to other species. The data among White-rumped Sandpipers was unique because they were all tagged outside of the Study Area and passed through the Study Area during non-stop migratory flights. The remaining six species were either tagged at staging areas within the Study Area, or had individuals that were tagged elsewhere but used staging areas within the Study Area before departing offshore. Shorebirds that stage along the US Atlantic coast are likely at higher risk of cumulative exposure to multiple offshore WEAs within a migratory season, if they make regional movements that transit Federal waters among staging sites, relative to those passing through the area once per season during non-stop flights. For this reason, we recommend that future studies explore regional movements of at-risk species that stage along the US Atlantic coast during migration, particularly at high-use staging areas such as Delaware Bay, coastal New Jersey, and Cape Cod, MA that located near offshore WEAs in adjacent Federal waters.

Calendar date was the second most influential covariate in the Boosted GAM model, describing exposure to Federal Waters during for fall migration. Offshore movements were most likely in July, decreased into October and increased slightly in November. Peak offshore movements occurred when winds were blowing to the south-southeast (offshore) and atmospheric pressure was high, indicating fair weather conditions for sustained offshore flights. Researchers have studied relationships between weather and migration for over a century (Cooke 1885), and the associations between migratory departures and conditions such as wind assistance and rising atmospheric pressure have been widely documented (Brooks 1965, Able 1973, Richardson 1978).

The boosted GAM models applied to a subset of two species (Red Knot and Semipalmated Sandpiper) with sufficient sample sizes of individuals in the Study Area ($n \geq 10$) during spring migration predicted that exposure to Federal waters was highest in moderately strong winds (~10 m/s) blowing to the north in May and early June. There was a higher occurrence of exposure under adverse weather conditions (i.e. low visibility and some precipitation) in the spring in contrast to the fall, when exposure was highest during fair weather (high visibility, no precipitation). This is consistent with previous research showing that shorebirds are more likely to migrate during adverse weather conditions (including headwinds,

reduced visibility, and precipitation) in spring due to less stable atmospheric conditions and greater time constraints to reach breeding areas (O'Reilly and Wingfield 1995). Migratory flights during poor conditions could lead to increased collision risk with offshore wind turbines because of impaired visibility, depleted energy reserves, and reduced flight altitudes (Newton 2007).

Wind direction was an important predictor of exposure to Federal waters in both spring and fall, and peaks in probability of offshore flights were consistent with supportive winds. This aligns with recent research showing that shorebirds are highly wind selective in both seasons during migration and regardless of migration distance (Anderson et al. 2019, Duijns et al. 2019). During both fall and spring, flights in Federal waters occurred most often during late-afternoon and nocturnal hours. Nocturnal migration is thought to be advantageous for some species due to increased diurnal foraging opportunities prior to and after a migration bout, and reduced predation risk from raptors (Kerlinger and Moore 1989, Lank 1989, Alerstam 2009). In addition, atmospheric conditions may be more favorable to migratory flights at night due to reductions in turbulence and evaporative water loss, relative to daytime conditions when winds tend to be stronger and the air less humid (Kerlinger and Moore 1989).

4.5 Altitude and Collision Risk

Information on flight altitudes relative to the RSZ of offshore wind turbines is important for collision risk assessments, particularly in the context of daylight, which directly affects visibility and avoidance behavior (Exo et al. 2003). During both spring and fall migration, the majority of shorebirds' flights over Federal waters occurred above the RSZ (>250 m). Nevertheless, exposure to the RSZ was not trivial; 24% of mean flight altitudes occurred within the RSZ during spring and 36% during fall. During fall, approximately half of the flights in the RSZ occurred during day versus night, whereas in spring, all flights in the RSZ occurred during the day. These diurnal and seasonal variations are important to understand because risk of collision is potentially higher at night due to reduced visibility of turbines (Exo et al. 2003) and disorientation effects from artificial lighting on turbine towers that may attract birds towards the rotor-swept zone (Richardson 2000; Drewitt and Langston 2006). Thus, around-the-clock monitoring of flight paths and altitudes of migratory birds within offshore WEAS will be especially important for assessments of collision with lighted infrastructure during the construction and operation phases of lease areas. Although many of our altitude estimates fell above the currently assumed upper limit of the RSZ (250 m), even after accounting for the substantial uncertainty in our models, offshore wind turbines are projected to increase in size in the future (Musial et al. 2019) resulting in a larger zone of collision risk.

In the present study, we applied models based on the theoretical relationship between horizontal detection range of VHF signals received by automated radio telemetry stations to estimate flight altitudes when tagged individuals were detected by two or more spatially separated stations simultaneously. More detailed information on variation in flight altitudes of shorebirds relative to timing, distance travelled, and meteorological conditions is needed to fully assess risks of exposure to the RSZ during offshore flights. Offshore radar studies have recorded shorebirds migrating at altitudes exceeding 1 to 2 km (Richardson 1976, Williams and Williams 1990), whereas nearshore studies documented local and migratory flights of shorebirds occurring at altitudes <100 m (Dirksen et al. 2000, Langston and Pullan 2003). Therefore, risk of exposure to rotor swept altitudes may be greatest during takeoff and landing from stopover areas,

which emphasizes the need for determining setback distances when developing turbines near migratory stopover and staging areas (Howell et al. 2019). In addition, flight altitudes of migratory birds may vary in response to weather as they search to find suitable tailwinds (Shamoun-Baranes et al. 2010; Senner et al. 2018). Migratory birds may also descend to lower altitudes during periods of limited visibility, low cloud ceiling, and/or inclement weather, increasing their risk of collision with offshore wind turbines (Hüppop et al. 2006; Senner et al 2018). Detailed information on flight altitudes is beyond the ability of current VHF tracking technology within the Motus Network, although development of light-weight GPS transmitters (Senner et al. 2018) or VHF-tags with embedded altimeters (Bowlin et al. 2015) may provide viable options for tracking fine-scale 3-dimensional flight paths of small-bodied shorebirds in the near future.

4.6 Departure Bearings from Study Area

Although our land-based tracking stations were constrained in their ability to track flights more than 20 km offshore, we calculated the departure bearings of flights as birds left the Study Area to provide a general direction of outbound movement. During spring migration, all birds included in the analysis were tagged at staging areas within the Study Area and departed to the north and northeast towards the breeding grounds. Shorebirds tracked during fall migration primarily departed from the Study Area heading offshore to the south or southeast, with the exception of Sanderlings that primarily departed to the southwest along the coast. These results align with previous research on shorebird migration ecology, showing that many species of shorebirds, including Red Knots, White-rumped Sandpipers, Semipalmated Sandpipers, Least Sandpipers and Whimbrel, depart on transoceanic flights from the US Atlantic coast during fall migration to wintering areas that extend throughout the southern hemisphere (Parmelee 1992, Skeel and Mallory 1996, Nebel and Cooper 2008, Hicklin and Gratto-Trevor 2010, Baker et al. 2013). Sanderlings have a more dispersed wintering range that includes US Atlantic coast and extends through South America (Macwhirter et al. 2002).

Among our tagged sample, we found that variability in departure bearings was lowest for White-rumped Sandpipers, which all departed in an offshore direction. In contrast, Red Knots showed the highest variability in departure bearings, likely reflecting different (short distance versus mid- and long-distance) wintering populations. Short distance migrants typically fly along the Atlantic coastline to winter in areas as far north as Maryland and as far south as the Carribean or even the Venezuelan coast. Mid-distance and long-distance migrants typically fly directly from stopover areas in the Canadian Maritimes or the US Atlantic to their wintering grounds in Brazil and southern South America (Morrison and Ross 1989, Morrison et al. 2001, Niles and Aubry 2014). The variability in departure directions that we observed among species further highlights the need for additional technology and research aimed at collecting individual-based movement data of shorebirds in offshore environments. The degree of exposure to risk from wind energy facilities depends on the flight behavior and routes taken during migration, both of which can vary over time and among individuals.

5 Future Directions

Results from this study provided new information for baseline assessments of shorebird movements in offshore environments and gave some insight on priorities for targeted studies in the future. Most of the data available for analysis in this study were collected during fall migration. Although we provide some novel data here, there is still a large gap in our understanding of shorebird movements in the Atlantic OCS during spring migration. In the present study, all birds tracked during spring migration and included in our analysis of exposure to Federal waters within the Study Area were tagged at spring staging areas along the US Atlantic coast and, therefore, were not tracked prior to their arrival on the Atlantic coast from the wintering grounds. Most individuals then departed the Study Area to the north or northeast, towards their breeding grounds. Birds are perhaps most likely to cross the Atlantic OCS as they first arrive to the US coast from their more southerly staging grounds and wintering areas. However, some individuals tracked during spring migration crossed Federal waters while moving between staging areas along the US Atlantic coast prior to subsequent departure towards breeding areas. Future efforts to tag shorebirds on wintering grounds would provide more complete information on the exposure of shorebirds of Federal waters of the Atlantic OCS during spring migration. This information is especially needed for at-risk populations, such as the long-distance *rufa* Red Knot, that cross the Atlantic OCS during migratory flights from wintering and staging areas in South America (especially in coastal Brazil) to staging areas in Delaware Bay. Upon their approach into Delaware Bay, is possible that these birds may cross adjacent offshore WEAs with depleted energy reserves from long-distance migratory flights, and potentially in adverse weather conditions that are more prevalent during the spring migration season relative to fall. Therefore, the relative risk of collision with offshore wind turbines may be especially high for *rufa* Red Knots during spring migration and thus warrants future study.

Fully estimating exposure and collision risk of shorebirds to offshore wind turbines requires tracking technology capable of collecting high-resolution movement and altitude data throughout the entire migratory range and full annual cycle. Satellite-based tracking technology may provide a viable solution for collecting high-resolution, three-dimensional movement data of small-bodied shorebirds in the near future, as light-weight transmitters become more widely available (Senner et al. 2018). Current options for small-bodied species (< 100 g) include light-weight GPS data loggers that collect a limited number of 2-dimensional locations and require that the bird be recaptured at a later date to recover the data. Satellite transmitters suitable for medium-bodied species (> 150 g) are currently available that uplink 2-dimensional location data to the internet via the Argos system. Larger GPS-GSM transmitters that collect fine-scale 3-dimensional data, relayed to users over cellular networks, are currently available for larger-bodied species (weighing > 800 g). Devices continue to get smaller, and these fine-scale data describing routes and altitudes throughout the migratory range and full annual cycle will greatly improve accuracy of collision risk estimates and assessments of cumulative effects in the coming years.

Despite the advantages of satellite-based tracking technologies, radio telemetry remains a viable method for tracking movements of small bodied species (<150 g) with very high spatial and temporal precision within range of tracking stations. The key strengths of automated radio telemetry are the extremely high temporal precision of the tags (which can emit signals as often as every 2 seconds) and the around-the-clock monitoring capabilities of automated radio telemetry stations. The high temporal precision of transmitters, combined with the constant monitoring capabilities of receiving stations, can be highly

effective for monitoring movements of tagged individuals through geographic areas where networks of receiving stations are located. Since the tags are very small and light-weight, the technology is suitable for tracking nearly all taxa of birds and bats. The collaborative Motus network leverages the benefits of this technology, and currently manages data from over 20,000 individuals representing over 200 different species detected by several hundred tracking stations across the western Hemisphere and beyond.

The large geographic scale and sample sizes made possible through collaboration with the Motus network demonstrate the potential of future collaborations to track movements of high priority species offshore. Coordinated deployment of automated radio telemetry stations on offshore infrastructure would help increase the utility of using radio telemetry for assessments of bird movements in the Atlantic OCS. We are currently field-testing automated radio telemetry equipment on two offshore structures: a monitoring buoy in New York Bight and a wind turbine at the Block Island Wind Farm. We intend to use results from these deployments to inform future guidance for establishing a network of automated radio telemetry stations on offshore structures throughout the US Atlantic OCS. For example, a calibration study conducted by Paton et al (2020) at the Block Island Wind Farm tested several different configurations of automated radio telemetry receivers and antennas, providing valuable information on ways to optimize detection probability from automated radio telemetry systems on offshore wind turbines. Recommendations from this study include methods to configure tracking systems to detect signals from tags among multiple antennas and stations simultaneously in order to improve estimates of movements within the scale of an individual lease area. In addition, Paton et al. (2020) recommend that researchers employ newly available receiving technology that allows for remote (satellite-based) data acquisition to improve reliability of offshore stations.

As offshore lease areas move into development phases, a standardized, coordinated network of automated radio telemetry equipment mounted on offshore structures offers a promising approach for collecting the data needed for collision risk models, including detailed information on passage rates through individual lease areas, diurnal versus nocturnal flight activity, as well as coarse information on avoidance rates and flight altitudes. In collaboration with Motus, a network of receivers at multiple lease areas throughout the US Atlantic OCS could be used in assessments of cumulative impacts from exposure of birds and bats to multiple lease areas throughout their migratory range and annual cycle. Future efforts to track full-annual-cycle movements of shorebirds will be critical for assessments of population-level risks, as widespread development of offshore lease areas progresses throughout a large portion of the Atlantic OCS (Bureau of Ocean Energy Management 2019).

6 References

Able KP. 1973. The role of weather variables and flight direction in determining the magnitude of nocturnal bird migration. Ecology 54: 1031-1041

Agostinelli C and Lund U. 2017. R Package Circular: Circular Statistics (version 0.4-93). https://r-forge.r-project.org/projects/circular/.

Alerstam T. 2009. Flight by night or day? Optimal daily timing of bird migration. Journal of Theoretical Biology 258: 530-536.

Anderson AM, Duijns S, Smith PA, Friis C, Nol E. 2019. Migration distance and body condition influence shorebird migration strategies and stopover decisions during southbound migration. Frontiers in Ecology and Evolution 7:251.

Andres, BA, Gratto-Trevor C, Hicklin P, Mizrahi D, Morrison RIG, Smith PA. 2012. Status of the semipalmated sandpiper. Waterbirds 35:146–148. doi: 10.1675/063.035.0114

Baker AJ, Gonzalez PM, Piersma T, Niles LJ, de Lima Serrano do Nascimento I, Atkinson, Clark NA, Minton CDT, Peck MK, Aarts G. 2004. Rapid population decline in Red Knots: Fitness consequences of decreased refueling rates and late arrival in Delaware Bay. Proc. R. Soc. Lond. B 271(1541): 875-882.

Baker AJ, Gonzalez PM, Morrison RIG, Harrington BA. 2013. Red Knot (Calidris canutus), version 2.0. In The Birds of North America (P. G. Rodewald, editor). Cornell Lab of Ornithology, Ithaca, New York, USA. https://doi.org/10.2173/bna.563.

Bivand R, Lewin-Koh N. 2016. R package 'Maptools' (version 0.9-2); [accessed 2017 July 1]. https://cran.rproject.org/web/packages/maptools/.

Bureau of Ocean Energy Management [BOEM]. 2017. Environmental Studies Program Studies Development Plan, 2018-2020; [accessed 2019 October 20]. https://www.boem.gov/FY-2018-2020-SDP/.

BOEM. 2019. Renewable Energy GIS Data (version 13 Feb 2019); [accessed 2019 August 20]. https://www.boem.gov/Renewable-Energy-GIS-Data/.

Bowlin MS, Enstrom DA, Murphy BJ, Plaza E, Jurich P, Cochran J. 2015. Unexplained altitude changes in a migrating thrush: long-flight altitude data from radio-telemetry. The Auk: Ornithological Advances 132(4): 808-816.

Brooks WS. 1965. Effect of weather on autumn shorebird migration in east-central Illinois. 77: 45-54.

Brown S, Gratto-Trevor C, Porter R, Weiser E, Mizrahi D, Bentzen R, Boldenow M, Clay R, Freeman S, Giroux M, Kwon E, Lank DB, Lecomte N, Liebezeit J, Loverti V, Rausch J, Sandercock BK, Schulte S, Smith P, Taylor A, Winn B, Yezerinac S, Lanctot RB. 2017. Migratory connectivity of Semipalmated Sandpipers and implications for conservation. Condor 119:207–224. doi: 10.1650/CONDOR-16-55.1

Brzustowski J and LePage D. 2019. R Package motus: Fetch and use data from the Motus Wildlife Tracking System (version 2.0.0). https://github.com/jbrzusto/motus.

Bühlmann P, Hothorn T. 2007. Boosting Algorithms: Regularization, Prediction and Model Fitting. Statistical Science 22(4):477-505.

Burger J, Gordon C, Niles L, Newman J, Forcey G, Vlietstra L. 2011. Risk evaluation for Federally listed (Roseate Tern, Piping Plover) or candidate (Red Knot) bird species in offshore waters: A first step for managing the potential impacts of wind facility development on the Atlantic Outer Continental Shelf. Renewable Energy 36: 338–351.

Burger J, Niles LJ, Porter RR, Dey AD, Koch S, Gordon C. 2012. Migration and over-wintering of Red Knots *(Calidris canutus rufa*) along the Atlantic coast of the United States. Condor 114: 302–313.

Cooke WW. 1885. The relation of migration to barometric pressure and temperature. Ornithology and Oologist 10: 65-68.

Cremers J and Klugkist I. 2018. One Direction? A Tutorial for Circular Data Analysis Using R With Examples in Cognitive Psychology. Frontiers in psychology 9:2040. doi:10.3389/fpsyg.2018.02040.

Dirksen S, Spaans AL, van der Winden J. 2000. Studies on Nocturnal Flight Paths and Altitudes of Waterbirds in Relation to Wind Turbines: A Review of Current Research in the Netherlands. In Proceedings of the National Avian-Wind Power Planning Meeting III, San Diego, California, May 2000. Prepared for the National Wind Coordinating Committee. Ontario: LGL Ltd.

Drewitt AL, Langston RH. 2008. Collision effects of wind-power generators and other obstacles on birds. Annals of the New York Academy of Sciences 1134(1):233-266.

Duijns S, Anderson AM, Aubry Y, Dey A, Flemming SA, Francis CM, Friis C, Gratto-Trevor C, Hamilton DJ, Holberton R, Koch S, McKellar AE, Mizrahi D, Morrissey CA, Neima SG, Newstead D, Niles L, Nol E, Paquet J, Rausch J, Tudor L, Turcotte Y, Smith PA. 2019. Long-distance migratory shorebirds travel faster towards their breeding grounds, but fly faster post-breeding. Scientific Reports 9:9420.

Environment and Climate Change Canada (ECCC). 2019. The Status of Birds in Canada Website, Data-version 2019. Environment and Climate Change Canada, Gatineau, Quebec, Canada.

Environment and Climate Change Canada. 2016. Recovery Strategy and Management Plan for the Red Knot (Calidris canutus) in Canada [Proposed]. Species at Risk Act Recovery Strategy Series. Environment and Climate Change Canada, Ottawa. ix + 54 pp.

Exo KM, Huppop O, Garthe S. 2003. Birds and offshore wind farms: a hot topic in marine ecology. Wader Study Group Bulletin 100:50-53.

Farmer A, Holmes RT, Pitelka FA. 2013. Pectoral Sandpiper (Calidris melanotos), version 2.0. In The Birds of North America (P. G. Rodewald, editor). Cornell Lab of Ornithology, Ithaca, New York, USA. https://doi.org/10.2173/bna.348.

Fox AD, Desholm M, Kahlert J, Christensen TK, Petersen IBK. 2006. Information needs to support environmental impact assessment of the effects of European marine offshore wind farms on birds. Ibis 148:129-144.

Fox AD, Petersen IK. 2019. Offshore Wind Farms and their effects on birds. Dansk Ornitologisk Forenings Tidsskrift 113: 86-101.

Galbraith H, DesRochers DW, Brown, Reed JM. 2014. Predicting vulnerabilities of North American shorebirds to climate change. PLoS ONE 9(9):e108899.

Gómez C, Bayly NJ, Norris DR, Mackenzie SA, Rosenberg KV, Taylor PD, Hobson KA, Cadena CD. 2017. Fuel loads acquired at a stopover site influence the pace of intercontinental migration in a boreal songbird. Scientific Report 7:3405.

Goodale MW, Milman A. 2016. Cumulative adverse effects of offshore wind energy development on wildlife. Journal of Environmental Planning and Management 59(1):1-21.

Gratto-Trevor CL, Dickson HL. 1994. Confirmation of elliptical migration in a population of Semipalmated Sandpipers. Wilson Bulletin 106:78–90.

Gratto-Trevor C, Morrison RIG, Mizrahi D, Lank DB, Hicklin P, Spaans AL. 2012a. Migratory connectivity of Semipalmated Sandpipers: winter distribution and migration routes of breeding populations. Waterbirds 35:83–95. doi: 10.1675/063.035.0109

Gratto-Trevor C, Smith PA, Morrison RIG, Aubry Y, Cotter R. 2012b. Population trends in Semipalmated Sandpipers from migration counts. Waterbirds 35:96–105. doi: 10.1675/063.035.0110

Grönroos J, Green M, Alerstam T. 2012. To fly or not to fly depending on winds: shorebird migration in different seasonal wind regimes. Animal Behaviour 83:1449-1457.

Hedenström A, Alerstam T. 1994. Optimal climbing flight in migrating birds: predictions and observations of knots and turnstones. Animal Behaviour 48: 47-54.

Hicklin P, Gratto-Trevor CL. 2010. Semipalmated Sandpiper (Calidris pusilla), version 2.0. In The Birds of North America (P. G. Rodewald, editor). Cornell Lab of Ornithology, Ithaca, New York, USA. https://doi.org/10.2173/bna.6.

Holberton RL, Taylor PD, Tudor LM, O'Brien KM, Mittelhauser GH, Breit A. 2019. Automated VHF radiotelemetry revealed site-specific differences in fall migration strategies of Semipalmated Sandpipers on stopover in the Gulf of Maine. Frontiers in Ecology and Evolution 7:327. doi: 10.3389/fevo.2019.00327

Hope DD, Pekarik C, Drever MC, Smith PA, Gratto-Trevor C, Paquet J, Aubry Y, Donaldson G, Friis C, Gurney K, Rausch J, McKellar AE, Andres B. 2019. Shorebirds of conservation concern in Canada – 2019. Wader Study 126(2): 88-100.

Howell JE, McKellar AE, Espie RH, Morrissey CA. 2019. Predictable shorebird departure patterns from a staging site can inform collision risks and mitigation of wind energy developments. Ibis doi:10.1111/ibi.12771.

Hüppop O, Dierschke J, Exo KM, Fredrich E, Hill R. 2006. Bird Migration Studies and Potential Collision Risk with Offshore Wind Turbines. Ibis 148: 90-109.

Johnson, A, Perz J, Nol E, Senner N. 2016. Dichotomous strategies: The migration of Whimbrel (Numenius phaeopus) breeding in the Eastern Canadian Sub-Arctic. Journal of Field Ornithology. Journal of Field Ornithology 87:371-383.

Kays R, Tilak S, Crofoot M, Fountain T, Obando D, Ortega A, Kuemmeth F, Mandel J, Swenson G, Lambert T, Hirsch B. 2011. Tracking animal location and activity with an automated radio telemetry system in a tropical rainforest. The Computer Journal, 54(12): 1931-1948.

Kerlinger P, Moore FR. 1989. Atmospheric structure and avian migration. Current Ornithology 6: 109-142.

Langston RH, Pullan JD. 2003. Wind farms and birds: an analysis of the effects of wind farms on birds, and guidance on environmental assessment criteria and site selection issues. Council of Europe.

Lank DB. 1989. Why fly by night? Inferences from tidally-induced migratory departures of sandpipers. Journal of Field Ornithology 60:154-161.

Loring PH, McLaren JD, Smith PA, Niles LJ, Koch SL, Goyert HF, Bai H. 2018. Tracking movements of threatened migratory rufa Red Knots in U.S. Atlantic Outer Continental Shelf Waters. Sterling (VA): US Department of the Interior, Bureau of Ocean Energy Management. OCS Study BOEM 2018-046. 145 p.

Loring PH, Paton PWC, McLaren JD, Bai H, Janaswamy R, Goyert HF, Griffin CR, Sievert PR. 2019. Tracking Offshore Occurrence of Common Terns, Endangered Roseate Terns, and Threatened Piping Plovers with VHF Arrays. Sterling (VA): US Department of the Interior, Bureau of Ocean Energy Management. OCS Study BOEM 2019-017. 140 p.

Macwhirter RB, Austin-Smith Jr. P, Kroodsma DE. 2002. Sanderling (Calidris alba), version 2.0. In The Birds of North America (P. G. Rodewald, editor). Cornell Lab of Ornithology, Ithaca, New York, USA. https://doi.org/10.2173/bna.653.

Mckinnon EA, Laplante M, Love OP, Fraser KC, Mackenzie S, Vezina F. 2019. Tracking landscape-scale movements of Snow Buntings and weather-driven changes in flock composition during the temperate winter. Frontiers in Ecology and Evolution 7:329.

Morrison RIG, Ross RK. 1989. Atlas of nearctic shorebirds on the coast of South America. Canada, 2 vols. Special Publication, Canadian Wildlife Service, Ottawa, Ontario.

Morrison RIG, Aubry Y, Butler RW, Beyersbergen GW Donaldson GW, Gratto-Trevor CL, Hicklin PW, Johnston VH, Ross RK. 2001. Declines in North American shorebird populations. Wader Study Group Bulletin 94:34-38.

Motus Wildlife Tracking System. 2016. Motus Wildlife Tracking System Collaboration Policy. January 2016; [accessed 2017 August 20]. https://motus.org/wp-content/uploads/2016/01/MotusCollaborationPolicy.January2016.pdf.

Musial WD, Beiter PC, Spitsen P, Nunemaker J, Gevorgian V. 2019. 2018 Offshore Wind Technologies Market Report (No. NREL/TP-5000-74278; DOE/GO-102019-5192). National Renewable Energy Lab (NREL), Golden, CO, USA.

Nebel S, Cooper JM. 2008. Least Sandpiper (Calidris minutilla), version 2.0. In The Birds of North America (P. G. Rodewald, editor). Cornell Lab of Ornithology, Ithaca, New York, USA. https://doi.org/10.2173/bna.115.

Nettleship DN. 2000. Ruddy Turnstone (Arenaria interpres), version 2.0. In The Birds of North America (P. G. Rodewald, editor). Cornell Lab of Ornithology, Ithaca, New York, USA. https://doi.org/10.2173/bna.537.

Newton I. 2007. Weather-related mass-mortality events in migrants. Ibis 149:453-467.

Niles LJ, Sitters HP, Dey AD, Atkinson PW, Baker AJ, Bennett KA, Carmona R, Clark KE, Clark NA, Espoz C, et al. 2008. Status of the Red Knot (*Calidris canutus rufa*) in the Western Hemisphere. Studies in Avian Biology No. 36.

Niles LJ, Burger J, Porter RR, Dey AD, Minton CDT, Gonzalez PM, Baker AJ, Fox JW, Gordon C. 2010. First results using light level geolocators to track red knots in the Western Hemisphere show rapid and long intercontinental flights and new details of migration pathways. Wader Study Group Bull. 117(2): 123-130.

Niles LJ, Aubry Y. 2014. Status of Migratory Shorebirds in French Guiana and Guadeloupe With Emphasis On Red Knots And Ruddy Turnstones. Report to Canadian Wildlife Service. 32 pp.

Nisbet ICT. 1963. Measurements with Radar of the Height of Nocturnal Migration over Cape Cod, Massachusetts. Bird-Banding 34(2):57-67.

Nol E, Blanken MS. 2014. Semipalmated Plover (Charadrius semipalmatus), version 2.0. In The Birds of North America (P. G. Rodewald, editor). Cornell Lab of Ornithology, Ithaca, New York, USA. https://doi.org/10.2173/bna.444.

North American Bird Conservation Initiative (NABCI) Canada. 2019. The State of Canada's Birds, 2019. Environment and Climate Change Canada, Ottawa, Canada. www.stateofcanadasbirds.org.

O'Connell A, Spiegel CS, Johnston S. 2011. Compendium of Avian Occurrence Information for the Continental Shelf Waters along the Atlantic Coast of the United States, Final Report (Database Section - Shorebirds). Prepared by the U.S. Fish and Wildlife Service, Hadley, MD for the USGS Patuxent Wildlife Research Center, Beltsville, MD. U.S. Department of the Interior, Geological Survey, and Bureau of Ocean Energy Management Headquarters, OCS Study BOEM 2012-076.

O'Reilly K, Wingfield JC. 1995. Spring and autumn migration in Arctic shorebirds: same distance, different strategies. American Zoologist 35:222-233.

Paton PWC, Cooper-Mullin, C., Kouhi, S. Loring PH. 2020. Assessing movements of birds using digital VHF transmitters: A validation study. Sterling (VA): US Department of the Interior, Bureau of Ocean Energy Management. OCS Study BOEM 2020-0xx. 140 p.

Parmelee DF. 1992. White-rumped Sandpiper (Calidris fuscicollis), version 2.0. In The Birds of North America (P. G. Rodewald, editor). Cornell Lab of Ornithology, Ithaca, New York, USA. https://doi.org/10.2173/bna.29.

Poole AF, Pyle P, Patten MA, Paulson DR. 2016. Black-bellied Plover (Pluvialis squatarola), version 3.0. In The Birds of North America (P. G. Rodewald, editor). Cornell Lab of Ornithology, Ithaca, New York, USA. https://doi.org/10.2173/bna.bkbplo.03.

Richardson WJ. 1976. Autumn migration over Puerto Rico and the Western Atlantic: a radar study. Ibis 118(3):309-332.

Richardson WJ. 1978. Timing and amount of bird migration in relation to weather: a review. Oikos 30:224-272.

Richardson WJ. 2000. Bird migration and wind turbines: migration timing, flight behavior, and collision risk. Pp. 132-140 in Proceedings of the National Avian-Wind Power Planning Meeting III, San Diego, California, USA.

Rodewald, P. (Editor). 2015. The Birds of North America: https://birdsna.org. Cornell Laboratory of Ornithology, Ithaca, NY.

Rosenberg KV, Pashley D, Andres B, Blancher PJ, Butcher GS, Hunter WC, Mehlman D, Panjabi AO, Parr M, Wallace G, Wiedenfeld D. 2014. The State of the Birds 2014 Watch List. North American Bird Conservation Initiative, U.S. Committee. Washington, D.C.

Senner NR, Stager M, Verhoeven MA, Cheviron ZA, Piersma T, Bouten W. 2018. High-altitude shorebird migration in the absence of topographical barriers: Avoiding high air temperatures and searching for profitable winds. Proceedings of the Royal Society B 285:20180569.

Shamoun-Baranes J, Leyrer J, van Loon E, Bocher P, Robin F, Meunier F, Piersma T. 2010. Stochastic atmospheric assistance and the use of emergency staging sites by migrants. Proceedings of the Royal Society B 277:1505-1511.

Skeel MA, Mallory EP. 1996. Whimbrel (Numenius phaeopus), version 2.0. In The Birds of North America (P. G. Rodewald, editor). Cornell Lab of Ornithology, Ithaca, New York, USA. https://doi.org/10.2173/bna.219.

Smith PA, Gratto-Trevor CL, Collins BT, Fellows SD, Lanctot RB, Liebezeit J, McCaffery B, Tracy D, Rausch J, Kendall S, Zack S, and Gates HR. 2012. Trends in abundance of Semipalmated Sandpipers: evidence from the Arctic. Waterbirds 35:106-119.

Smith PA, McKinnon L, Meltofte H, Lanctot RB, Fox AD, Leafloor JO, Soloviev M, Franke A, Falk K, Golovatin M, Sokolov V, Sokolov A, Smith AC. Accepted. Status and trends of tundra birds across the circumpolar Arctic. Ambio.

Taylor PD, Crewe TL, Mackenzie SA, Lepage D, Aubry Y, Crysler Z, Finney G, et al. 2017. The Motus Wildlife Tracking System: A Collaborative Research Network to Enhance the Understanding of Wildlife Movement. Avian Conservation and Ecology 12(1):8.

Tibbitts TL, Moskoff W. 2014. Lesser Yellowlegs (Tringa flavipes), version 2.0. In The Birds of North America (P. G. Rodewald, editor). Cornell Lab of Ornithology, Ithaca, New York, USA. https://doi.org/10.2173/bna.427.

USFWS. 2014. Endangered and Threatened Wildlife and Plants; Threatened Species Status for the rufa Red Knot; Final Rule. Department of the Interior, Fish and Wildlife Service, 50 CFR Part 17. 79 Federal Register (FR) 238: 73706-73748; [accessed 12 December 2017]. http://www.gpo.gov/fdsys/pkg/FR-2014-12-11/pdf/2014-28338.pdf.

U.S. Shorebird Conservation Plan Partnership. 2016. U.S. Shorebirds of Conservation Concern ─ 2016. http://www.shorebirdplan.org/science/assessment-conservation-status-shorebirds/.

van der Velde M, Haddrath O, Verkuil YI, Baker AJ, Piersma T. 2017. New primers for molecular sex identification of waders. Wader Study 124, 147–151. doi: 10.18194/ws.00069

Warnock ND, Gill RE. 1996. Dunlin (Calidris alpina), version 2.0. In The Birds of North America (P. G. Rodewald, editor). Cornell Lab of Ornithology, Ithaca, New York, USA. https://doi.org/10.2173/bna.203.

Western Hemisphere Shorebird Reserve Network (WHSRN). https://whsrn.org/ [accessed 1 November 2019]

Williams TC, Williams JM. 1990. Open ocean bird migration. IEEE Proceedings F - Radar and Signal Processing 137:133-137.

Wright JR, Powell LL, Tonra CM. 2018. Automated telemetry reveals staging behavior in a declining migratory passerine. Auk 135:461-476.

Zockler C, Delany S, Hagemeijer W. 2003. Wader population are declining – how will we elucidate the reasons? Wader Study Group Bulletin. 100:202-211.

Appendix A: Metadata for Tag Deployments

As supplementary material to this report, we have provided tag deployment data and results of exposure analysis for each nano-tagged bird in this study submitted to BOEM ('Appendix_A_Tag_Metadata.rds'). Note: deployment locations were rounded to the nearest degree and some were grouped with nearby locations

Descriptions of each field appear below:

Fields:

tag_id: tag ID number in the Motus database

proj_id: Motus project number

spp: species (AMGP - American Golden-Plover, BBPL - Black-bellied Plover, DUNL - Dunlin, LESA - Least Sandpiper, LEYE - Lesser Yellowlegs, PESA - Pectoral Sandpiper, PUSA - Purple Sandpiper, REKN - Red Knot, REPH - Red Phalarope, RNPH - Red-necked Phalarope, RUTU - Ruddy Turnstone, SAND – Sanderling, SBDO - Short-billed Dowitcher, SEPL - Semipalmated Plover, SESA - Semipalmated Sandpiper, WHIM - Whimbrel, WRSA - White-rumped Sandpiper)

dep_loc: geographic location of tag deployment

dep_lat: approximate latitude of tag deployment

dep_lon: approximate longitude of tag deployment

dep_date: Date of tag deployment

age: age of bird. AHY = After Hatch Year, HY = Hatch Year, U = unknown (or not determined)

sex: sex of bird. M = male, F = female, U = unknown (or not determined)

incl_exposure_analysis = yes (included in analysis of exposure), no (not included)

migration_season: fall, spring, both (NA if incl_exposure_analysis = no)

fed_waters: 1 = movement model estimated locations over Federal waters of US Atlantic during nonstop flight, 0 = movement model did not estimate locations over Federal waters of US Atlantic (NA if incl_exposure_analysis = no).

Appendix B: Metadata for BOEM Automated Radio Telemetry Stations, 2014-2017

Table B-1. Detailed description of automated receiving stations comprising the BOEM radio telemetry array by site, station code, geographic coordinates (decimal degrees), start year of operation, end year of operation, and installation specifications.

Site	Code	Lat	Long	Start Year	End Year	Installation
Monomoy NWR - N, Chatham, MA	MNYN	41.6088	-69.9870	2014	Still operational	Six, 9-element (11.1 dBd) Yagi antennas oriented radially (60 degree separation) on 12.2-m mast
Monomoy NWR - S, Chatham, MA	MNYS	41.5526	-70.010	2014	Still operational	Six, 9-element (11.1 dBd) Yagi antennas oriented radially (60 degree separation) on 12.2-m mast
Monomoy NWR – Tern Colony, Chatham, MA	TERN	41.6197	-69.9849	2014	2015	One, 5-element (9 dBd) Yagi antenna (oriented S) on 1.4 m post.
Nantucket NWR (Great Point), Nantucket, MA	GTPT	41.3906	-70.0490	2014	Still operational	Six, 9-element (11.1 dBd) Yagi antennas oriented radially (60 degree separation) on 12.2-m mast
Coatue Point, Nantucket, MA	CTPT	41.3073	-70.0640	2014	2017	Six, 9-element (11.1 dBd) Yagi antennas oriented radially (60 degree separation) on 12.2-m mast
Eel Point, Nantucket, MA	CTPT	41.2934	-70.1972	2014	2015	Six, 9-element (11.1 dBd) Yagi antennas oriented radially (60 degree separation) on 12.2-m mast
Muskeget Island, Nantucket, MA	MUSK	41.3373	-70.3050	2014	2017	Six, 9-element (11.1 dBd) Yagi antennas oriented radially (60 degree separation) on 12.2-m mast
Nomans Land Island NWR, MA	NOMA	41.2613	-70.8150	2014	Still operational	Six, 9-element (11.1 dBd) Yagi antennas oriented radially (60 degree separation) on 12.2-m mast

Site	Code	Lat	Long	Start Year	End Year	Installation
Nomans Land Island NWR, MA - Summit	NOMS	41.2531	-70.8130	2014	Still operational	One, 9-element (11.1 dBd) Yagi antenna oriented SW on a 3 m (10 ft) mast at the summit (110 ft. elevation) of Nomans Land Island
Sachuest Point NWR, Middletown, RI	SACH	41.4787	-71.2440	2014	Still operational	Six, 9-element (11.1 dBd) Yagi antennas oriented radially (60 degree separation) on 12.2-m mast
Southeast Light, Block Island, RI	BISE	41.1532	-71.5530	2014	2017	Six, 9-element (11.1 dBd) Yagi antennas oriented radially (60 degree separation) on 12.2-m mast
Napatree Point, Westerly, RI	NAPA	41.3063	-71.8840	2014	Still operational	Six, 9-element (11.1 dBd) Yagi antennas oriented radially (60 degree separation) on 12.2-m mast
Montauk Point, Montauk, NY	MNTK	41.0723	-71.8560	2014	Still operational	Six, 9-element (11.1 dBd) Yagi antennas oriented radially (60 degree separation) on 12.2-m mast
Great Gull Island, NY	GGIS	41.2018	-72.1190	2014	Still operational	Four 5-element (9 dBd) Yagi antennas oriented radially (90 degree separation) on 11-m observation tower
Race Point, Cape Cod National Seashore, Provincetown, MA	RCPT	42.0658	-70.2440	2015	2017	Six, 9-element (11.1 dBd) Yagi antennas oriented radially (60 degree separation) on 12.2-m mast
Marconi, Cape Cod National Seashore, Wellfleet, MA	WELL	41.9147	-69.9720	2015	Still operational	Six, 9-element (11.1 dBd) Yagi antennas oriented radially (60 degree separation) on 12.2-m mast
Waquoit Bay National Estuarine Research Reserve, Mashpee, MA	WAQT	41.5518	-70.5070	2015	Still operational	Six, 9-element (11.1 dBd) Yagi antennas oriented radially (60 degree separation) on 12.2-m mast
Trustom Pond NWR, South Kingston, RI	TRUS	41.3734	-71.5760	2015	Still operational	Six, 9-element (11.1 dBd) Yagi antennas oriented radially (60

Site	Code	Lat	Long	Start Year	End Year	Installation
						degree separation) on 12.2-m mast
Fire Island National Seashore, Long Island, NY	FRIS	40.6328	-73.2160	2015	Still operational	Six, 9-element (11.1 dBd) Yagi antennas oriented radially (60 degree separation) on 12.2-m mast
Wings Neck, Bourne, MA	WING	41.6807	-70.6615	2016	Still operational	Two, 9-element antennas on 11-m observation tower
Old Saybrook, CT	OSCT	41.2875	-72.3240	2016	Still operational	Six, 9-element (11.1 dBd) Yagi antennas on 8-m tower
Plum Island Animal Disease Center, Orient, NY	PLIS	41.1894	-72.1630	2016	2017	Six, 9-element (11.1 dBd) Yagi antennas oriented radially (60 degree separation) on 12.2-m mast
New York Aquarium, Coney Is, NY	CONY	40.5738	-73.9770	2016	Still operational	Four, 9-element (11.1 dBd) antennas on 12 m building
Jamaica Bay Unit, Gateway National Recreation Area, NY	JMBY	40.6163	-73.8240	2016	Still operational	Four, 5-element (9 dBd) antennas on 12.2 m utility pole
Sandy Hook Unit, Gateway National Recreation Area, NJ	SHNJ	40.4301	-73.9868	2016	Still operational	Six, 9-element (11.1 dBd) Yagi antennas oriented radially (60 degree separation) on 12.2-m mast
Rutgers Marine Field Station, NJ	RTNJ	39.5090	-74.3240	2016	Still operational	Four, six-element (9 dBd) antennas attached to roof of 12-m building
North Brigantine Natural Area, NJ	NBNJ	39.4218	-74.3477	2016	Still operational	Six, 9-element (11.1 dBd) Yagi antennas oriented radially (60 degree separation) on 12.2-m mast
Avalon Fishing Pier, Avalon, NJ	AVNJ	39.0919	-74.7179	2016	Still operational	Four, 9-element (11.1 dBd) antennas attached to 7-m mast
Cape Henlopen State Park, DE	CHSP	38.7702	-75.0852	2016	Still operational	Six, 9-element (11.1 dBd) Yagi antennas oriented radially (60 degree separation) on 12.2-m mast

Site	Code	Lat	Long	Start Year	End Year	Installation
Parramore Island, VA Coast Reserve, VA	PARR	37.5737	-75.6174	2016	Still operational	Four, six-element (9 dBd) antennas on existing 21-m tower
Chincoteague NWR, VA	CHIN	37.8627	-75.3703	2016	Still operational	Six, 9-element (11.1 dBd) Yagi antennas oriented radially (60 degree separation) on 12.2-m mast
Eastern Shore NWR, Skidmore Island, VA	SKID	37.1340	-75.9258	2016	Still operational	Six, 9-element (11.1 dBd) Yagi antennas oriented radially (60 degree separation) on 12.2-m mast
Back Bay NWR, VA	BBVA	36.6718	-75.9156	2016	Still operational	Six, 9-element (11.1 dBd) Yagi antennas oriented radially (60 degree separation) on 12.2-m mast

Appendix C. Summary of geospatially referenced detection and modeled location data from all shorebirds in this study submitted to BOEM as a supplemental material to this report

As supplementary material to this report, we have provided movement model output and associated meteorological covariate data on a 1-minute time step for all birds by migration season and species (Appendix_C_Location_Estimates_and_Weather_Data_[spp]_[migration_season].rds). In addition, we provide all processed data from the BOEM array and broader Motus Wildlife Tracking System for all birds in this study (Appendix_C_Motus_Detection_Data_[spp].rds).

Field descriptions of each file appear below:

File name: Appendix_C_Location_Estimates_and_Weather_Data_[spp]_[migration_season].rds

Fields:

tag_id: tag ID number in the Motus database

spp: species (BBPL - Black-bellied Plover, DUNL - Dunlin, LESA - Least Sandpiper, LEYE - Lesser Yellowlegs, PESA - Pectoral Sandpiper, REKN - Red Knot, RUTU - Ruddy Turnstone, SAND – Sanderling, SEPL - Semipalmated Plover, SESA - Semipalmated Sandpiper, WHIM - Whimbrel, WRSA - White-rumped Sandpiper)

migration_season: fall, spring

ts_gmt: time stamp of estimated location, in Greenwich Mean Time (GMT)

x: mean x-coordinate of location estimate in UTM Zone 18N (units in m)

y: mean y-coordinate of location estimate in UTM Zone 18N (units in m)

z: mean altitude estimate (units in m)

stdx: standard deviation of x-coordinate of location estimate in UTM Zone 18N (units in m)

stdy: standard deviation of y-coordinate of location estimate in UTM Zone 18N (units in m)

lqz: lower quartile of z (units in m)

uqz: upper quartile of z (units in m)

nonstop: yes (nonstop flight), no (stopover or staging movement)

wind_sp: wind speed (m/s), at estimated flight altitude

wind_dir: the direction wind blows toward, measured in degrees clockwise from geographic North, at estimated flight altitude

air_temp: air temperature (units in Kelvins, surface level)

precipn: precipitation accumulation (units in kg/m^2, surface level)

visibility: visibility (units in m, surface level)

pressure: barometric pressure (units in Pa, surface level)

File name: Appendix_C_Motus_Detection_Data_[spp].rds

Fields:

tag_id: tag ID number in the Motus database

spp: species (BBPL - Black-bellied Plover, DUNL - Dunlin, LESA - Least Sandpiper, LEYE - Lesser Yellowlegs, PESA - Pectoral Sandpiper, REKN - Red Knot, RUTU - Ruddy Turnstone, SAND – Sanderling, SEPL - Semipalmated Plover, SESA - Semipalmated Sandpiper, WHIM - Whimbrel, WRSA - White-rumped Sandpiper)

ts_gmt: time stamp of detection, in GMT

recv_proj: id number in the Motus database of the project that deployed automated radio telemetry station (NA if not available)

recv_name: name of automated radio telemetry station that recorded the detection (NA if not available)

recv_type: type of receiver detection recorded on (Sensorgnome, Lotek)

recvLat: latitude of automated radio telemetry station (in decimal degrees)

recvLon: longitude of automated radio telemetry station (in decimal degrees)

antenna: receiving antenna number

sig: signal strength of detection (dBm if recv_type = Sensorgnome, scale of 0-255 if recv_type = Lotek)

Department of the Interior (DOI)

The Department of the Interior protects and manages the Nation's natural resources and cultural heritage; provides scientific and other information about those resources; and honors the Nation’s trust responsibilities or special commitments to American Indians, Alaska Natives, and affiliated island communities.

Bureau of Ocean Energy Management (BOEM)

The mission of the Bureau of Ocean Energy Management is to manage development of U.S. Outer Continental Shelf energy and mineral resources in an environmentally and economically responsible way.